ABSTRACT

Imaging Surface Reactions at Molecular Level on TiO_2 Surfaces

Yaobiao Xia, Ph.D.

Mentor: Zhenrong Zhang, Ph.D.

Understanding the structure and properties of TiO_2 surfaces is critical to achieve a better understanding of heterogeneous catalytic reactions on TiO_2. In this thesis, rutile TiO_2 (110) and anatase TiO_2 (001) surfaces have been investigated using scanning tunneling microscopy (STM). The approach of comparison of the same nanoscale area during reaction allows the site-specific molecular-level understanding of surface catalytic reactions.

The rutile TiO_2(110) (1 × 1) surface prepared by cycles of Ar-ion sputtering and e-beam annealing was studied using acetone as a probe molecule. It was found that acetone molecules preferably adsorb on the oxygen vacancy sites at room temperature. The sequential isothermal STM images show acetone either diffuse along the bridge-bonded oxygen row or from the oxygen row to the titanium row and then moving along the titanium row.

By exposing the reduced TiO_2(110) (1 × 1) surface to O_2, the surface became partially oxidized. The consecutive reaction steps of acetone molecules with the partially oxidized surface was studied. It was found that acetone molecules react with the oxygen

adatoms and the bridge-bound oxygen vacancies. As a result of reactions, two different types of species were formed.

With more cleaning cycles at higher temperatures, TiO_2(110) transformed from the reduced (1×1) phase to the cross-linked (1×2) phase. The structure of cross-linked (1×2) TiO_2(110) was studied through the interaction of trimethyl acetic acid (TMAA) with various sites on the surfaces. At low coverage, TMAA molecules mostly adsorb in troughs and on cross-links. With increasing coverage, they form a chain in the trough. At higher coverage, TMAA molecules adsorb on strands in both centered and off-centered configurations. Comparing three different models, the adsorption of TMAA strongly supports the Ti_2O model.

The atomic structure of anatase TiO_2(001) expitaxial thin films has been studied. Three types of features were found on the bright rows of the (1×4) reconstructed surface from the high bias STM images. High resolution STM images taken at the same area at different bias voltages show that these features are originated from two basic atomic building blocks. Based on these data, a modified added molecule model was proposed.

Imaging Surface Reactions at Molecular Level on TiO_2 Surfaces

by

Yaobiao Xia, B.S.

A Dissertation

Approved by the Department of Physics

_____

Dwight P. Russell, Ph.D., Chairperson

Submitted to the Graduate Faculty of
Baylor University in Partial Fulfillment of the
Requirements for the Degree
of

Doctor of Philosophy

Approved by the Dissertation Committee

_____

Zhenrong Zhang, Ph.D., Chairperson

_____

Kenneth T. Park, Ph.D.

_____

Gregory A. Benesh, Ph.D.

_____

Howard Lee, Ph.D.

_____

Jonathan Hu, Ph.D.

Accepted by the Graduate School

December 2017

_____

J. Larry Lyon, Ph.D., Dean

Page bearing signatures is kept on file in the Graduate School.

TABLE OF CONTENTS

LIST OF FIGURES

LIST OF TABLES

ACKNOWLEDGMENTS

First of all, I would like to thank my advisor Dr. Zhenrong Zhang, for her support, advice and guidance through all these years. It is my pleasure to be the first graduate student in her group. We worked together to build the lab up, make the apparatus work, solve the problems and overcome the difficulties, collect the data and publish the articles. From the beginning of my graduate research till now, I learned from her the knowledge and skills for scientific research and all the efforts finally bore fruit with this dissertation completed. Also, I would like to give thanks to Dr. Kenneth T. Park, for his kindness, helpfulness, and the encouraging words. It is full of joy working with him and by himself he showed me the characters of a good mentor. In addition, I would like to express my appreciation to Dr. Gregory A. Benesh, Dr. Howard Lee, and Dr. Jonathan Hu for their assistance and service on the dissertation committee.

Then, I want to thank all the professors teaching me physics courses, Dr. Anzhong Wang, Dr. B.F.L. Ward, Dr. Gerald B. Cleaver, Dr. Kenneth T. Park, Dr. Yumei Wu and Dr. Zhenrong Zhang. Thank Dr. Walter Wilcox and Dr. Gerald B. Cleaver for their help and service as graduate program director. Also I would like to thank Dr. Linda Kinslow and Mr. Randy Hall for help with physics lab teaching. Thank Mrs. Baker Chava and Mrs. Marian Nunn-Graves for their help with great patience year after year.

More, I would like to thank all the colleagues with whom I have worked in our group during these years. I cherished the experience working with Razieh Yousefi, Bo

Zhang, Amir M. Ali, Stephen M. Pickett, Murray Patrick, Blake Birmingham and Ke Zhu.

Finally, special thanks are given to my parents for bringing me up and supporting me whenever and wherever. I owe thanks to my sister Huiqing Xia for helping me and taking care of our parents for me when I am thousands of miles away. More thanks goes to my wife Jia Guo for loving me and taking care of the family day and night. To my beloved boys and girls, Helen, Peter, Jude and Rachel, thank you for being my little angels and making my life full. At last, sincere thanks are given to the brothers and sisters all around and the lamb upon the throne.

In Memory of My Grandparents

CHAPTER ONE

Introduction

Over the past thirty years, the surface science of metal oxides has drawn rapidly increasing attention.[1] As a model system in the surface science of metal oxides, titanium dioxide (TiO_2) is one of the most investigated oxide surfaces, due to its wide range of industrial applications.[2,3] The main use of TiO_2 is as white pigment in paints, coatings, paper and cosmetic products, taking advantage of its brightness and high refractive index. TiO_2 nanoparticles and thin film have also been used as supports for metal nanoparticles in heterogeneous catalysis, as photo-catalysts, as gas sensors, as optical coatings, and as self-cleaning surfaces, etc.

Indoor air pollutants including oxygenated organic compounds such as ketones, aldehydes and alcohols present an increasing environmental concern.[4-9] Heterogeneous photocatalysis using TiO_2 is a promising strategy for remediating volatile organic compounds. Thus, the chemistry and photochemistry of organic compounds containing C=O groups has been widely studied on various forms of TiO_2.[7-10]

TiO_2 crystallizes in many different structures, mainly occurs in these three polymorphs, rutile, anatase and brookite.[2] Only rutile and anatase are found to be active in the applications of TiO_2 and therefore most studies are focused rutile and anatase surfaces.[2]

1.1 Rutile Titanium Dioxide (110) Surface

Rutile is the most common natural form of TiO_2, thermodynamically most stable. It has a tetragonal unit cell with unit cell parameters a=b=4.584 Å and c=2.953 Å.[11] The

basic building block consists a titanium atom at the center surrounded by six oxygen atoms at the apices in a slightly distorted octahedral configuration, as shown in Fig. 1.1(a). The length of the two bonds between the centered titanium and the oxygen atoms at the apices is 1.983 Å, slightly bigger than the length of the four bonds between the centered titanium and the co-planar oxygen atoms 1.946 Å. The octahedron shares one corner with its neighboring along [001] direction then they are stacked with their long axis alternating by 90°, in other words, by sharing the co-planar oxygen atom of one with the apical oxygen atom of the other one. The stacking of the octahedron leads to threefold coordinated oxygen atoms.

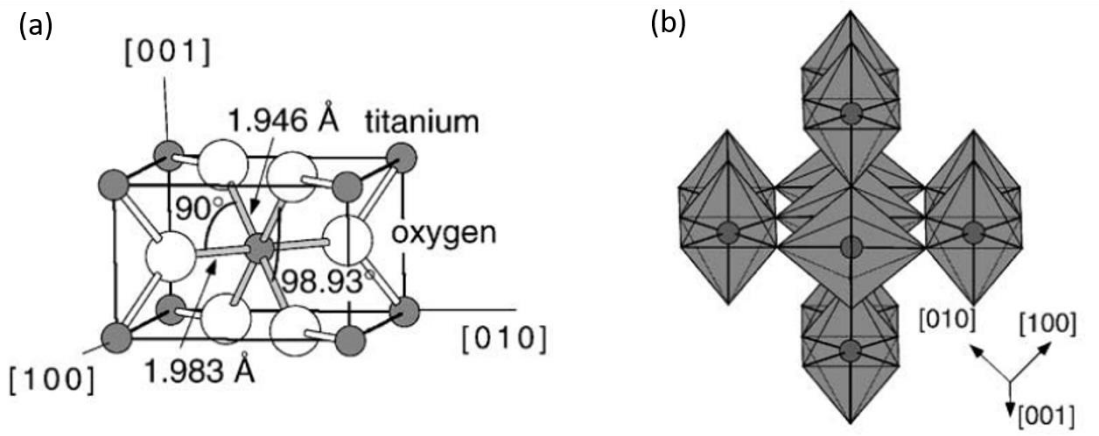

Figure 1.1 (a) The tetragonal bulk unit cell of rutile has the dimensions, a=b=4.584 Å, c=2.953 Å. (b) The stacking of the octahedron in rutile.[2]

From theoretic calculation, the (110) surface is the most stable one with the lowest surface energy compared to (001) and (100) surfaces.[12] On this basis, rutile TiO_2(110) has become the most studied low Miller index single crystal metal oxide surface.

Point defects are of fundamental importance for the chemistry and photochemistry of metal oxides. In heterogeneous catalysis, adsorption and dissociation of molecular

species are usually initiated at surface defect sites. It is well established that the most prevalent surface defect, the bridge-bonded oxygen (O_b) vacancy (V_O) site, as shown in Fig. 1.2, initiates the adsorption and dissociation of alcohols and water.[12-19] Recently, a subsurface defect, Ti interstitial, has been recognized to also influence the surface chemistry of TiO_2(110).[20-22]

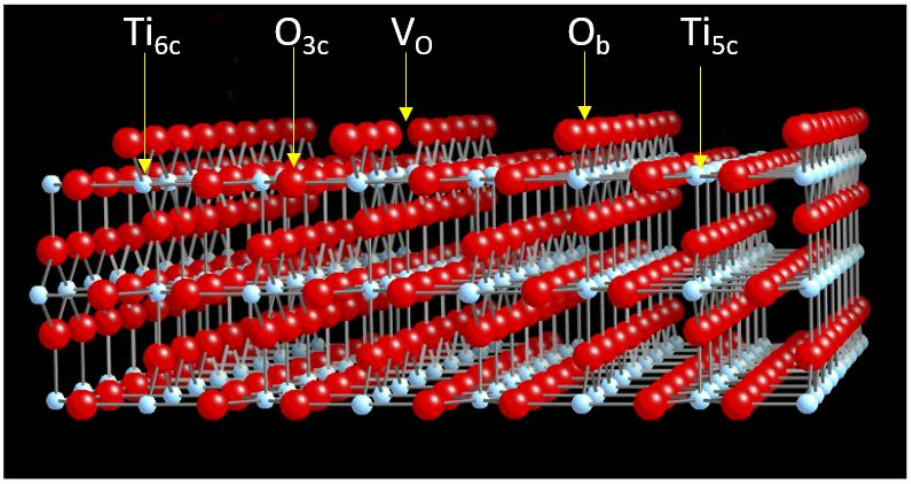

Figure 1.2 The structure of rutile TiO_2(110) 1 × 1 surface termination, bulk and point defect sites

The chemistry and photochemistry of organic compounds containing C=O groups has been widely studied on various forms of TiO_2 for remediating the volatile organic compounds found indoors and for probing photoreaction mechanisms.[23-27] The role of defects on the chemistry of ketones and aldehydes on TiO_2(110) is still not clear. In some experimental studies, no evidence is observed for preferential or dissociative adsorption of acetone,[28,29] acetaldehyde,[30] and formaldehyde[24] on V_O sites. While another study reported that formaldehyde preferentially binds to V_O sites.[31] Theoretically, acetone adsorption on V_O sites is reported to be slightly more stable (~ 0.16 eV) than the adsorption on the five

coordinated Ti^{4+} sites,[32] while formaldehyde and benzaldehyde are reported to be stabilized by Ti interstitial and show a lack of binding to V_O sites.[21,33]

The surface diffusion process is a vital step in most surface mediated reactions. Many catalytic reactions rely on the dynamic interplay between the addition and removal of oxygen atoms on the oxide surface, for example, in the photo-oxidation of cyclohexane via a Mars-van Krevelen mechanism over TiO_2[34-26] and the reductive coupling of aldehydes in the McMurry reaction on TiO_2.[21,30,31,37,38] Understanding the dynamic interactions between adsorbates and defects is critical in determining the catalytic reaction mechanism. However, less attention has been paid to the interplay of the diffusion dynamics between defects and adsordates.[39] Recently, the V_O site on TiO_2(110) has been shown to assist the diffusion of alkoxy species formed by the dissociation of alcohols on V_O sites.[40] Surface hydroxyls formed by H_2O dissociation on a V_O can enhance the diffusivity of adsorbed catecholates.[41]

It is clear that the presence of surface oxygen is crucial in controlling the reaction pathways in both thermal and photoinduced reactions taking place at the TiO_2–gas phase interface.[5,42-44] As a result, O_2 on the TiO_2(110) single crystal surface has been extensively studied to understand how molecular oxygen binds to titania surfaces and forms the various active species.[45-54] Recently, the interaction of O_2 with organics has been studied on TiO_2(110) surfaces to understand the role of oxygen species in the reactions.[55-58] Oxygen is often used as a scavenger of photo-excited electrons to prevent negative charge accumulation. Oxygen species can directly participate in the oxidation chemistry. For example oxygen adatoms thermally dissociate methanol to a photoactive methoxy species.[59,60] An extensive series of studies by Henderson has shown that through a thermal

process, adsorbed oxygen converts the photo-inactive form of carbonyl molecules (e.g. acetone, acetaldehyde, butanone, and acetophenone) into photoactive carbonyl molecule-oxygen complex species on TiO_2(110).[10,61-69] Vibrational spectroscopy, isotopic labeling studies and DFT calculations identified the configuration of these photoactive intermediates as η^2-diolate species. However, the atomic-level details of how the O_2 active species interact with organic species is far from fully understood. Scanning tunneling microscopy (STM) has been very helpful in unraveling the atomic-level details of the interaction between O_2 and defects on TiO_2.[55-58] STM studies of butyrophonone[70] and acetone[56] on oxidized TiO_2(110) show the formation of the ketone-O complex. However, the exact configuration of the complex is still not clear.

Here, we studied the dynamic interaction between ketone and surface defects on reduced TiO_2(110) using acetone, the smallest ketone, as a probe molecule. Further, the interaction of acetone with adsorbed oxygen on partially oxidized TiO_2(110) surfaces was investigated.

1.2 Anatase Titanium Dioxide (001) Surface

The anatase polymorph of TiO_2 appears to be an even more potent catalyst than rutile due to its higher photoactivity. Anatase nanoparticles most frequently expose (101) surfaces, together with small amount of (001) facets. Experimental results[71-75] and theoretical evidence[76] on anatase nanocrystals suggest that the minority (001) surface is photo-catalytically more reactive than the majority (101) surfaces and plays a key role in the reactivity of anatase nanoparticles. Some investigations recently reported contrary results.[77,78] Clearly, a molecular-level understanding of the reaction mechanism on different anatase surfaces is needed. However, experimental studies of surface reactions on

well-defined anatase surfaces are limited.[79-81] This is mainly due to the difficulty of synthesizing pure anatase single crystals with sufficient size. High-quality anatase epitaxial thin films have been synthesized by molecular beam epitaxy (MBE)[82-84] and chemical vapor deposition[85] on $SrTiO_3$(100) and $LaAlO_3$(100) substrates. Adopting these films offers an alternative approach to undertake molecular-level well-controlled surface reaction studies on anatase surfaces.[81,86-88]

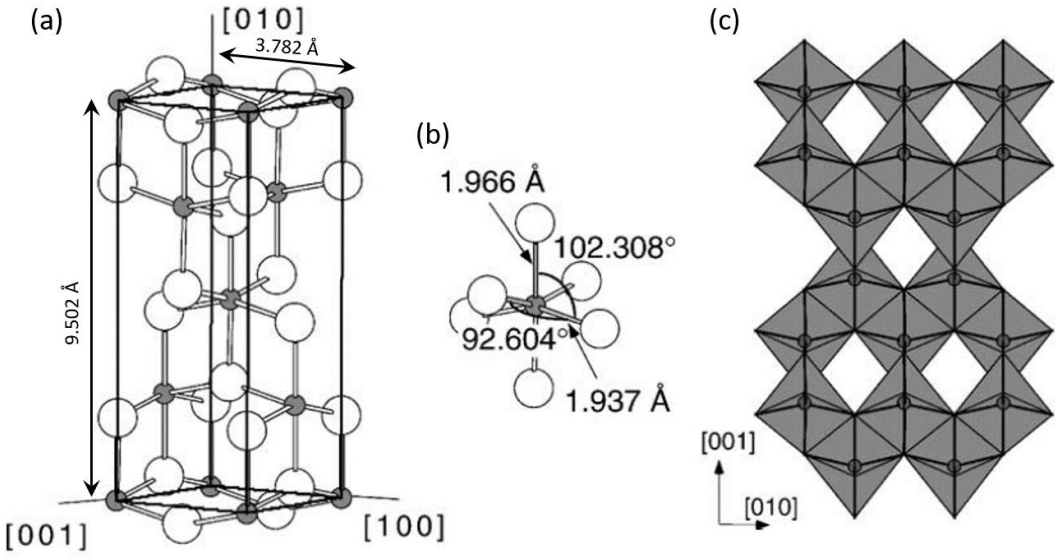

Figure 1.3 (a) The tetragonal bulk unit cell of anatase has the dimensions, a=b=3.782 Å, c=9.502 Å. (b) The unit of octahedron. (c) The stacking of the octahedron in anatase.[2]

Like rutile, anatase has a tetragonal unit cell as well with unit cell parameters, a=b=3.782 Å and c=9.502 Å.[89] The basic building block in anatase also consists of a titanium atom surrounded by six oxygen atoms in a slightly octahedral configuration, as shown in Fig. 1.3. The two bonds between the titanium and the apical oxygen atoms, 1.966 Å, are slightly longer than the four bonds between the titanium and the co-planar oxygen atoms, 1.937 Å. The neighboring octahedrons share the corner and form (001) planes, then

connected with their edges with the plane of octahedron below. The stacking of the octahedron results in threefold coordinated oxygen atoms.

Surface science is the study of physical and chemical properties of material surfaces. Since the early 1960s, the growth in the study of solid surfaces has been enormous, prompted by the commercial availability of ultra-high vacuum (UHV) and the development of various surface analytical techniques. UHV is extremely important for modern surface science mainly for two reasons: one is to reduce the number of molecules in the chamber to achieve low gas density which makes it possible for electrons and ions to be used as probe without significant interference from gas phase scattering, the other is to provide an environment in which the sample surface can be cleaned and maintained for durations of time needed for experiments. A number of modern techniques such as x-ray photoelectron spectroscopy (XPS), auger electron spectroscopy (AES), ion scattering spectroscopy (ISS), secondary ion mass spectrometry (SIMS), low-energy electron diffraction (LEED), reflection high-energy electron diffraction (RHEED), temperature programmed desorption (TPD), scanning electron microscopy (SEM), transmission electron microscopy (TEM), scanning tunneling microscopy (STM), atomic force microscopy (AFM), etc. have been developed and applied in investigations of the properties of surfaces. Especially, the STM technique makes it possible to obtain real space images of surfaces with atomic resolution which greatly changed the way how we study surface phenomena.

Here, we utilized the UHV STM to study the surface structure of epitaxial anatase TiO_2(110) thin film.

Chapter two explains the importance of ultra-high vacuum (UHV), how to obtain and maintain UHV with pumping system. The principle of scanning tunneling microscopy (STM) is discussed and two UHV VT-STM systems with STM images obtained from each STM are shown. The procedure of sample preparation is also explained.

Chapter three is published as: Yaobiao Xia, Bo Zhang, Jingyun Ye, Qingfeng Ge, Zhenrong Zhang Acetone-Assisted Oxygen Vacancy Diffusion on TiO_2(110). J. Phys. Chem. Lett.,2012, 3, 2970, DOI: 10.1021/jz301293y. Dr. Zhenrong Zhang supervised the project. I built the experimental setup, Bo Zhang and I performed all measurements with data processing. Bo Zhang and I analyzed the data and Dr. Zhang wrote the manuscript. Dr. Ye and Dr. Ge performed the DFT theoretical calculations.

Chapter four is published as: Yaobiao Xia, Jingyun Ye, Patrick Murray, Amir Ali, Qingfeng Ge, Zhenrong Zhang Imaging reactions of acetone with oxygen adatoms on partially oxidized TiO_2(110). Phys. Chem. Chem. Phys., 2013, 15, 13897, reproduced by permission of The Royal Society of Chemistry. Dr. Zhang supervised the project. I performed all the experimental measurements and data processing. Patrick Murray and Amir Ali, as undergraduate students, joined me in some experiments. Dr. Zhang and I analyzed the data and wrote the manuscript. Dr. Ye and Dr. Ge provided DFT theoretical calculations.

Chapter five is published as: Yaobiao Xia, Ke Zhu, Tiffany C. Kaspar, Yingge Du, Blake Birmingham, Kenneth T. Park, Zhenrong Zhang Atomic Structure of the Anatase TiO2(001) Surface. J. Phys. Chem. Lett, 2013, 4, 2958. Dr. Zhang and Dr. Park supervised the project. I performed all the measurements with STM and data processing. Ke Zhu and Blake Birmingham assisted me in some experiments. Dr. Kaspar and Dr. Du prepare the

anatase TiO_2 thin film samples and performed the measurements with RHEED and XPS. Dr. Zhang and I analyzed the data and wrote the manuscript.

Chapter six is published as: Ke Zhu, Yaobiao Xia, Zhenrong Zhang, Kenneth T. Park Probing Structure of Cross linked (1 × 2) Rutile TiO_2(110): Adsorption of Trimethyl Acetic Acid. J. Phys. Chem. C, 2016, 120, 15257. Dr. Park and Dr. Zhang supervised the project. Ke Zhu and I performed the measurements. I performed most of data processing and analysis. Dr. Park and Dr. Zhang wrote the manuscript.

Chapter seven summaries the results and presents some suggestions for future research based on this work.

CHAPTER TWO

Experiment

2.1 Ultra-high Vacuum (UHV)

To characterize surfaces of materials at an atomic level, the composition of the surface should remain essentially constant over the duration of an experiment. To achieve that, the experiments need to be conducted in vacuum. All the experiments involved in this thesis are carried out under UHV conditions. Conventionally, vacuum better than 10^{-9} Torr is defined as an ultra-high vacuum.

Normally, vacuum is described in terms of molecular density, mean free path and the time constant to form a monolayer. From the kinetic theory of gases,[90] the flux *I* of molecules and atoms colliding the surface is given by the expression

$$I = \frac{p}{\sqrt{2\pi m k_B T}}$$

Here p is the pressure, m is the mass of the molecule, k_B is the Boltzmann's constant and T is the temperature. The vacuum can be described in terms of the molecular density n, mean free path λ and time constant to form a monolayer τ. They can be obtained as

$$\mathrm{n} = \frac{p}{k_B T}$$

$$\lambda = \frac{1}{\pi d^2 n}$$

$$\tau = \frac{n_0}{I} = \frac{n_0 \sqrt{2\pi m k_B T}}{p}$$

where d is the diameter of the molecules and n_0 is the number of atoms in a monolayer.[91] Assuming the sticking coefficient to be 1, the density of one monatomic layer is defined to be $n_0 = 10^{15}\ cm^{-2}$, for nitrogen molecules at room temperature 293 K.

At pressure 10^{-6} Torr (1 Torr = 1.33x10^{-2} Ncm^{-2}),

$$\tau = \frac{10^{15}\sqrt{2\pi \times (\frac{28}{1000 \times 6.02 \times 10^{23}}) \times (1.38 \times 10^{-23}) \times 293}}{1.33 \times 10^{-2} \times 10^{-6}} \text{s} = 2.6 \text{ s}$$

It takes only 2.6 s to form a monolayer of gas molecules on the surface. Similarly, at pressure 10^{-9} Torr, τ = 0.7 hour while at pressure 10^{-10} Torr τ = 7.2 hours. It shows that a vacuum of the order of 10^{-10} Torr or better is necessary in order to prevent surface contamination during the experiments lasting several hours. Besides that, a longer mean free path of gas molecules under UHV conditions means less scattering from gas molecules to the electrons or ions before received by the analyzer, which reduces the influence on experimental measurements.

To achieve these stringent conditions, a UHV system is required. A typical UHV system consists of one chamber made of stainless steel, flanges and glass viewports, a pumping system including several different types of pumps, gauges and valves, process equipment including load lock, manipulator, heater, ion gun and evaporator, and surface analysis equipment.

The pumping system is used to obtain and maintain vacuum in the chamber. A rotary vane vacuum pump, also called a mechanic pump or roughing pump, is used to take the system from atmospheric pressure down to about 10^{-3} Torr, normally connected to the fore line to back the turbo pump. The turbo-molecular pump, also called a turbo pump for short, sweeps the gas molecules to the exhaust connected to the fore line by high speed

rotating blades. It further evacuates the system to 10^{-8} or 10^{-9} Torr. The ion pump, as the most popular UHV main pump, can lower the vacuum to 10^{-11} Torr level by chemically ionizing the gas molecules, accelerating the ionized molecules by the electric field and embedding them into the cathode. A titanium sublimation pump is used intermittently in addition to the ion pump. By sublimating titanium from the heated Ti-covered filament, it coats the tubes, the cathode, and the walls with a fresh thin Ti film, which react with the gas molecules to form stable compounds.

In order to measure the pressure, different gauges are used. Thermocouple and Pirani gauges measure a vacuum in the range of 10-10^{-3} Torr while ionization gauges cover the range of 10^{-4}-10^{-11} Torr. The thermocouple gauge contains a heated filament, when molecules hit the filament and remove heat energy, the thermocouple measures filament temperature as a function of gas pressure. The Pirani gauge reads the pressure from the change in the resistance of the heated filament, and have about the same pressure measurement range. They are used in fore line monitoring. The ionization gauge uses thermionic emission of electrons from a heated filament which ionize atoms and gas molecules. The ions are then attracted towards the fine-wire grounded collector and produce current which is converted to a pressure reading.

Conventionally, it takes a very long time (~one month) to pump the system from atmospheric pressure to UHV, because the vapor pressure from residual gas (mainly water) which is absorbed to the chamber walls is very high. Chamber bakeout is necessary to accelerate this process. Heating the apparatus up to 100-200°C with silicone rubber heaters, heating tapes, or a heating tent, helps to desorb the water and other gases from the walls and pumped out of chamber in a relatively short period of time (several days). The system

is usually covered with aluminum foil and/or a heating tent to assure uniform heating monitored with thermocouple wires at several different spots. The viewports and electrical feedthroughs also need to be covered with aluminum foil to avoid thermal stress. Usually the bakeout takes 2 to 3 days. After the bakeout is finished, all filaments need to be degassed a few times while the apparatus cools down but is still warm. This process removes the impurities absorbed on the filaments.

2.2 Scanning Tunneling Microscopy (STM)

The first scanning tunneling microscope was developed by Binnig and Rohrer et al. in 1981[92], which earned Binnig and Rohrer the Nobel Prize in Physics in 1986. Since then, it has revolutionized surface science and became the most widely used surface science technique. Compared with other surface analytical techniques, STM has many advantages such as, STM can achieve atomic-level resolution and be performed in different environments; STM provides a direct probe of truly local interaction on the atomic scale and three-dimensional images of the surface; STM can be employed to modify the surface and manipulate atoms and molecules through tip-sample interactions,[93] etc.

STM is based on the concept of quantum tunneling. In quantum mechanics, the wavefunction $\psi(z)$ of the electron in a potential $V(z)$ satisfies the Schrodinger equation,[94]

$$-\frac{\hbar^2}{2m}\frac{d^2}{dz^2}\psi(z) + V(z)\psi(z) = E\psi(z). \quad (1.1)$$

where *m* is the electron mass and E is the energy.

The solution for Eq. 1.1 in the classically forbidden region, $V > E$

$$\psi(z) = \psi(0)e^{-kz} \quad (1.2)$$

where $k = \frac{\sqrt{2m(V-E)}}{\hbar}$ is the decay constant. In this model, where $V(z)$ is a simple rectangular potential barrier V_0 with thickness *d* as shown in Fig. 2.1.

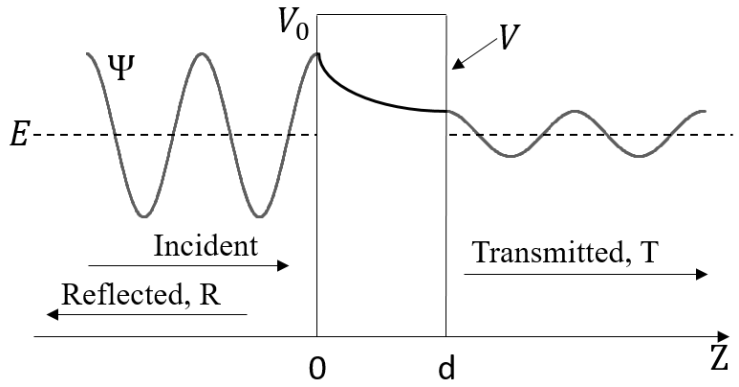

Figure 2.1 Rectangular barrier of potential V_0 and electron wave function ψ

The transmission coefficient is given by:

$$T = (1 + \frac{{V_0}^2 sinh^2(kd)}{4E(V-E)})^{-1} \tag{1.3}$$

In the $kd \gg 1$ limit, we assuming the potential is much smaller than the value of the work function,

$$T \propto e^{-2kd} \tag{1.4}$$

When the tip and the sample are brought sufficiently close together (within nanometer range), a tunneling current *I* is generated by applying a small bias voltage between the tip and the sample.

$$I \propto e^{-2kd} \tag{1.5}$$

For a work function of a few eV and $k \approx 1$ Å^{-1}, the tunneling current decreases by almost an order of magnitude when the separation of the tip and sample is increased by 1 Å. Based

on the effect that the current is exponentially sensitive to the separation, STM can obtain atomic resolution images showing surface corrugations of almost 1 Å with an atomically sharp conducting tip.

There are two basic modes for the STM scanning process: constant current mode and constant height mode. In the basic constant current mode, the tip is scanned across the surface at constant tunneling current I_t by continuously adjusting the height of the tip with the feedback voltage V_z, as shown in Fig. 2.2. The topographic height of the sample surface can be measured as the tip height derived from V_z. Alternatively, in the constant height mode, the tip is rapidly scanned across the surface at nominally constant height and constant voltage V_z. By monitoring the rapid variations in the tunneling current, the signal can be read and processed, displayed as an image on screen.

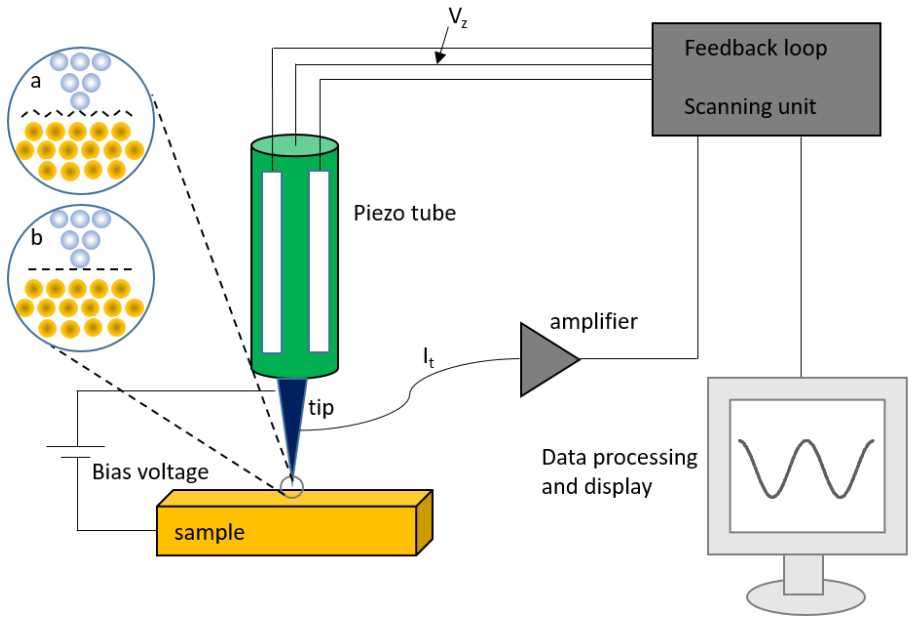

Figure 2.2 The schematic view of STM. Two basic modes for STM scanning: (a) Constant current mode, (b) Constant height mode

Since the tunneling current depends exponentially on the separation between tip and sample, any type of vibration can affect the operation of STM. The vibration isolation system is, therefore, very important for STM to observe the atomic corrugations. There are two types of vibration isolation systems, inertial suspension-spring system in which the stage is suspended from springs with viton spacers and eddy-current damper used for damping components, and external air-support system in which a bulky stage is supported by inflated supports such as vibration isolators.

Two UHV STM systems were used for the work involved in the thesis. The SPECS UHV VT-STM system, located in the Baylor Science Building, consists of a custom designed STM chamber, equipped with manipulator, filament heater, sputter ion gun, molecular dozer, light source, mass spec, SPECS STM, etc.

A picture of the SPECS VT-STM system is shown in Figure 2.3.

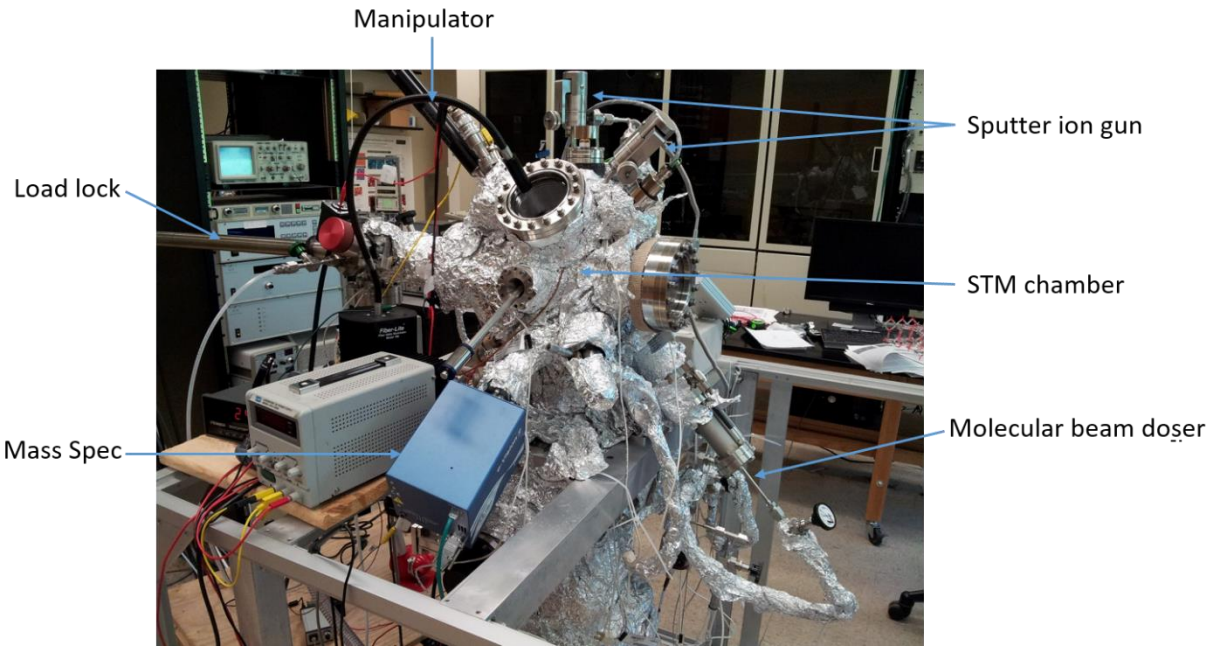

Figure 2.3 The SPECS VT-STM system

As shown in Figure 2.4, the STM stage sits on a heavy metal block, called a cradle, and is suspended by three springs. Viton bands can be inserted between the cradle and the STM support frame for damping. Before scanning, the STM is unlocked by retracting the cooling piston to make the cradle hanging free in its spring mount. During sample transfer and tip exchange, the cradle must be locked. The chamber is pumped down by a full pumping system including one rotatory pump, two turbomolecular pumps, one ion pump and one titanium sublimation pump, with the base pressure at 10^{-11} Torr level. To work at reduced temperatures, the sample is cooled by pumping liquid nitrogen through the tubes of the cooling piston while the cradle is locked. To work at elevated temperature, the sample is heated by a filament located right above the sample, which can be then moved away during sample transfer.

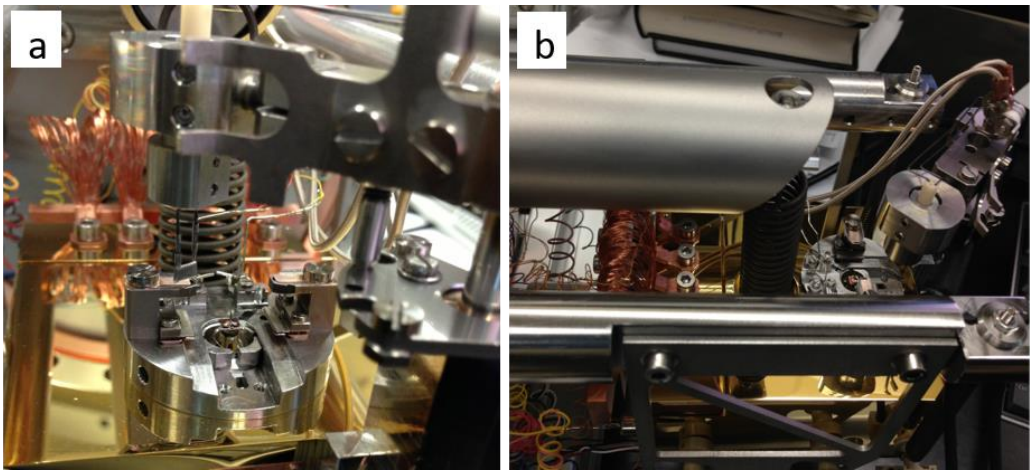

Figure 2.4 The Specs VT-STM stage on the cradle (a) Front view. (b) Side view

STM tips are of key importance in order to obtain high resolution STM images. Scanning with a double-tip or even multiple-tip would make it difficult to obtain stable STM images with high resolution. Homemade tungsten tips are electrochemically etched

and spot-welded onto tip holders. After tip exchange, the tip can be treated in-situ with Ar-ion sputtering for about 15 min, with typical accelerating voltage of 3 kV, and an ion current 5 μA. To avoid sputtering ions hitting and harming the piezoelectric scanner or the approach motor, the tip must be approached through a tiny bore hole without touching the sputter shield while the cradle is locked.

Highly Ordered Pyrolytic Graphite (HOPG) was used to test STM scanning. High resolution STM images of HOPG are shown in Fig. 2.5, clearly reveal the hexagonal atomic lattice.

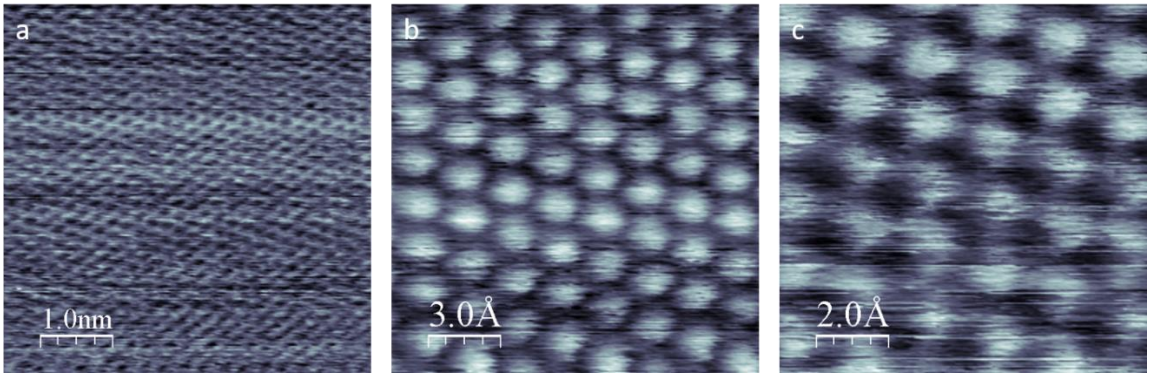

Figure 2.5 High resolution STM images of HOPG on different area sizes, (a) 5 nm x 5 nm, (b) 15 Å x 15 Å, (c) 10 x 10 Å

The RHK UHV VT-STM system, located in the Baylor Research and Innovation Collaborative (BRIC), consists of a preparation chamber and an STM chamber. The preparation chamber is equipped with a manipulator, a filament heater, a sputter ion gun, and a LEED/AES. The STM chamber houses an RHK VT-STM and a sample storage. The system sits on a bulky table which lands on four air leg dampers to provide vibration isolation.

Using the same electrochemically etched W tip, the tip inserted into the tip holder can be annealed in-situ on a tip-annealing stage. It is convenient to transfer the tip from the STM scan head to the sample storage or to the tip annealing stage with a wobble stick.

A picture of the RHK VT-STM system is shown in Figure 2.6.

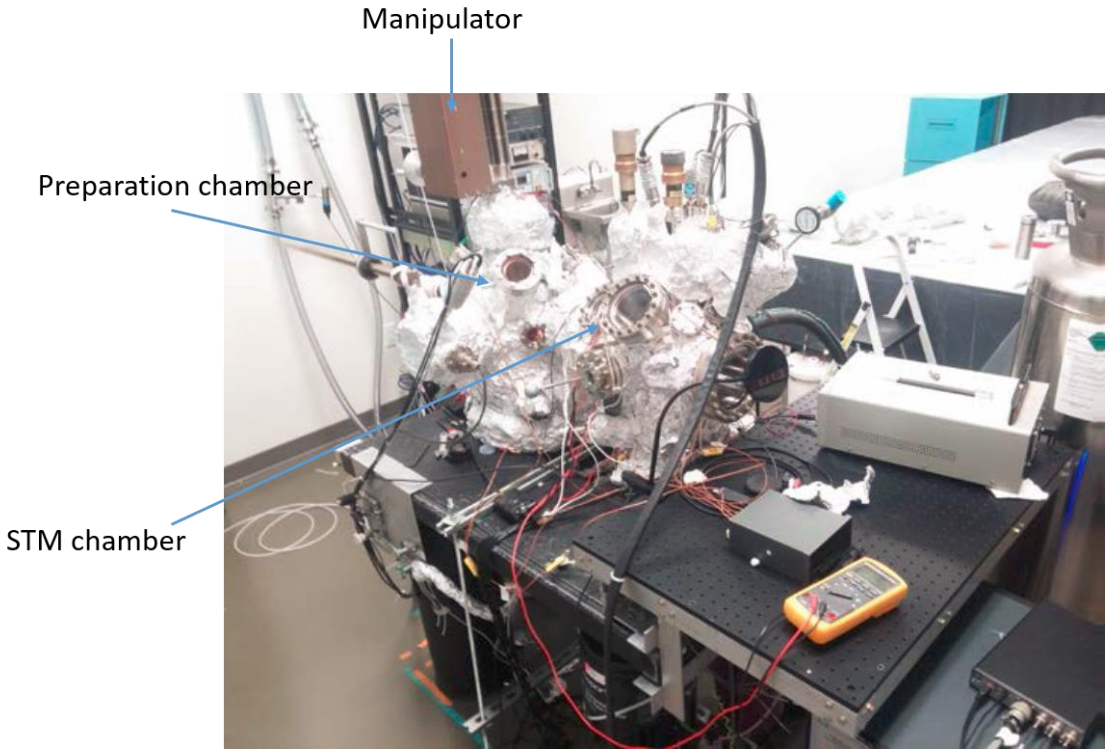

Figure 2.6 The RHK VT-STM system

The Ag(111) sample was scanned before and after copper (II) phthalocyanine (CuPc) deposition, as shown in Fig. 2.7. The lattice spacing of the hexagonal lattice is about 2.89 Å. A CuPc multilayer film was obtained by thermal evaporating CuPc onto the Ag(111) surface and then it was annealed to form a uniform CuPc monolayer film.

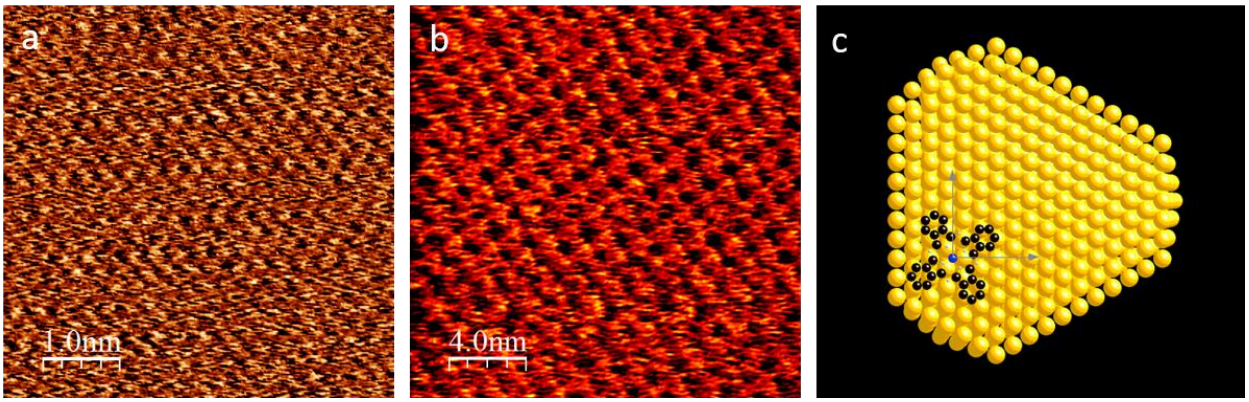

Figure 2.7 (a) Atomic resolution image of Ag(111), (b) Molecular resolution of CuPc monolayer on Ag(111), (c) Ball model for CuPc molecule adsorbed on Ag(111) surface

2.3 Sample Preparation

The rutile TiO_2(110) single crystal is cleaned by repeated cycles of Ar-ion sputtering and annealing. A typical Ar-ion sputtering lasted for 15 minutes with Ar partial pressure of 3×10^{-6} Torr. The ion beam current is about 2 μA using the accelerating voltage 1 KV. After Ar sputtering, the sample is annealed by electron beam heating for 5 minutes. To form (1×1) surface, the sample need to be annealed up to 900 K while it need be higher to 1050 K to form (1×2) surface.

The anatase TiO_2(001) epitaxial thin films were grown on atomically smooth Nb-doped $SrTiO_3$(001) single crystal substrates by oxygen plasma assisted molecular beam epitaxy at Pacific Northwest National Laboratory. The thickness of the thin films is 50 nm. The samples were then cleaned at Baylor by cycles of Ar-ion sputtering and electron-beam annealing. Sputtering lasted for 1 minute with the beam current of 2 μA at 1 KV while annealing was up to 900 K for 5 minutes.

Acetone and TMAA were cleaned by several freeze-pump-thaw cycles using liquid nitrogen before dosing to the surface via a retractable tube doser containing a pinhole. The

gas-line system and doser assembly were purged with fresh chemical vapor each day before preparing the sample.

The partially oxidized TiO_2(110) was prepared using a reduced TiO_2(110) surface with O_2 exposure. Oxygen was dosed by backfilling the chamber.

CHAPTER THREE

Acetone-Assisted Oxygen Vacancy Diffusion on TiO_2(110)[1]

This chapter published as: Y. Xia, B. Zhang, J. Ye, Q. Ge, Z. Zhang Acetone-Assisted Oxygen Vacancy Diffusion on TiO_2(110). J. Phys. Chem. Lett.,2012, 3, 2970

Abstract

We have studied the dynamic relationship between acetone and bridge-bonded oxygen (O_b) vacancy (V_O) defect sites on the TiO_2(110)-1 x 1 surface using scanning tunneling microscopy (STM) and density function theory (DFT) calculations. We report an adsorbate-assisted V_O diffusion mechanism. The STM images taken at 300 K show that acetone preferably adsorbs on the V_O site and is mobile. The sequential isothermal STM images directly show that the mobile acetone effectively migrates the position of Vo by a combination of two acetone diffusion channels: one is the diffusion along the O_b row and moving as an alkyl group, which heals the initial V_O; another is the diffusion from O_b row to five coordinated Ti^{4+} row and then moving along the Ti^{4+} row as an acetone, which leaves a V_O behind. The calculated acetone diffusion barriers for the two channels are comparable and agree with experimental results.

3.1 Introduction

Point defects are of fundamental importance for the chemistry and photochemistry of metal oxides. In heterogeneous catalysis, adsorption and dissociation of molecular species are usually initiated at surface defect sites. The surface chemistry of rutile TiO_2(110) has been extensively studied due to the wide application of titania.[1-3] It is well

[1] http://pubs.acs.org/doi/abs/10.1021/jz301293y

established that the most prevalent surface defect, the bridge-bonded oxygen (O_b) vacancy (V_O) site, initiates the adsorption and dissociation of alcohols and water.[4-11] Recently, a subsurface defect, Ti interstitial, has been recognized to also influence the surface chemistry of TiO_2(110).[12-14]

The chemistry and photochemistry of organic compounds containing C=O groups has been widely studied on various forms of TiO_2 for remediating the volatile organic compounds found indoors and for probing photoreaction mechanisms.[15-19] The role of defects on the chemistry of ketones and aldehydes on TiO_2(110) is still not clear. In some experimental studies, no evidence is observed for preferential or dissociative adsorption of acetone,[20, 21] acetaldehyde,[22] and formaldehyde[16] on V_O sites. While other study reported formaldehyde preferentially binds to V_O sites.[23] Theoretically, acetone adsorption on V_O sites is reported to be slightly more stable (~ 0.16 eV) than the adsorption on the five coordinated Ti^{4+} sites,[24] while formaldehyde and benzaldehyde are reported to be stabilized by Ti interstitial and show a lack of binding to V_O sites.[13, 25]

The surface diffusion process is a vital step in most surface mediated reactions. Many catalytic reactions rely on the dynamic interplay between the addition and removal of oxygen atoms on the oxide surface, for example, in the photo-oxidation of cyclohexane via a Mars-van Krevelen mechanism over TiO_2[26-28] and the reductive coupling of aldehydes in the McMurry reaction on TiO_2.[13, 22, 23, 29, 30] Understanding the dynamic interactions between adsorbates and defects is critical in determining the catalytic reaction mechanism. However, less attention has been paid to the interplay of the diffusion dynamics between defects and adsordates.[31] Recently, the V_O site on TiO_2(110) has been shown to assist the diffusion of alkoxy species formed by the dissociation of alcohols on V_O sites.[32] Surface

hydroxyls formed by H_2O dissociation on a V_O can enhance the diffusivity of adsorbed catecholates.[33]

In this study, we choose acetone, the smallest ketone, as a probe molecule to study the dynamic interaction between ketone and surface defects on reduced TiO_2(110). We report that acetone preferentially adsorbs on the V_O site of the TiO_2(110) surface. More importantly, we present an acetone-assisted V_O diffusion which is mediated by two acetone diffusion channels, namely, the diffusion along the O_b row as alkyl and the diffusion along the Ti^{4+} row as acetone. The adsorbate-assisted point defects diffusion has not been directly observed in any previous experimental studies on oxide surfaces.

3.2 Experimental and Computational Methods

Experiments were performed in an ultrahigh vacuum chamber (base pressure < 3×10^{-11} Torr) equipped with variable temperature STM (SPECS), quadrupole mass spectrometry (SRS) and ion gun (SPECS). The single crystal TiO_2(110) surface (Princeton Scientific) was prepared by multiple cycles of sputtering (1~ 3 keV) and e-beam heating annealing (~ 900 K).

Acetone (EMD, 99.5+ %), was cleaned by several freeze-pump-thaw cycles using liquid nitrogen prior to use and was introduced onto the TiO_2(110) surface at the STM stage via a retractable tube doser containing a pinhole. All STM images (empty states) were collected at 300 K in a constant-current (<0.1 nA) mode at positive sample bias voltages of 0.8 – 1.3 V. Images were processed using WSxM software (Nanotech, freeware).[35] The vacancy concentration and species coverage were obtained by a direct counting from STM images and expressed in monolayer (ML) units (1 ML corresponds to 5.2×10^{14} cm^{-2} Ti atoms).

Periodic DFT calculations reported herein were performed using the VASP code.[36, 37] We use projector augmented wave potentials[38] with the 3d and 4s valence states of Ti being expanded in a plane-wave basis set with a cutoff energy of 400 eV and PW91 form[39] of exchange-correlation functional. Theoretical derived lattice constants of rutile TiO_2 were used in the construction of slabs to model the surface oxygen vacancies. The (110) surface was modeled by a supercell with a dimension of 6.58 Å × 11.87 Å ×20.16 Å. A 4 × 2 × 1 k-point grid generated by the Monkhorst-Pack method was found to give converged results for the surface calculations. Spin polarization was necessary as the defective surface unit cell with one oxygen vacancy is in a triplet state. Two top trilayers were relaxed while the bottom trilayer was fixed. Diffusional transition states of adsorbed acetone were determined by a combined nudged elastic band method[40] and quasi-Newton optimization. Normal mode harmonic vibrational analysis was performed for the transition states.[41] Similar setup and parameters were used in previous calculations.[42]

3.3 Results and Discussions

Figure 3.1 shows two consecutive STM images taken on a TiO_2(110) surface at 300 K after exposed to 0.03 ML of acetone (1 ML = 5.2×10^{14} cm^{-2}). In the empty state STM images of TiO_2(110), the low lying five coordinated Ti^{4+} ions are imaged as protrusions while the rows of O_b ions are imaged as depressions due to the inverse electronic contrast of these two ions. The V_O site appears as the bridging spot (blue dot) on the dark row. Upon acetone adsorption, acetone is observed as a bright protrusion centered on O_b row (red dot). We assign the bright features as the acetone molecules adsorbed on V_O sites. This assignment is supported by DFT calculations and confirmed by the diffusion of acetone observed experimentally as shown below. The results indicate acetone preferably adsorbs

on V_O sites. We did not observe Ti^{4+}-bounded acetone at 300 K as reported by Yasuo and co-workers.[21]

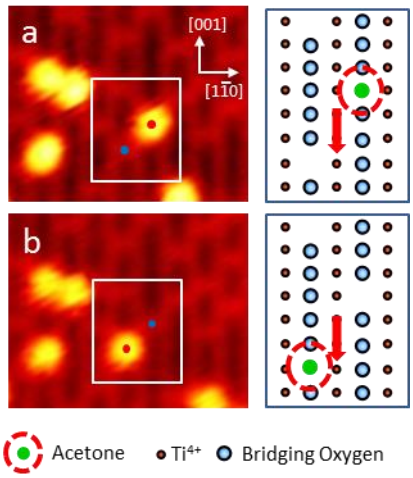

Figure 3.1. Two consecutive STM images, taken 66 s apart, represent the across-row diffusion of acetone from one V_O to an unoccupied V_O. Red dot marks acetone species and blue dot marks unoccupied V_O.

Interestingly, we observe that the bright acetone species are mobile at 300 K. Both across- and along-row motions are observed by imaging the same area of a TiO_2(110) surface for extended periods of time ranging from 30 minutes to 3 hours at 300 K. Two consecutive STM images in Figure 3.1 represent the typical across-row diffusion. The comparison of the marked regions shows that a bright acetone species on Figure 3.1a (red dot) has hopped to the unoccupied V_O (Figure 3.1a, blue dot) located on the adjacent O_b row. This confirms that acetone preferably adsorbs on V_O sites and agrees with previous DFT calculations.[24] After acetone hopped away, a V_O (Figure 3.1b, blue dot) appears on the exact position where the acetone was located before hopping. This suggests that during the cross-row diffusion, acetone takes oxygen with it and moves as a whole molecule. Statistically, evaluation of over 200 events shows that all the apparent cross-row motion

events reveal V_O sites. At 300 K, we did not observe the decrease in acetone coverage over a period of up to 3 hours. This indicates almost no acetone molecule desorbs from surface at the coverage below the V_O concentration (0.13 ML).

The across-row motion can be explained by the proposed diffusion mechanism shown in Figure 1 using the ball model. The acetone molecules preferentially adsorb on V_O sites. The V_O-bounded acetone can move out of V_O to Ti^{4+} row at 300 K. Then instead of desorbing, acetone diffuses along the Ti^{4+} row and adsorbs on the next available unoccupied V_O site, which may locate on the adjacent/same O_b row, as we observed experimentally (S1). We emphasize that in this diffusion channel (along the Ti^{4+} row), the original V_O positions do not change because acetone takes its oxygen and moves as a whole molecule. Since no Ti^{4+}- bounded acetone is observed at 300 K, the diffusion rate of Ti^{4+}-bounded acetone at 300 K should be much faster than the scan speed of STM ranging from 55 nm/s to 85 nm/s.

As for the along-row diffusion, detailed analysis reveals that there is a second diffusion channel (Channel 2) coexisting with the diffusion channel (Channel 1) presented above. As illustrated in Figure 3.2, the combination of the two channels results in the shifting of V_O positions. The images are the snap shots of STM movie recorded on same area of a TiO_2(110) surface at 300 K after exposed to 0.01 ML of acetone. From Figure 3.2a to Figure 3.2b (taken 12 minutes after Figure 3.2a), a V_O-bounded acetone (Figure 3.2a, red dot) hops to the unoccupied V_O (Figure 3.2a, blue dot) located on the same O_b row and appears as bright V_O-bounded acetone species (Figure 3.2b, red dot). As with the cross-row diffusion, after acetone hopped away, a new V_O (Figure 3.2b, blue dot) appears on the exact position where the acetone was located before the motion. The emergence of

the V_O indicates the along-row diffusion from 2a to 2b is via diffusion on the Ti^{4+} row as a whole molecule (Channel 1).

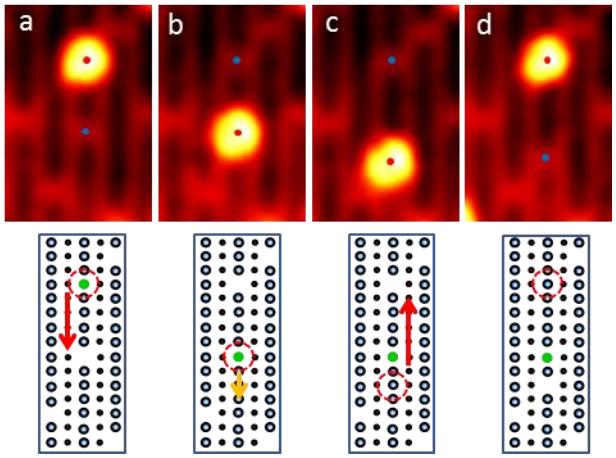

Figure 3.2. STM images recorded as a function of time (t = 0, 12, 18, 21 min) on the same area of acetone pre-adsorbed TiO_2(110). The corresponding ball models illustrate the diffusion of V_O mediated by acetone diffusion at 300 K. Red arrows represent the direction of acetone diffusion on the Ti row and yellow arrow represents the direction of alkyl group diffusion on the O_b row. Green balls represent the oxygen atom from the acetone.

After another 6 minutes, this bright V_O-bounded acetone (Figure 3.2b, red dot) moves two lattice spaces downward (Figure 3.2c, red dot). In contrast to Channel 1, this acetone did not hop to an unoccupied V_O. In addition, no V_O is observed after its motion (Figure 3.2c). This means that acetone heals the V_O by losing its oxygen and diffuses as an alkyl group on O_b row (ball model). Apparently the diffusion process from Figure 3.2b to Figure 3.2c is different from Channel 1.

Finally, the bright acetone species (Figure 3.2c, red dot) diffuses back to the upper unoccupied V_O site (Figure 3.2d, red dot). A V_O (Figure 3.2d, blue dot) appears after the motion. This indicates that alkyl group picks an O_b atom and diffuses to the next unoccupied V_O (Figure 3.2d) via Channel 1. Comparison between Figure 3.2a and 3.2d

clearly shows that the V_O (Figure 3.2a, blue dot) shifted two lattice spaces downward (Figure 3.2d, blue dot).

The overall change in V_O pattern upon adsorption of acetone is further examined by the comparison of images that were taken a certain period of time apart on the same area of the TiO_2(110) surface. The V_O pattern changed dramatically at 300 K due to diffusion of acetone on the surface. For example, 26% of V_O sites changed their positions in 34 minutes on the TiO_2(110) surface with 0.05 ML of acetone (S2).

We can exclude that the change of the V_O positions is related to the intrinsic V_O diffusion. A previous study on clean TiO_2(110) surfaces shows that V_O can diffuse intrinsically along the O_b row at temperatures above 350 K.[32] However, V_O is stationary at 300 K on clean TiO_2(110). It is known that the onset of the Ti interstitial diffusion is at about 400 K.[34] The observed diffusion processes presented here are at 300 K. This excludes that they are related to the diffusion of Ti interstitials. Both the acetone diffusion channels can be accessed through thermal activation. As the first acetone diffusion mechanism (Channel 1) will not result in the diffusion of V_O sites, our results show that both diffusion channels are necessary for the shift in V_O positions.

To obtain a detailed understanding of the acetone-assisted V_O diffusion on reduced TiO_2(110), we simulated the two diffusion channels by performing DFT calculations (Figure 3.3). The adsorption geometries and the energetics of acetone are examined on both Ti^{4+} and V_O sites. In accord with the previous reported results,[24] the most stable adsorption configuration is on V_O site with the acetone symmetry plane parallel to the O_b row (V_O ,II Figure 3.3a) and with the adsorption energy (E_{abs}) of -1.24 eV. Compared with the perpendicular configuration (V_O⊥, Figure 3.3b) which is 0.26 eV less stable, the V_O II

configuration would allow the maximization of the attractive van-der-Waals (vdW) force between methyl group and neighboring O_b atom, although we have not quantified the contribution of vdW interaction using DFT. On Ti^{4+} sites, the acetone favors the top site with perpendicular configuration (Ti⊥, Figure 3.3k). The E_{abs} (-0.87 eV) is slightly higher than the parallel configuration (Ti||, Figure 3.3j) with the E_{abs} of -0.80 eV. Similarly, the Ti⊥ configuration allows the maximization of the attractive vdW force between methyl group and neighboring O_b atom. The E_{abs} (-0.87 eV) of acetone on Ti^{4+} sites is 0.37 eV higher than V_O enoteca taht noitavresbo latnemirepxe eht htiw seerga sihT .noitarugifnoc || adsorption takes place preferentially on V_O sites.

The elementary steps calculated for the acetone diffusion along the O_b row (Channel 2) are shown in Figure 3.3 (a to f). The initial step is the rotation of the acetone from the V_OV ot noitarugifnoc ||$_O$⊥ configuration (a-b). Since the energy difference (0.26 eV) between these two configurations is mainly due to the weak attractive vdW force, the calculated rotational barrier is small (0.34 eV) as expected. This indicates the acetone is free to rotate about the C=O bond on V_O at 300 K. The next step is the breaking of the C=O bond and the formation of the diolate intermediate (c-d) with a barrier of 0.56 eV. The adsorption energy of the diolate (0.91 eV) is comparable with the V_O⊥ configuration (0.98 eV). Assuming that the diffusion process is Arrhenius-like, the hopping rate r is given as

$$r = \nu_0 \exp(-\Delta E_B / k_B T) \quad (3.1)$$

where ν_0 is the attempt frequency, ΔE_B the activation energy barrier, k_B the Boltzmann constant, and T the temperature. The rotational barrier from V_OV ot ||$_O$⊥ (a-b) is much higher (0.34 eV) than the barrier (0.08 eV) of the reverse process (b-a). It is reasonable to assume that the frequency factors are the same. Thus, the coverage of acetone in V_O 4 si ||

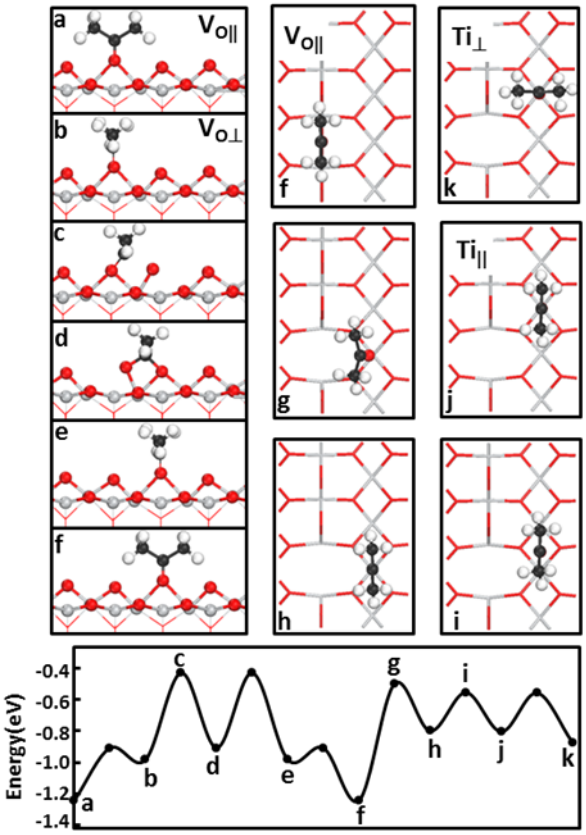

Figure 3.3. Calculated configurations in ball-stick model and their corresponding locations on the calculated potential energy diagram (bottom panel) along two acetone diffusion channels. (a)-(f) Side view of alkyl diffusion along an O_b row (Channel 2). (f)-(k) Top view of acetone diffusion from V_O to Ti^{4+} row and along the Ti^{4+} row (Channel 1).

orders of magnitude higher than that in $V_{O\perp}$ at 300 K. Therefore, although the acetone diffusion along the O_b row is a two-step process, it can be treated as an effective one-step process with an apparent diffusion barrier of 0.82 eV (a-f). A similar diffusion mechanism was proposed for formaldehyde on TiO_2(110).[23]

The elementary steps calculated for the diffusion of V_O- bounded acetone to and along Ti row (Channel 1) are shown in Figure 3(f to k). The calculated barrier for V_O-

bounded acetone moving to Ti^{4+} is 0.74 eV (f-h) with the small barrier (0.25 eV) for acetone diffusion along Ti^{4+} row (h-j).

This indicates that the rate limiting step for this diffusion channel is moving out of V_O. The results agree with experimental observation that only acetone moving out of V_O is observed at 300 K and the diffusion of acetone on Ti row is not observed due to the fast motion on Ti row. The overall diffusion barriers for Channel 1 (0.74 eV) and Channel 2 (0.82 eV) are comparable. This also agrees with experimental observation that both diffusion channels are observed at 300 K. Experimentally, the residence time of the acetone/alkyl can be determined from the STM movies by the decaying of the number of stationary acetone molecules with time. The determined residence time is 90 s which corresponds to the estimated energy barrier of 0.95 eV using the Arrhenius equation. We used a typical attempt frequency of $\sim 10^{13}$ s^{-1} for the estimation which did not include the coexistence of both channels and that Channel 1 is a two-step process. Nevertheless, the estimated value agrees well with the calculated barriers.

In summary, we present the diffusion of V_O on reduced TiO_2 (110)-1 x 1 surface mediated by the combination of two acetone diffusion channels. The STM images show that at 300 K acetone prefers to adsorb on V_O sites. The sequential isothermal STM images directly show V_O-bounded acetone can diffuse both along the Ti row and along the O_b row. On O_b row, acetone heals the oxygen vacancy by losing its oxygen and diffuses as an alkyl group. Subsequently, the alkyl group can combine with an O_b atom and diffuse to and then along Ti^{4+} row as an acetone which creates a new oxygen vacancy. The acetone diffusion barriers calculated using DFT agree with experimental results.

References

(1) Diebold, U. The Surface Science of Titanium Dioxide. *Surf. Sci. Rep.* 2003, *48*, 53-229.

(2) Henderson, A. M. A Surface Science Perspective on Photocatalysis. *Surf. Sci. Rep.* 2011, *66*, 185-297.

(3) Dohnalek, Z.; Lyubinetsky, I.; Rousseau, R. Thermally-Driven Processes on Rutile TiO_2(110)-(1x1):A Direct View at the Atomic Scale. *Prog. Surf. Sci.* 2010, *85*, 161-205.

(4) Brinkley, D.; Engel, T. Evidence for Structure Sensitivity in the Thermally Activated and Photocatalytic Dehydrogenation of 2-Propanol on TiO_2. *J. Phys. Chem. B* 2000, *104*, 9836-9841.

(5) Farfan-Arribas, E.; Madix, R. Different Binding Sites for Methanol Dehydrogenation and Deoxygenation on Stoichiometric and Defective TiO_2(110)Surfaces. *Surf. Sci.* 2003, *544*, 241-260.

(6) Zhang, Z.; Bondarchuk, O.; White, J. M.; Kay, B. D.; Dohnalek, Z. Imaging Adsorbate O-H Bond Cleavage: Methanol on TiO_2(110). *J. Am. Chem. Soc.* 2006, *128*, 4198-4199.

(7) Gamble, L.; Jung, L.; Campbell, C. Decomposition and Protonation of Surface Ethoxys on TiO_2(110). *Surf. Sci.* 1996, *348*, 1-16.

(8) Wendt, S.; Schaub, R.; Matthiesen, J.; Vestergaard, E. K.; Wahlstrom, E.; Rasmussen, M. D.; Thostrup, P.; Molina, L. M.; Laegsgaard, E.; Stensgaard, I. et al. Oxygen Vacancies on TiO_2(1 1 0) and their Interaction with H_2O and O_2: A Combined High-Resolution STM and DFT Study. *Surf. Sci.* 2005, *598*, 226-245.

(9) Hugenschmidt, M. B.; Gamble, L.; Campbell, C. T. The Interaction of H_2O with a TiO_2(110) Surface. *Surf. Sci.* 1994, *302*, 329-340.

(10) Henderson, M. A. Structural Sensitivity in the Dissociation of Water on TiO_2 Single-Crystal Surfaces. *Langmuir* 1996, *12*, 5093-5098.

(11) Bikondoa, O.; Pang, C. L.; Ithnin, R.; Muryn, C. A.; Onishi, H.; Thornton, G. Direct Visualization of Defect-Mediated Dissociation of Water on TiO_2(110). *Nat. Mater.* 2006, *5*, 189-192.

(12) Wendt, S.; Sprunger, P. T.; Lira, E.; Madsen, G. K. H.; Li, Z.; Hansen, J. O.; Matthiesen, J.; Blekinge-Rasmussen, A.; Laegsgaard, E.; Hammer, B. et al. The Role of Interstitial Sites in the Ti3d Defect State in the Band Gap of Titania. *Science* 2008, *320*, 1755-1759.

(13) Haubrich, J.; Kaxiras, E.; Friend, C. M. The Role of Surface and Subsurface Point Defects for Chemical Model Studies on TiO_2: A First-Principles Theoretical Study of Formaldehyde Bonding on Rutile TiO_2(110). *Chem. Eur. J.* 2011, *17*, 4496-4506.

(14) Bowker, M.; Bennett, R. A. The Role of Ti_{3+} Interstitials in TiO_2(110) Reduction and Oxidation. *J. Phys. Condens. Matter.* 2009, *21*, 474224.

(15) Mattsson, A.; Osterlund, L. Adsorption and Photoinduced Decomposition of Acetone and Acetic Acid on Anatase, Brookite, and Rutile TiO_2 Nanoparticles. *J. Phys. Chem. C* 2010, *114*, 14121-14132.

(16) Kim, J.; Kay, B. D.; Dohnalek, Z. Formaldehyde Polymerization on $(WO_3)_3/TiO_2$(110) Model Catalyst. *J. Phys. Chem. C* 2010, *114*, 17017-17022.

(17) Henderson, M. A. Photooxidation of Acetone on TiO_2(110): Conversion to Acetate Via Methyl Radical Ejection. *J. Phys. Chem. B* 2005, *109*, 12062-12070.

(18) El-Maazawi, M.; Finken, A.; Nair, A.; Grassian, V. Adsorption and Photocatalytic Oxidation of Acetone on TiO_2: An in Situ Transmission FT-IR Study. *J. Cata.* 2000, *191*, 138-146.

(19) Hernandez-Alonso, M. D.; Tejedor-Tejedor, I.; Coronado, J. M.; Anderson, M. A.; Soria, J. Operando FTIR Study of the Photocatalytic Oxidation of Acetone in Air Over TiO_2-ZrO_2 Thin Films. *Catal. Today* 2009, *143*, 364-373.

(20) Henderson, M. A. Acetone Chemistry on Oxidized and Reduced TiO_2(110). *J. Phys. Chem. B* 2004, *108*, 18932-18941.

(21) Yasuo, M.; Sasahara, A.; Onishi, H. Acetone Adsorption on Oxidized and Reduced TiO_2(110): A Scanning Tunneling Microscope Study. *J. Phys. Chem. C* 2010, *114*, 14579-14582.

(22) Henderson, M. A. Effect of Coadsorbed Water on the Photodecomposition of Acetone on TiO_2(110). *J. Cata.* 2008, *256*, 287-292.

(23) Qiu, H.; Idriss, H.; Wang, Y.; Woell, C. Carbon-Carbon Bond Formation on Model Titanium Oxide Surfaces: Identification of Surface Reaction Intermediates by High-Resolution Electron Energy Loss Spectroscopy. *J. Phys. Chem. C* 2008, *112*, 9828-9834.

(24) Marquez, A. M.; Plata, J. J.; Fdez Sanz, J. Role of Coverage and Surface Oxidation Degree in the Adsorption of Acetone on TiO_2(110). A Density Functional Study. *J. Phys. Chem. C* 2009, *113*, 19973-19980.

(25) Benz, L.; Haubrich, J.; Jensen, S. C.; Friend, C. M. Molecular Imaging of Reductive Coupling Reactions: Interstitial-Mediated Coupling of Benzaldehyde on Reduced TiO_2(110). *ACS Nano* 2011, *5*, 834-843.

(26) Almeida, A. R.; Moulijn, J. A.; Mul, G. Photocatalytic Oxidation of Cyclohexane Over TiO_2: Evidence for a Mars-Van Krevelen Mechanism. *J. Phys. Chem. C* 2011, *115*, 1330-1338.

(27) Trovarelli, A. In *Catalysis by Ceria and Related Materials;* Catalytic science series; Imperial College Press: London, 2002; Vol. 2, pp 508.

(28) Masel, R. I. In *Chemical Kinetics and Catalysis;* Wiley-Interscience: New York, 2001; pp 952.

(29) Zehr, R. T.; Henderson, M. A. Acetaldehyde Photochemistry on TiO_2(110). *Surf. Sci.* 2008, *602*, 2238-2249.

(30) Pierce, K. G.; Barteau, M. A. Ketone Coupling on Reduced TiO_2 (001) Surfaces: Evidence of Pinacol Formation. *J. Org. Chem.* 1995, *60*, 2405-2410.

(31) Cheng, H.; Selloni, A. Energetics and Diffusion of Intrinsic Surface and Subsurface Defects on Anatase TiO_2(101). *J. Chem. Phys.* 2009, *131*, 054703.

(32) Zhang, Z.; Rousseau, R.; Gong, J.; Li, S. C.; Kay, B. D.; Ge, Q.; Dohnalek, Z. Vacancy-Assisted Diffusion of Alkoxy Species on Rutile TiO_2(110). *Phys. Rev. Lett.* 2008, *101*, 156103.

(33) Li, S. C.; Chu, L. N.; Gong, X. Q.; Diebold, U. Hydrogen Bonding Controls the Dynamics of Catechol Adsorbed on a TiO_2(110) Surface. *Science* 2010, *328*, 882-884.

(34) Henderson, M. A. A Surface Perspective on Self-Diffusion in Rutile TiO_2. *Surf. Sci.* 1999, *419*, 174-187.

(35) Horcas, I.; Fernandez, R.; Gomez-Rodriguez, J. M.; Colchero, J.; Gomez-Herrero, J.; Baro, A. M. WSXM: A Software for Scanning Probe Microscopy and a Tool for Nanotechnology. *Rev. Sci. Instrum.* 2007, *78*, 013705.

(36) Kresse, G.; Hafner, J. *Ab Initio* Molecular Dynamics for Open-Shell Transition Metals. *Phys. Rev. B* 1993, *48*, 13115-13118.

(37) Kresse, G.; Furthmuller, J. Efficient Iterative Schemes for Ab Initio Total-Energy Calculations using a Plane-Wave Basis Set. *Phys. Rev. B* 1996, *54*, 11169-11186.

(38) Kresse, G.; Joubert, D. From Ultrasoft Pseudopotentials to the Projector Augmented-Wave Method. *Phys. Rev. B* 1999, *59*, 1758-1775.

(39) Perdew, J.; Chevary, J.; Vosko, S.; Jackson, K.; Pederson, M.; Singh, D.; Flolahais, C. Atoms, Molecules, Solids, and Surfaces: Applications of the Generalized Gradient Approximation for Exchange and Correlation. *Phys. Rev. B* 1992, *46*, 6671-6687.

(40) Mills, G.; Jonsson, H.; Schenter, G. Reversible Work Transiton State Theory: Application to Dissociative Adsorption of Hydrogen. *Surf. Sci.* 1995, *324*, 305-337.

(41) Jonsson, H. Theoretical Studies of Atomic-Scale Processes Relevant to Crystal Growth. *Annu. Rev. Phys. Chem.* 2000, *51*, 623-653.

(42) Zhang, Z.; Ge, Q.; Li, S. C.; Kay, B. D.; White, J. M.; Dohnalek, Z. Imaging Intrinsic Diffusion of Bridge-Bonded Oxygen Vacancies on TiO_2(110). *Phys. Rev. Lett.* 2007, *99*, 126105.

CHAPTER FOUR

Imaging Reactions of Acetone with Oxygen Adatoms on Partially Oxidized $TiO_2(110)$[1]

This chapter published as: Y. Xia, J. Ye, P. Murray, A. Ali, Q. Ge, Z. Zhang Imaging reactions of acetone with oxygen adatoms on partially oxidized $TiO_2(110)$.Phys. Chem. Chem. Phys., 2013, 15, 13897

Abstract

Understanding the interaction of O_2 with ketones on metal oxide surfaces is important for the photo-oxidation of toxic organic molecules. The consecutive reaction steps of acetone molecules with oxygen adatoms (O_a's) on partially oxidized $TiO_2(110)$ surfaces have been studied using high-resolution scanning tunneling microscopy (STM) at 300 K. The sequential isothermal STM images reveal two types of acetone-O_a species as a result of reactions of acetone with an oxygen adatom and a bridging bound oxygen vacancy (V_O). One species is the Ti_{5c}-bound acetone-O_a diolate formed from Ti_{5c}-bound acetone reacting with O_a. The diolate is mobile at 300 K and can assist the diffusion of surface O_a by exchanging the acetone oxygen with the O_a. The second acetone-O_a species is V_O-bound acetone-O_a complex formed from a V_O-bound acetone reacting with an O_a located on the neighboring Ti row. The V_O-bound complex is stationary at 300 K. This species has not been reported previously.

4.1 Introduction

Indoor air pollutants including oxygenated organic compounds such as ketones, aldehydes and alcohols present an increasing environmental concern.[1-6] Heterogeneous

[1] http://pubs.rsc.org/en/Content/ArticleLanding/2013/CP/c3cp51695d#!divAbstract.

photocatalysis using TiO_2 is a promising strategy for remediating volatile organic compounds. Thus, the chemistry and photochemistry of organic compounds containing C=O groups has been widely studied on various forms of TiO_2.[4-7]

It is clear that the presence of surface oxygen is crucial in controlling the reaction pathways in both thermal and photoinduced reactions taking place at the TiO_2–gas phase interface.[2, 8-10] As a result, O_2 on the TiO_2(110) single crystal surface has been extensively studied to understand how molecular oxygen binds to titania surfaces and forms the various active species.[11-20] Recently, the interaction of O_2 with organics has been studied on TiO_2(110) surfaces to understand the role of oxygen species in the reactions.[21-24] Oxygen is often used as a scavenger of photo-excited electrons to prevent negative charge accumulation. Oxygen species can directly participate in the oxidation chemistry. For example oxygen adatoms thermally dissociate methanol to a photoactive methoxy species.[25, 26] An extensive series of studies by Henderson has shown that though a thermal process, adsorbed oxygen converts the photo-inactive form of carbonyl molecules (e.g. acetone, acetaldehyde, butanone, and acetophenone) into photoactive carbonyl molecule-oxygen complex species on TiO_2(110).[7, 27-35] Vibrational spectroscopy, isotopic labeling studies and DFT calculations identified the configuration of these photoactive intermediates as η^2-diolate species. However, the atomic-level details of how the O_2 active species interact with organic species is far from fully understood. Scanning tunneling microscopy (STM) has been very helpful in unraveling the atomic-level details of the interaction between O_2 and defects on TiO_2.[21-24] STM studies of butyrophonone[36] and acetone[22] on oxidized TiO_2(110) show the formation of the ketone-O complex. However, the exact configuration of the complex is still not clear.

In our previous study, we reported the dynamic relationship between acetone and surface bridging bonded oxygen vacancy (V_O) defect sites on reduced TiO_2(110) surface.[37] In this study, we focus on the interaction of acetone with adsorbed oxygen on partially oxidized TiO_2(110) surfaces. High-resolution STM followed the consecutive reaction steps of acetone with oxygen adatoms (O_a) and V_O's. We report here the direct imaging of two key acetone-oxygen species. One species is the Ti_{5c}-bound acetone-O_a diolate which is reported to be critical in photoreaction and the other is the V_O-bound acetone-O_a complex which has not been reported in the literature. By tracking species resulted from a sequence of reactions, we show molecular-level details of the underlying reaction mechanism.

4.2 Experimental Section

Experiments were performed in an ultrahigh vacuum chamber (base pressure < 3×10^{-11} Torr) equipped with variable temperature STM (SPECS), quadrupole mass spectrometry (SRS) and ion gun (SPECS). The single crystal TiO_2(110) surface (Princeton Scientific) was prepared by multiple cycles of sputtering (1~ 3 keV) and e-beam heating annealing (~ 900 K). The cleanness of the reduced surface is checked by STM before the surface is exposed to oxygen. Oxygen was dosed by backfilling the chamber. The STM tip was withdrawn about 1 μm from the surface during O_2 exposure. The vacancy concentration and species coverage were obtained by a direct counting from STM images and expressed in monolayer (ML) units (1 ML corresponds to 5.2×10^{14} cm^{-2} Ti atoms). On prepared partially oxidized TiO_2(110) surfaces, less than 0.005 ML of hydroxyl (OH_b) is observed indicating that the background H_2O adsorption is negligible. Acetone (EMD, 99.5+ %), was cleaned by several freeze-pump-thaw cycles using liquid nitrogen prior to use and was introduced onto the partially oxidized TiO_2(110) surfaces at the STM stage

via a retractable tube doser containing a pinhole. All STM images (empty states) were collected at 300 K in a constant-current (<0.1 nA) mode at positive sample bias voltages of 0.8 – 1.3 V. Images were processed using WSxM software (Nanotech, freeware).[38]

4.3 Results

To probe the reaction of acetone with an oxygen adatom, we prepared the partially oxidized TiO_2(110) surface where only a fraction of the V_O's is converted to O_a. Figure 1 shows snap shots from a representative STM movie taken after acetone adsorbs on the partially oxidized TiO_2(110) surface with 0.07 ML of O_a and 0.06 ML of V_O at 300 K. In the empty state STM images of TiO_2(110), the low lying five coordinated Ti_{5c} ions are imaged as protrusions while the rows of bridging bonded oxygen (O_b) ions are imaged as depressions. The V_O site appears as the bridging spot (highlighted by small white arrows in Figure 4.1a) on the dark O_b row. When O_2 adsorbs on reduced TiO_2(110) at 300 K, oxygen dissociates on the surface via two dissociation channels forming either oxygen adatom (O_a) pairs or single O_a's.[12, 39, 40] The O_a's show up as bright dots (blue arrows) on the Ti_{5c} rows which are surrounded by slightly darker regions. The distance between the two O_a's of the O_a pair is two lattice constants at 300 K.[12, 18, 19]

After acetone adsorption at 300 K (Figure 4.1a), two types of bright acetone features are observed on O_b rows. One type (small circles) is V_O-bound acetone which is symmetric with respect to the row. The assignment of the V_O-bound acetone is based on the adsorption sites and their mobility on clean TiO_2(110).[37] The V_O-bound acetone readily diffuses on the surface at 300 K via two diffusion channels: one is diffusion along the O_b row and moving as an alkyl group, which heals the initial V_O; another is diffusion from O_b row to the five coordinated Ti_{5c} row and then moving along the Ti_{5c} row as an acetone,

which leaves a V_O behind. The combination of the two acetone diffusion channels mediates the diffusion of V_O.[37] Due to the small diffusion barrier (~ 0.25 eV) along the Ti row, the Ti_{5c}-bound acetone molecules (η^1-acetone) diffuse faster than the STM scan speed (~ 80 nm/ s) and show up as occasional streaks on the STM images.

The other type (small square) is not symmetric and has a faint lobe protruding to the Ti row. In figure 4.1a, the faint lobe protrudes from upper–left side of the feature (small square) to the Ti row. This type of bright feature is assigned as V_O-bound acetone-O_a complex. We call it the V_O-bound complex from here on. To explore the formation of the V_O-bound complex, we acquired time lapsed images over extended periods of time (53 min) on the same area after acetone exposure. Figure 4.1 shows the formation of two V_O-bound complexes. From Figure 4.1a to Figure 4.1b, the upper V_O-bound acetone (upper small circle) diffuses to an unoccupied V_O site (white arrow on the right, Figure 1a) which has a faint single O_a (upper blue arrow) located one lattice spacing downward on the neighboring Ti row. A V_O appears at where the acetone was originally located indicating that the whole acetone molecule diffuses via Ti row to the unoccupied V_O as shown in the ball model.[37] The V_O-bound acetone combined with nearby O_a appears as bright V_O-bound complex (Figure 1b, upper square). In the meantime, the bottom V_O-bound acetone molecule (black circle) diffused back and forth several times through both the two diffusion channels and ended one lattice constant downward from figure 4.1a to 4.1b. Compared to the V_O-bound acetone, the V_O-bound complex is also located on V_O, but it has a small faint protrusion extended into the Ti row onto the neighboring O_a. Figure 1c shows another example of a V_O-bound complex appearing at the Vo marked by the left white arrow on

Figure 4.1a. This V_O has an O_a pair sitting on the neighboring Ti row with one of the O_a's located one lattice spacing upward to the left of the V_O.

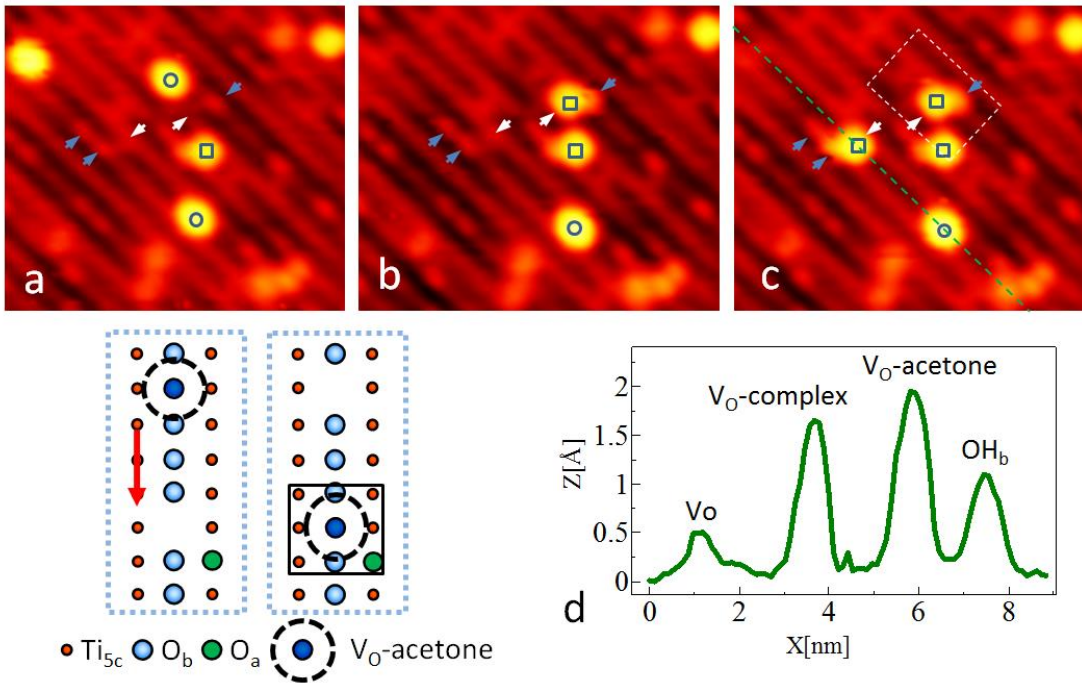

Figure 4.1. Snap shots (a-c) from an STM movie taken on the partially oxidized surface after acetone exposure at 300 K. The ball model illustrates the conversion of the V_O-bound acetone to the V_O–bound acetone–O_a complex. d) The line scan of the green line on image c). Symbols on the STM images indicate O_a (blue arrow), V_O (white arrow), V_O-bound acetone (small circle), and V_O–bound acetone–O_a complex (small square) respectively.

To further illustrate the different appearances of the V_O-bound acetone and the V_O-bound complex, we have also included the line scan (dotted line on Figure 4.1c) along the O_b row of such isolated features at a typical bias of 1.3 V. The apparent height of the V_O-bound acetone (~ 0.18 nm) measured relative to the O_b row is slightly larger than that of V_O-bound complex (~0.15 nm). For comparison, the heights of V_O and OH_b are also examined and included on the line scan. The OH_b feature is higher than V_O as expected at a typical bias voltage (1.0-1.5 V).[39, 41, 42]

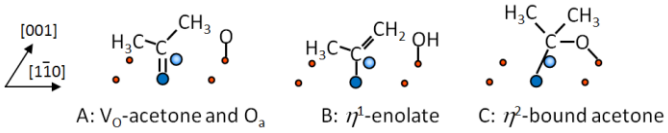

Figure 4.2. The possible configurations of the Vo-bound acetone O_a complex.

The major difference between the V_O-bound acetone and the V_O-bound complex is their mobility. The V_O-bound acetone readily diffuses at 300 K with an average lifetime of 90 s.[37] However, once formed, the V_O-bound complex becomes stationary. No diffusion is observed from three separate isothermal experiments with the total imaging time of ~150 min. Interestingly, if the O_a is located two lattice spacings away from the V_O-bound acetone as shown below, the formation of the V_O-bound complex is not observed.

Figure 4.2 shows several possible configurations for the observed V_O-bound complex. One is that the V_O-bound acetone rotates 45° to maximize the attractive van-der-Waals (vdW) force between methyl group and O_a (configuration A). This attractive force may increase the diffusion barrier for V_O-bound acetone to move from a V_O site to the Ti row. On the reduced surface, this is the rate limiting step (–0.74 eV) for the diffusion of acetone via the Ti row since the diffusion barrier for acetone motion along the Ti row is only 0.25 eV.[37] Another possibility is the formation of η^1-enolate (configuration B). In this case, the V_O-bound acetone rotates 45° and transfers a hydrogen atom from the methyl group to O_a and forms the η^1-enolate which becomes a stable species. This is feasible as O_a has shown higher reactivity than O_b due to an excess amount of charge associated with the O_a.[19] On CeO_2, stable η^1-enolate has been observed on reduced surfaces which involves the reaction of acetone with V_O and lattice oxygen.[3] Many groups have observed H/D

exchange between acetone and OH groups on other oxide-based materials.[5, 43-47] The consensus mechanism involves formation of an acetone enolate species in which a hydrogen atom from one of the acetone's methyl groups is transferred to the surface resulting in rehybridization of acetone to the enolate. We excluded the possibility of η^2-bound acetone where carbonyl carbon atom coordinates with O_a (configuration C), because the distance between the V_O site and the O_a located one lattice spacing away on the neighboring Ti row is ~ 4.2 Å. This distance is too far for the O-C-O η^2-configuration. In addition, Henderson et. al reported the adsorption energy (E_{ads}) of a similar configuration, η^2-bound acetone, where carbonyl carbon atom coordinates to O_a located directly across the V_O. The calculated E_{ads} (–45 kJ/mol) is much higher than that (–72 kJ/mol) of the Ti_{5c}-bound acetone.[35]

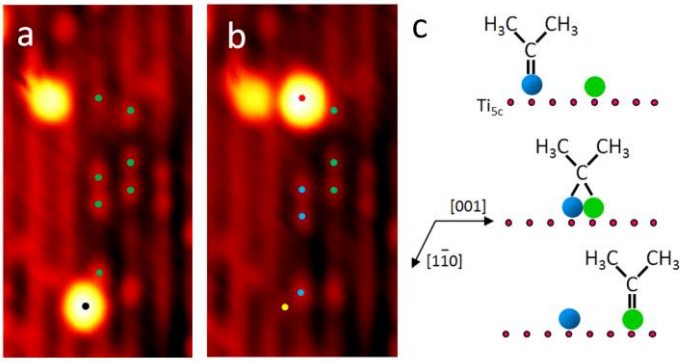

Figure 4.3. Two subsequent STM images (a, b) showing the diffusion of the O_a and c) the ball model of acetone assisted O_a diffusion via the formation the Ti_{5c}-bound acetone-O_a diolate. Symbols on the STM images indicate O_a (green dot), shifted O_a (blue dot), V_O-bound acetone (black dot), and Ti_{5c}-bound acetone-O_a diolate (red dot) respectively.

Figure 4.3 presents two subsequent images illustrating the formation of the second type of acetone-O_a complex — the Ti_{5c}-bound acetone-O_a diolate. When an acetone molecule diffuses along a Ti row and passes an O_a, the O_a is observed to shift by one lattice

constant via a diolate intermediate. For example, from figure 4.3a to 4.3b, the V_O-bound acetone (black dot, Figure 4.3a) moves to the Ti row leaving a vacancy (yellow dot, Figure 4.3b) behind suggesting that the acetone moves along the Ti row upward as an acetone molecule.[37] The acetone passes a single O_a and an O_a pair (blue dots, Figure 4.3b) and stops on a single O_a appearing as a bright feature (red dot, Figure 4.3b) which is centered on the Ti row. Compared to Figure 4.3a, the positions of the three O_a's (blue dots, Figure 4.3b) on the path of the acetone diffusion are shifted by one lattice constant downward which is opposite to the diffusion direction (upward) of the acetone molecule. The bright feature located on O_a (red dot, Figure 4.3b) is assigned as a Ti_{5c}-bound diolate as proposed before.[27] A large set of O_a diffusion events (144) were evaluated from three separate experiments. For every observed O_a diffusion event, either the formation of diolate or the diffusion of a V_O-acetone to a new V_O was observed. It is worth noting that on Figure 4.3a, the lower O_a (green dot, Figure 4.3a) is located two lattice distances away from the V_O-bound acetone (black dot), thus the formation of the V_O-bound complex is not observed due to the large distance (~ 6 Å) from the O_a to V_O-bound acetone.

Figure 4.3c illustrates our interpretation for the O_a diffusion process via the diolate intermediate. The V_O-bound acetone moves to the Ti_{5c} row and binds on Ti_{5c} sites via the lone-pair electrons on the carbonyl oxygen atom becoming a η^1-acetone species.[27] The η^1-acetone species diffuses along the Ti_{5c} row rapidly at 300 K.[37] When η^1-acetone reaches an O_a, the O_a coordinates to electron-deficient acetone carbon forming Ti_{5c}-bound diolate species (η^2-diolate). The diolate can dissociate back to an O_a and an acetone. The acetone molecule continues to diffuse along Ti row, either forward as a new acetone with the oxygen that used to be the O_a, leaving behind its oxygen atom as a new O_a, or backward in

the form of original acetone. The former case results in the apparent motion of the O_a and the oxygen scrambling while the latter case leaves the O_a in its original position. Over 20 isolated diolates were evaluated by overlaying the lattice grid on the images to determine the position of diolate relative to O_a. Instead of centered on top of O_a, the diolate is centered between the two O_a's as expected. This O_a diffusion mechanism and the formation of the diolate are consistent with the mechanism proposed by Henderson and coworkers on the basis of isotope labeling studies.[27] A similar O_a diffusion mechanism has been observed when H_2O interacts with O_a.[48]

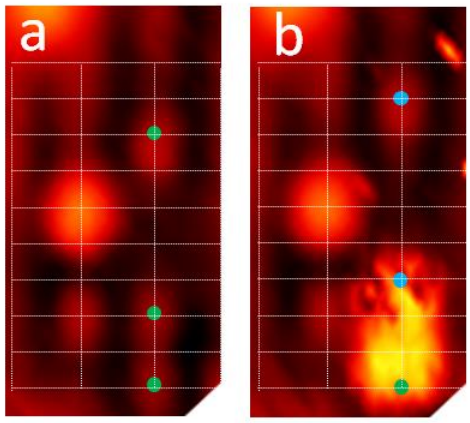

Figure 4.4. Two subsequent STM images overlaid with the lattice grid present the formation of a Ti_{5c}-bound acetone-O_a diolate (the fuzzy bright feature) on an O_a pair. Symbols on the STM images indicate O_a (green dot) and shifted O_a (blue dot) respectively.

A diolate can be observed on a single O_a as shown in Figure 4.3 and on an O_a pair as shown in Figure 4.4. Unlike the diolate on a single O_a, a majority (70%) of diolates formed on O_a pairs appear fuzzy (Figure 4.4b). Here, an acetone moves downward passing an O_a (upper green dot, Figure 4.4a). The O_a is shifted up by one lattice distance and stops on an O_a pair (lower pair of blue dots, Figure 4.4a). The distance of two O_a's in the pair is generally two lattice spacings apart.[12, 18, 19] The images overlaid by lattice grid (Figure 4.4)

shows that the fuzzy bright feature extends over four lattice positions. This indicates that the upper O_a of the O_a pair is shifted up one lattice spacing by exchanging oxygen with acetone when acetone moves downward and forms diolate with the lower O_a of the O_a pair. The acetone molecule can diffuse back and forth between the two O_a's and forms diolates with either of the O_a's which are now three lattice spacings apart. Therefore the fuzzy feature in our experiments represents the time average of acetone moving between the two O_a's. Later, like the diolate on a single O_a, the diolate on an O_a pair dissociates back to an O_a pair and an acetone. The acetone from the fuzzy diolate is observed to move on and adsorb on a nearby V_O (not shown). This indicates that the fuzzy diolate is not due to two acetone molecules adsorbing simultaneously on an O_a pair. From two sets of experiments with comparable concentrations of O_a pair and single O_a, the total number of diolate species observed on O_a pairs is about 4.5 (168/36) times of that of the diolate on the single O_a's. This value is higher than the expected value of 2.0 from the simple statistical probability of acetone encountering twice as many O_a's from pairs as isolated O_a's. This indicates that with another O_a nearby, the lifetime of the diolate slightly increases. This might relate to the different charge distributions near the single O_a and the O_a pair since they are formed from two different dissociation channels.

It should be noted that although the involvement of the acetone is observed, the diolate intermediates including both on single O_a's and O_a pairs are only directly observed in ~ 40% (59/144) of the total number of O_a diffusion events. This suggests that the average lifetime of diolate is slightly shorter than the data acquisition time (66 s/frame). Assuming that the diffusion process is Arrhenius-like, the hopping rate ν is given as $\nu = \nu_0 \exp(-\Delta E_B / k_B T)$ where ν_0 is the attempt frequency, ΔE_B the activation energy barrier,

k_B the Boltzmann constant, and T the temperature. The estimated lifetime (~ 1 min) corresponds to an energy barrier of 0.85 ~ 0.90 eV for the diolate to dissociate back to O_a and Ti_{5c}-bound acetone. A typical attempt frequency of ~10^{13}/s is used in the estimate. This barrier is comparable to the two V_O-acetone diffusion barriers (0.74 eV and 0.82 eV) for the two diffusion channels respectively.[37] Thus, the diffusion of V_O-acetone and the conversion of the diolate to O_a and Ti_{5c}-bound acetone are all observed on the same surface at 300 K. At low coverages (below V_O coverage) of acetone and when the coverages of the V_O and O_a are comparable, the populations of the diolate, V_O-bound acetone and Ti_{5c}-bound acetone reflect their relative adsorption energies (E_{ads}). From our experiments, the coverage ratio of the diolate to V_O-bound acetone is ~ 0.10 and no Ti_{5c}-bound acetone is resolved. This indicates E_{ads}'s of the diolate, V_O-bound acetone and Ti_{5c}-bound acetone follow $E_{ads}^{\text{Ti-bound acetone}} > E_{ads}^{\text{diolate}} > E_{ads}^{\text{Vo-bound acetone}}$. It is reported that the calculated E_{ads} of the diolate (–1.57 eV) is lower than that of the Ti-bound acetone (–0.75 eV)[35] which agrees with our results. However the energy difference between these two species indicates that the diolate is more stable than the V_O-bound acetone (–1.24 eV)[37] which is in contrast to our experiment results. Note that these three calculated E_{ads}'s are relative to different surfaces (the stoichiometric surface with an O_a for the diolate, the stoichiometric surface for the Ti-bound acetone, and the reduced surface for V_O-bound acetone) which could be the reason of the discrepancy between the experiment and the calculation.

4.4 Conclusion

The consecutive reaction steps of acetone with O_a and V_O on partially oxidized TiO_2(110) surfaces are imaged using STM at 300 K. Acetone reacts with the surface form two types of acetone–O_a complexes. A V_O-bound acetone combines with a nearby O_a

appearing as a bright V_O-bound acetone-O_a complex. Once formed, the V_O-bound acetone-O_a complex becomes stationary. A Ti_{5c}-bound acetone combines with an O_a as a Ti_{5c}-bound diolate which assists the diffusion of the surface O_a. The diolate can be observed both on a single O_a and on an O_a pair. The lifetimes of the Ti_{5c}-bound acetone-O_a diolate, the V_O-bound acetone and the Ti_{5c}-bound acetone indicate that their adsorption energies follow $E_{ads}^{\text{Ti-bound acetone}} > E_{ads}^{\text{diolate}} > E_{ads}^{\text{Vo-bound acetone}}$.

References

1 Schmidt, C. M.; Buchbinder, A. M.; Weitz, E.; Geiger, F. M., *J. Phys. Chem. A*, 2007, 111, 13023.

2 Carter, E.; Carley, A. F., Murphy, D. M., *ChemPhysChem*, 2007, 8, 113.

3 Senanayake, S. D.; Gordon, W. O.; Overbury, S. H., Mullins, D. R., *J. Phys. Chem. C*, 2009, 113, 6208.

4 Mattsson, A., Osterlund, L., *J. Phys. Chem. C*, 2010, 114, 14121.

5 El-Maazawi, M.; Finken, A.; Nair, A., Grassian, V., *J. Catal.*, 2000, 191, 138.

6 Hernandez-Alonso, M. D.; Tejedor-Tejedor, I.; Coronado, J. M.; Anderson, M. A., Soria, J., *Catal. Today*, 2009, 143, 364.

7 Henderson, M. A., *J. Phys. Chem. B*, 2005, 109, 12062.

8 Tatsuma, T.; Tachibana, S., Fujishima, A., *J. Phys. Chem. B*, 2001, 105, 6987.

9 Nakamura, R., Sato, S., *J. Phys. Chem. B*, 2002, 106, 5893.

10 Szczepankiewicz, S. H.; Colussi, A. J., Hoffmann, M. R., *J. Phys. Chem. B*, 2000, 104, 9842.

11 Yates, J. T., *Surf. Sci.*, 2009, 603, 1605.

12 Wendt, S.; Sprunger, P. T.; Lira, E.; Madsen, G. K. H.; Li, Z.; Hansen, J. O.; Matthiesen, J.; Blekinge-Rasmussen, A.; Laegsgaard, E.; Hammer, B., Besenbacher, F., *Science*, 2008, 320, 1755.

13 Pang, C. L.; Bikondoa, O.; Humphrey, D. S.; Papageorgiou, A. C.; Cabailh, G.; Ithnin, R.; Chen, Q.; Muryn, C. A.; Onishi, H., Thornton, G., *Nanotechnology*, 2006, 17, 5397.

14 Du, Y.; Deskins, N. A.; Zhang, Z.; Dohnalek, Z.; Dupuis, M., Lyubinetsky, I., *J. Phys. Chem. C*, 2009, 113, 666.

15 Petrik, N. G., Kimmel, G. A., *J.Phys.Chem.C*, 2011, 115, 152.

16 Henderson, M. A.; Epling, W. S.; Perkins, C. L.; Peden, C. H. F., Diebold, U., *J. Phys. Chem. B*, 1999, 103, 5328.

17 Scheiber, P.; Riss, A.; Schmid, M.; Varga, P., Diebold, U., *Phys.Rev.Lett.*, 2010, 105, 216101.

18 Lira, E.; Hansen, J. Ø.; Huo, P.; Bechstein, R.; Galliker, P.; Lægsgaard, E.; Hammer, B.; Wendt, S., Besenbacher, F., *Surf.Sci.*, 2010, 604, 1945.

19 Du, Y.; Deskins, N. A.; Zhang, Z.; Dohnalek, Z.; Dupuis, M., Lyubinetsky, I., *Phys. Chem. Chem. Phys.*, 2010, 12, 6337.

20 Tan, S.; Ji, Y.; Zhao, Y.; Zhao, A.; Wang, B.; Yang, J., Hou, J. G., *J.Am.Chem.Soc.*, 2011, 133, 2002.

21 Jayaweera, P. M.; Quah, E. L., Idriss, H., *J.Phys.Chem.C*, 2007, 111, 1764.

22 Yasuo, M.; Sasahara, A., Onishi, H., *J. Phys. Chem. C*, 2010, 114, 14579.

23 Brinkley, D., Engel, T., *J. Phys. Chem. B*, 2000, 104, 9836.

24 Idriss, H.; Légare, P., Maire, G., *Surf.Sci.*, 2002, 515, 413.

25 Shen, M.; Henderson, M. A., *J. Phys. Chem. Lett.*, 2011, 2, 2707.

26 Phillips, K. P.; Jensen, S. C.; Baron, M.; Li, S. C.; Friend, C. M., *J. Am. Chem. Soc.*, 2012, 135, 574.

27 Henderson, M. A., *J. Phys. Chem. B*, 2004, 108, 18932.

28 Henderson, M. A., *J. Catal.*, 2008, 256, 287.

29 Henderson, M. A., *J. Phys. Chem. C*, 2008, 112, 11433.

30 Henderson, M. A., *Surf.Sci.*, 2008, 602, 3188.

31 Zehr, R. T., Henderson, M. A., *Surf.Sci.*, 2008, 602, 2238.

32 Zehr, R. T.; Deskins, N. A.; Henderson, M. A., *J. Phys. Chem. C*, 2008, 114, 16900.

33 Zehr, R. T.; Henderson, M. A., *Phys. Chem. Chem. Phys.*, 2010, 12, 8085.

34 Wang, T.; Dixon, D. A., Henderson, M. A., *J. Phys. Chem. B*, 2010, 114, 14083.

35 Henderson, M. A.; Deskins, N. A.; Zehr, R. T., Dupuis, M., *J. Catal.*, 2011, 279, 205.

36 Jensen, S. C.; Shank, A.; Madix, R. J., Friend, C. M., *ACS Nano*, 2012, 6, 2925.

37 Xia, Y.; Zhang, B.; Ye, J.; Ge, Q., Zhang, Z., *J. Phys. Chem. Lett.*, 2012, 3, 2970.

38 Horcas, I.; Fernandez, R.; Gomez-Rodriguez, J. M.; Colchero, J.; Gomez-Herrero, J., Baro, A. M., *Rev.Sci.Instrum.*, 2007, 78, 013705.

39 Bikondoa, O.; Pang, C. L.; Ithnin, R.; Muryn, C. A.; Onishi, H., Thornton, G., *Nat. Mater.*, 2006, 5, 189.

40 Du, Y.; Dohnalek, Z., Lyubinetsky, I., *J. Phys. Chem. C*, 2008, 112, 2649.

41 Wendt, S.; Schaub, R.; Matthiesen, J.; Vestergaard, E. K.; Wahlstrom, E.; Rasmussen, M. D.; Thostrup, P.; Molina, L. M.; Laegsgaard, E.; Stensgaard, I.; Hammer, B., Besenbacher, F., *Surf.Sci.*, 2005, 598, 226.

42 Zhang, Z.; Bondarchuk, O.; Kay, B. D.; White, J. M., Dohnalek, Z., *J. Phys. Chem. B*, 2006, 110, 21840.

43 Luo, S., Falconer, J. L., *J. Catal.*, 1999, 185, 393.

44 Xu, W., Raftery, D., *J. Catal.*, 2001, 204, 110.

45 Zaki, M. I.; Hasan, M. A., Pasupulety, L., *Langmuir*, 2001, 17, 768.

46 Griffiths, D. M., Rochester, C. H., *J.Chem.Soc. Faraday Trans.*, 1978, 74, 403.

47 Hasan, M. A.; Zaki, M. I., Pasupulety, L., *Appl. Catal. A-Gene.*, 2003, 243, 81.

48 Du, Y.; Deskins, N. A.; Zhang, Z.; Dohnalek, Z.; Dupuis, M., Lyubinetsky, I., *Phys. Rev. Lett.*, 2009, 102, 096102.

CHAPTER FIVE

Atomic Structure of the Anatase TiO_2(001) Surface[1]

This chapter published as: Y. Xia, K. Zhu, T. C. Kaspar, Y. Du, B. Birmingham, K. T. Park, Z. Zhang Atomic Structure of the Anatase TiO2(001) Surface. J. Phys. Chem. Lett, 2013, 4, 2958

Abstract

Understanding the structure of well-defined anatase TiO_2 surfaces is critical for deciphering site-specific thermal and photo- reaction mechanisms on anatase TiO_2. Using ultrahigh vacuum scanning tunneling microscopy (STM), we have studied the atomic structure of anatase TiO_2(001) epitaxial thin films grown by oxygen plasma assisted molecular beam epitaxy. Bright rows of the (1×4) reconstructed surface are resolved as three types of features with different sizes. High-resolution STM images taken from the same area at different bias voltages show that these individual features are originated from combinations of two basic atomic building blocks. We propose a modified added molecule model for the anatase TiO_2(001) surface structure.

5.1 Introduction

Driven by various applications, thermal and photo- catalytic reactions on various forms of TiO_2 including thin films, nanoparticles and single crystals have been extensively studied.[1-3] From the fundamental reaction mechanism point of view, numerous studies have been performed on the well-defined single crystal rutile TiO_2(110) surface and have provided important molecular-level details of reaction processes and mechanisms.[4, 5] The

[1] http://pubs.acs.org/doi/abs/10.1021/jz401284u

anatase polymorph of TiO_2 appears to be an even more potent catalyst than rutile due to its higher photoactivity. Anatase nanoparticles most frequently expose (101) surfaces, together with small amount of (001) facets. Experimental results [6-10] and theoretical evidence[11] on anatase nanocrystals suggest that the minority (001) surface is photo-catalytically more reactive than the majority (101) surfaces and plays a key role in the reactivity of anatase nanoparticles. Some investigations recently reported contrary results.[12, 13] Clearly, a molecular-level understanding of the reaction mechanism on different anatase surfaces is needed. However, experimental studies of surface reactions on well-defined anatase surfaces are limited.[14-16] This is mainly due to the difficulty of synthesizing pure anatase single crystals with sufficient size. High-quality anatase epitaxial thin films have been synthesized by molecular beam epitaxy (MBE)[17-19] and chemical vapor deposition[20] on $SrTiO_3$(100) and $LaAlO_3$(100) substrates. Adopting these films offers an alternative approach to undertake molecular-level well-controlled surface reaction studies on anatase surfaces.[17, 21-23]

The surface structure of epitaxial anatase TiO_2(001) thin films has been studied both *in situ* and *ex situ* the growth chamber.[18, 21, 23, 24] The surface exhibits a (1×4) reconstruction detected by low-energy electron diffraction (LEED),[18, 21, 23, 24] scanning tunneling microscopy (STM),[18, 21, 23, 24] atomic force microscopy[16], angle-resolved mass spectroscopy of recoiled ions,[20] and reflection high-energy electron diffraction (RHEED) [18, 21, 23, 24]. High-resolution XPS indicates that the surface is fully oxidized to Ti^{4+}, with no Ti^{3+} present even for surface sensitive grazing emission.[18, 20] Several models have been proposed for the (1×4) reconstructed structure.[18, 20, 25, 26] The reconstruction was best explained by the added molecule (ADM) model,[26] in which surface tensile stress was

relieved by rows of TiO_3 species periodically replacing rows of surface bridging oxygen in the (1×1) surface. However, the ADM model along with all other previous models propose that the added bright row is uniform[26-33] since no periodic corrugation has been observed on LEED pattern. Since the (1x4) reconstruction was recently predicted to occur on the {001} facets of micrometer-sized anatase crystals in humid environments,[28] determining the structure of this reconstruction is critical to understanding the catalytic chemistry of the anatase surface. In this work, we study the surface structure of anatase TiO_2(001) using scanning tunneling microscopy (STM). High resolution images show that the atomic corrugation of the bright row is not uniform and is originated from two different atomic building blocks. We propose a modified added molecule model for the anatase TiO_2(001) surface structure.

5.2 Experimental Methods

Anatase TiO_2(001) epitaxial thin films were grown on atomically smooth Nb-doped (0.1 at. %, MTI) $SrTiO_3$(001) single-crystal substrates by oxygen plasma assisted molecular beam epitaxy (OPAMBE) at Pacific Northwest National Laboratory. The substrate preparation method, which results in atomically flat, TiO_2-terminated surfaces, has been described elsewhere.[18] The thickness of our thin films is 50 nm. XPS and RHEED analyses were performed before samples were taken out of the growth system. XPS showed no Ti^{3+} from as-grown (1×4) reconstructed anatase surfaces (S1) with a typical detection limit of 1% atomic concentration. A clear (1×4) reconstruction is visible in the [100] azimuth on the RHEED pattern for all the samples, characteristic of a well-ordered atomically flat anatase (001) surface (S1).

Anatase (001) films were shipped to Baylor after growth. STM experiments were carried out in an ultrahigh vacuum (UHV) chamber (base pressure < 3×10^{-11} Torr) equipped with variable temperature STM (SPECS), quadrupole mass spectrometry (SRS) and ion gun (SPECS). The thin films were cleaned by several cycles of Ar ion sputtering (1000 eV, 2 μA sample current,1 min) and e-beam heating annealing (~ 900 K) in UHV, resulting in a (1×4) reconstructed surface. All STM images (empty states) were collected at 300 K in a constant-current (~ 0.2 nA) mode at positive sample bias voltages of 0.8 – 2.8 V. STM tips are the electrochemically etched W tips (SPECS) and were cleaned *in situ* in the UHV chamber by Ar ion sputtering. Images were processed using WSxM software (Nanotech, freeware).[34]

5.3 Results and Discussions

Figure 5.1 shows representative STM images of an anatase (001) thin film surface. Large terraces with an average size of ~30 nm are observed. (4×1) and (1×4) reconstructed terraces, which are the result of the two types of equivalent orthogonal domains, are clearly visible. The distance between the adjacent bright rows is ~15 Å, approximately four times the value of the (1×1) in-plane lattice spacing *a* (*a* = 3.786 Å) which is characteristic of the (1×4)/(4×1) surface reconstruction.[18, 20, 25] In agreement with previous reports, the step height between the two terraces with orthogonal domains is 2.4 Å, whereas the step height between two like-domains is 5.0 Å. [24] These measured values correspond to ¼-unit-cell height and ½-unit cell height respectively. We also observe small amounts of (1×3) and (1×5) periodicities which agrees with what has been reported previously.[21]

In the high resolution image (Figure 5.1b), each bright row is resolved into separate features elongated perpendicular to the row. The line scan along the bright row shows that

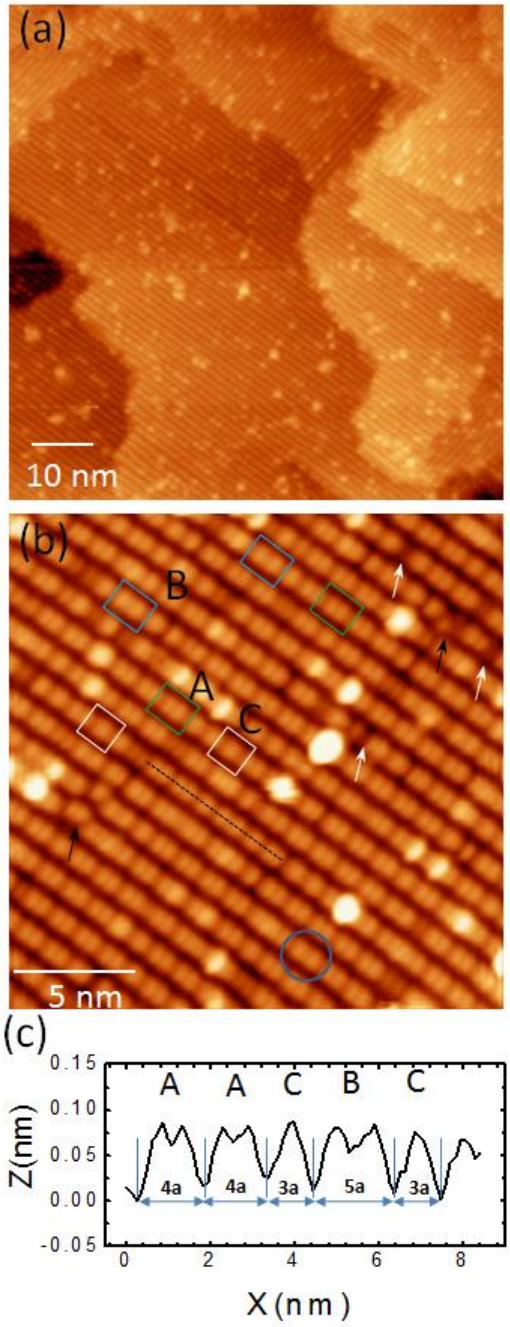

Figure 5.1. Representative STM images of an anatase (001) thin film surface. (a) 80 nm × 80 nm image, (b) high resolution image (20 nm × 20 nm) shows three types (A, B, and C) of features marked by the green, blue and white rectangles respectively. (c) Line profile along the black dotted line on b.

the sizes of these separated features are not uniform and some of them are paired up. Careful analyses indicate that the features can be grouped into three categories. Type A

(green rectangle) and type B (blue rectangle) are pairs of bright features but are not identical. Line profile measurements show that the type A pair occupies the space of four lattice constants (4*a*) along the row as shown in Figure 5.1c. The separation (~5.5 Å) between the two bright lobes in type A pair is slightly less than 2*a*. On the other hand, the type B pair occupies the space of five lattice constants (5*a*). The separation (~ 8.4 Å) between the two lobes in type B pair is greater than 2*a*. The last category of features is the single isolated feature without pairing (type C, white rectangle) that occupies the space of three lattice constants along the row. In addition to these features, there are kinks marked by black arrows and atomic-scale dark defects marked by white arrows on the surface. We examined several samples under similar sample preparation procedures. All three types (A, B, C) of features are observed on these samples. The number density of the type A pair varies in the range of ~ 40% to ~ 70%.

The surface structure was further examined by scanning at different bias voltages. Figure 5.2 shows two sets of high-resolution images. The images in each set are taken from the same area. The image (Figure 5.2a) taken at 2.5 V shows the three types of features (A, B, C) described above. The same area of Figure 5.2a imaged at the lower bias (1.8 V, Figure 5.2b) shows that the type A pair consists of four individual features with two brighter ones at the center and two dimmer ones on the sides. One bright individual feature and one dimmer feature together correspond to one of the two bright lobes of the type A pair (green rectangle) shown on the high bias image (Figure 5.2a). The type B pair (blue rectangle, Figure 5.2b) consists of five individual features with three bright individual features at the center and two dimmer individual features on the sides. The type C feature (white rectangle, Figure 5.2b) has one bright feature at the center and two dimmer features on the sides.

Another set of experiments, the image taken at high bias (Figure 5.2c) shows the three types of features again. The image taken from the same area at even lower bias (1.0 V, Figure 5.2d) clearly shows that the bright individual feature and the dimmer feature are two different atomic building blocks. The bright individual features appear as oval shapes elongated perpendicular to the row which is marked by ovals on the duplicate image (Figure 5.2f). The dimmer individual feature (marked by short line perpendicular to the row) further splits into two spots with respect to the row. The observation of the two bright spots and the non-uniformity in the bright row has been indicated in previous reported STM images but no explanation was provided.[21] We also observed the two faint rows in the trench between the bright rows on very low bias images (S2) which agrees with the literature.[21] A total of 11 sets of successful bias dependence experiments are obtained on two samples using three newly sputtered tips. The observed bias dependence of the features is reproducible which indicates that the dependence is not tip dependent.

The line profile (red line, Figure 5.2g) along the bright row in the low bias image (Figure 5.2d) shows that each of the ovals occupies one lattice position and so does each of the dimmer features. The line profile (black line, Figure 5.2g) along the same bright row on the high bias image (Figure 5.2c) shows that depressions (vertical red lines, Figure 5.2g) that separates the type A, B, and C features in the high bias image align with depressions between the two dimmer features in the low bias image. At high bias, depressions at the center of type A pairs align with the lattice positions. Each of the bright lobes in the type A pair consists of one oval block and one line block. Similarly, one line feature and one neighboring oval block correspond to one of the two bright lobes of the type B pair (Figure 5.2e). But there is one additional oval block in the middle of the type B pair. Interestingly,

at high bias (Figure 5.2g, black line), the oval block at the center of a type B pair appears dimmer than the bright lobe (i.e. the line-oval combination), while at low bias (Figure 5.2g, red line), the oval block at the center shows about the same brightness as the neighboring oval blocks. This indicates that the local density of states of the line blocks and the oval blocks respond differently with the bias voltage.

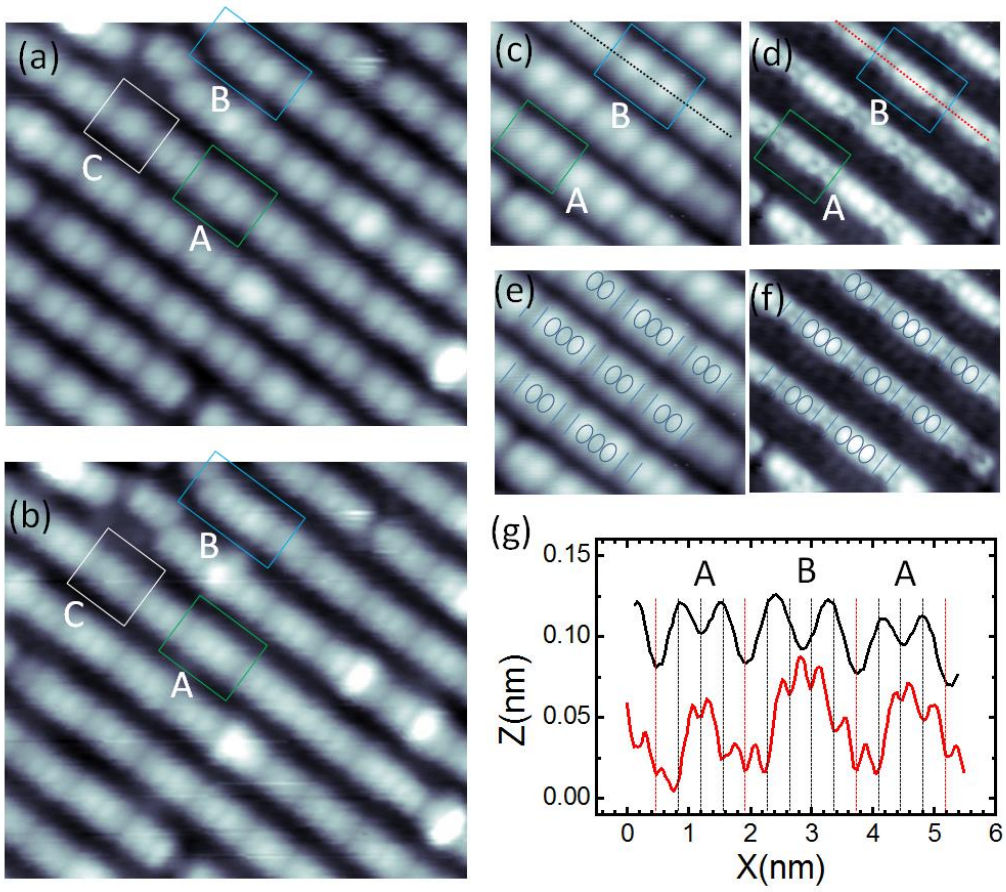

Figure 5.2. Two sets of high-resolution images taken at different bias voltages. (a-b) are taken from the same area: (a) V_s = 2.5 V, (b) V_s = 1.8 V. (c-d) are taken from another area: (c) V_s = 2.2 V, (d) V_s = 1.0 V. The (c) and (d) images are duplicated in (e) and (f), respectively, with two different atomic blocks (oval and line) been highlighted. (g) Line profiles along the black dotted line on (c) and along the red dotted line on (d). Vertical lines represent the (1×1) lattice spacing.

Several models have been proposed for the anatase TiO_2(001) structure since the report of the (1×4) reconstructed surface. The stoichiometric surface, based on evidence

from high-resolution XPS excludes the simple added TiO_3 row model[20] and the missing oxygen row model[20, 35]. The {103} nanofacet model[20] has difficulty explaining the periodicity of (1×3) and (1×5) periodicities observed on the STM images.[20] In {011} nanofacet model,[16] the height difference between the bright row and dark row is too large compared to the corrugation observed in STM and AFM images.[21, 25] Based on the stoichiometry obtained from XPS and the STM image, the added and missing row (AMR) model[13] (Figure 3a) and added molecule (ADM) model[26] (Figure 3b) are the most promising models. Lazzeri et al. calculated "theoretical STM images" of these two models within Tersoff-Hamann's approach.[26] The reconstruction is best explained by the ADM model. This model explains the two faint rows in the trench and the (1×3) and (1×5) periodicities. This model avoids the over-stoichiometric problem of the added TiO_3 row model[20] by the inclusion of a row of threefold coordinated bridging oxygen ($O(3)_{bridge,}$ green ball) beneath the Ti atoms in the bright added TiO_3 row.

However, all the previous models propose that the structure in the added bright row is uniform and therefore cannot explain the non-uniformity observed on the bright rows in Fig. 5.1 and Fig. 5.2. Figure 5.3c shows our modified added molecule model. Starting from the ADM model, we propose a mixture of the removal of the twofold oxygen at the center ($O(2)_{center}$, light blue ball) of the bright added row and the insertion of the $O(3)_{bridge}$ (green ball) beneath the added TiO_3 row. To form a type A pair (green rectangle, Figure 5.3c), two $O(2)_{center}$ atoms are removed from the first and fourth of four continuous Ti atoms (small grey balls) in the added row forming defects. In the meantime, $O(3)_{bridge}$ atoms (green balls) are inserted underneath the Ti atoms ($Ti(4)_{end}$) which are bound to the removed $O(2)_{center}$ atoms. In this way, Ti atoms at the center of type A pair ($Ti(4)_{center}$) and $Ti(4)_{end}$ atoms are

all fourfold coordinated. Similarly, to form a type B pair (blue rectangle, Figure 5.3c), two $O(2)_{center}$ atoms are removed from the first and the fifth of five continuous Ti(4) atoms. A Type C feature can be formed by removing two $O(2)_{center}$ atoms from the first and the third of three continuous Ti(4) atoms.

The bright row of our model can be viewed as a mixture of the bright row of ADM model and that of the AMR model. Therefore, our observed STM image may be qualitatively explained by the comparison with the reported "theoretical STM images" of the ADM and AMR models calculated within Tersoff-Hamann's approach.[26] The side view along the iii–iii line (Figure 5.3c) shows the plane perpendicular to the (001) surface passing through a $Ti(4)_{center}$ atom. The coordination and the geometry of the $Ti(4)_{center}$ atom and four coordinated oxygen atoms are exactly the same as those in ADM model (Figure 5.3b). In the calculated STM image (Figure 2a in ref 26), Ti(4) atoms in bright rows of the ADM model appear as bright ovals perpendicular to the row as illustrated by the grey area in Figure 5.3b. This suggests that our observed oval blocks correspond to Ti_{center} atoms.

The side view along the iv–iv line (Figure 5.3c) shows the plane perpendicular to the (001) surface passing through a $Ti(4)_{end}$ atom. Coordinations of $O(3)_{bridge}$ atom and O_{side} atoms are the same as those in the AMR model (Figure 3a). The difference is at the Ti atom. The $Ti(4)_{end}$ atom is fourfold coordinated in our model because one of two coordinated $O(2)_{center}$ atoms is removed, whereas the Ti(5) atom is fivefold coordinated in the AMR model. Interestingly, the "theoretical STM images" (Figure 2b in ref 26) of the bright row of the AMR model shows that the local density of the Ti(5) atoms splits in two as illustrated by the two grey areas in Figure 3a. This is because the nodal plane for the *d* states on these atoms is a plane perpendicular to the surface and the row. Our observed

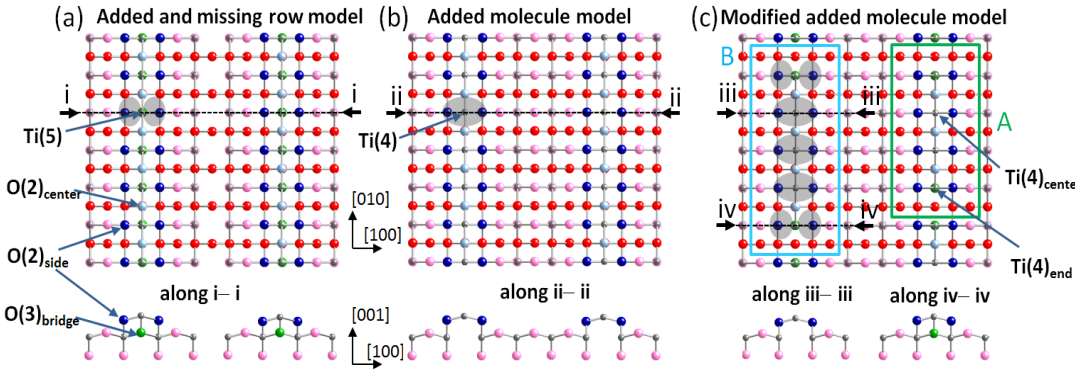

Figure 5.3. Three models for anatase TiO_2(001) (1×4) reconstruction: a) added and missing row (AMR) model[13]; b) added molecule (ADM) model[21]; c) our proposed modified added molecule model. Upper panel: top view of the models; Lower panel: the side view of the plane perpendicular to the surface passing through the surface of Ti atoms (small grey balls), corresponding to dotted lines in the upper panel. Pink/red balls represent in plane buckle upward/buckle downward oxygen atoms. Light/dark blue balls represent twofold buckle upward/downward oxygen atoms ($O(2)_{center}$/ $O(2)_{side}$) in the added row. Green balls represent threefold coordinated bridging oxygen atoms ($O(3)_{bridge}$) beneath the added TiO_3 row.

splitting of the line block into two spots is consistent with the nodal plane expected from the Ti(5) atoms in the AMR model. In our model, the breaking of symmetry for $Ti(4)_{end}$ is in the [010] direction, the row direction. It is possible that the splitting of the local density in the [100] direction, the direction perpendicular to the row, is partially preserved. In addition, the two oxygen atoms on the side (O_{side}) of the bright row also contribute to the density of the bright row (the dotted line on Figure 2d in ref 26). We expect the calculated detailed map of local density of states will be different compared to that from the AMR model. Nevertheless, the split of the $Ti(4)_{end}$ *d* states and the contribution from the O_{side} could explain the splitting of the dimmer individual figures into two bright spots at low bias, where the tip is close to the surface. As the $Ti(4)_{center}$ atoms and $Ti(4)_{end}$ atoms in our model have different configurations and therefore different local density of states, it is not surprising they appear as different brightnesses as shown on low bias images (Figure 5.2b, 5.2d).

It is worth noting that our proposed model is slightly over-stoichiometric because when one $O(2)_{center}$ is removed, two $O(3)_{bridge}$ are inserted under the two Ti_{end} atoms which were bound to the removed $O(2)_{center}$ atoms. This results in about 2.5 % more oxygen atoms on the reconstructed surface than the number of oxygen atoms on the stoichiometric surface. XPS experiments from Tanner *et. al*[25] reported that the surface layers of the (1×4) reconstructed surface contain Ti exclusively in the 4+ oxidation state after UHV annealing. Under similar sample preparation, it is reasonable to assume that our sample is also stoichiometric. A value of 2.5% is slightly above the limit of the XPS resolution. Some additional defects are shown as black spots on STM images (white arrows, Figure 1a). Those defects might contribute to maintaining stoichiometry. Another possibility to compensate the overall stoichiometry of our model is the possible existence of the subsurface oxygen vacancies. A recent theoretical calculation shows that unlike rutile, oxygen vacancies are significantly more stable at subsurface than at surface sites in the case of anatase (001) and (101) surfaces.[30] Detailed theoretical calculations are needed to fully understand the structure.

The understanding of the atomic surface structure of the (1×4) reconstructed surface impacts the chemistry and photo-chemistry of the anatase TiO_2(001). Experimentally, the structure of the (001) surface of the microscale and nanoscale anatase TiO_2 single crystals synthesized using hydrothermal/solvothermal methods is still unclear. A recent DFT calculation predicts that the {001} facets of anatase crystals prepared in HF aqueous solution will exhibit the (1×4) reconstruction in humid environments.[28] Until now, the theoretical calculations of the structure of anatase TiO_2(001) (1×4) are all based on the uniform atomic structure of the bright added row ridges.[26-33] In particular, the ADM has

been well accepted as the structure of the (1×4) reconstructed anatase TiO_2(001) surface.[26] The incorporation of N and C dopants and the formation of defects have been calculated based on this model.[29] The calculation of the reactivity of H_2O and formic acid on anatase TiO_2(001) shows that both H_2O and formic acid dissociate spontaneously on the highly reactive ridge of the reconstructed TiO_2(001) (1×4) surface.[32] The favorable adsorption structure for H_2O and formic acid is the dissociated OH or formate moiety bound to Ti(4) while H moves to the nearby bridging $O(2)_{center}$, so that the $O(2)_{center}$ - Ti(4) bond is broken. For formate, bidentate configurations are energetically more favored than monodentate ones. However, kinetics seems to favor the monodentate configuration. The STM experiments of formic acid[21] and trimethyl acetate (TMA)[23] suggest that formate and TMA bind to the ridges in a bridging bidentate fashion. However, our results clearly show that the ridges of the TiO_2(001) (1×4) surface are not uniform. The Ti(4) atoms in the line and the oval blocks of the ridge (see Figures 2 and 3) are different. The $O(2)_{center}$ atoms between the line blocks are missing. The changes in the chemical bonding of both Ti and O in the ridges are expected to affect the dissociation and the structure of H_2O, formic acid and potentially many other molecules on the anatase TiO_2(001) (1×4) surface. It is likely that there are two types of dissociation channels on the ridges. Site-specific STM experiments are needed to distinguish the difference.[36]

In summary, we have studied the structure of (1×4) anatase TiO_2(001) epitaxial thin films. High bias STM images show three types of features on the bright rows of the (1×4) reconstruction. The high-resolution images taken from the same area at different bias voltages show that the three types of features are made of two common types of atomic building blocks. We propose a modified added molecule model. In this model, the twofold

oxygen at the center of the added TiO_3 row is removed non-uniformly and replaced with surface bridging oxygen atoms of the (1×1) surface. The observed STM image can be qualitatively explained by the combination of reported "theoretical STM images" for the AMR model and ADM model.[26]

References

(1) Diebold, U. The Surface Science of Titanium Dioxide. *Surf. Sci. Rep.* 2003, *48*, 53-229.

(2) Fujishima, A.; Zhang, X.; Tryk, D. A. TiO_2 Photocatalysis and Related Surface Phenomena. *Surf. Sci. Rep.* 2008, *63*, 515-582.

(3) Pelaez, M.; Nolan, N. T.; Pillai, S. C.; Seery, M. K.; Falaras, P.; Kontos, A. G.; Dunlop, P. S. M.; Hamilton, J. W. J.; Byrne, J. A.; O'Shea, K.; et al. A Review on the Visible Light Active Titanium Dioxide Photocatalysts for Environmental Applications. *Appl. Catal. B-Environ.* 2012, *125*, 331-349.

(4) Henderson, A. M. A Surface Science Perspective on Photocatalysis. *Surf. Sci. Rep.* 2011, *66*, 185-297.

(5) Dohnalek, Z.; Lyubinetsky, I.; Rousseau, R. Thermally-Driven Processes on Rutile TiO_2(110)-(1x1):A Direct View at the Atomic Scale. *Prog. Surf. Sci.* 2010, *85*, 161-205.

(6) Zhang, D.; Li, G.; Yang, X.; Yu, J. C. A Micrometer-size TiO_2 Single-crystal Photocatalyst with Remarkable 80% Level of Reactive Facets. *Chem. Commun.* 2009, *45*, 4381-4383.

(7) Liu, S.; Yu, J.; Jaroniec, M. Tunable Photocatalytic Selectivity of Hollow TiO_2 Microspheres Composed of Anatase Polyhedra with Exposed {001} Facets. *J. Am. Chem. Soc.* 2010, *132*, 11914-11916.

(8) Han, X.; Kuang, Q.; Jin, M.; Xie, Z.; Zheng, L. Synthesis of Titania Nanosheets with a High Percentage of Exposed (001) Facets and Related Photocatalytic Properties. *J. Am. Chem. Soc.* 2009, *131*, 3152-3153.

(9) Yang, H. G.; Sun, C. H.; Qiao, S. Z.; Zou, J.; Liu, G.; Smith, S. C.; Cheng, H. M.; Lu, G. Q. Anatase TiO_2 Single Crystals with a Large Percentage of Reactive Facets. *Nature* 2008, *453*, 638-641.

(10) Wen, C. Z.; Zhou, J. Z.; Jiang, H. B.; Hu, Q. H.; Qiao, S. Z.; Yang, H. G. Synthesis of Micro-sized Titanium Dioxide Nanosheets Wholly Exposed with High-Energy {001} and {100} Facets. *Chem. Commun.* 2011, *47*, 4400-4402.

(11) Gong, X. Q.; Selloni, A. Reactivity of Anatase TiO_2 Nanoparticles: the Role of the Minority (001) Surface. *J. Phys. Chem. B* 2005, *109*, 19560-19562.

(12) Pan, J.; Liu, G.; Lu, G. Q.; Cheng, H. On the True Photoreactivity Order of {001}, {010}, and {101} Facets of Anatase TiO_2 Crystals. *Angew. Chem. Int. Ed.* 2011, *50*, 2133-2137.

(13) Zheng, Z.; Huang, B.; Lu, J.; Qin, X.; Zhang, X.; Dai, Y. Hierarchical TiO_2 Microspheres: Synergetic Effect of {001} and {101} Facets for Enhanced Photocatalytic Activity. *Chem. Eur. J.* 2011, *17*, 15032-15038.

(14) Scheiber, P.; Fidler, M.; Dulub, O.; Schmid, M.; Diebold, U.; Hou, W.; Aschauer, U.; Selloni, A. (Sub)Surface Mobility of Oxygen Vacancies at the TiO_2 Anatase (101) Surface. *Phys. Rev. Lett.* 2012, *109*, 136103.

(15) He, Y.; Dulub, O.; Cheng, H.; Selloni, A.; Diebold, U. Evidence for the Predominance of Subsurface Defects on Reduced Anatase TiO_2(101). *Phys. Rev. Lett.* 2009, *102*, 106105.

(16) Thomas, A. G.; Flavell, W. R.; Kumarasinghe, A. R.; Mallick, A. K.; Tsoutsou, D.; Smith, G. C.; Stockbauer, R.; Patel, S.; Gratzel, M. Resonant Photoemission of Anatase TiO_2 (101) and (001) Single Crystals. *Phys. Rev. B* 2003, *67*, 035110.

(17) Sandell, A.; Sanyal, B.; Walle, L. E.; Richter, J. H.; Plogmaker, S.; Karlsson, P. G.; Borg, A.; Uvdal, P. Probing and Modifying the Empty-State Threshold of Anatase TiO_2: Experiments and *Ab Initio* Theory. *Phys. Rev. B* 2008, *78*, 075113.

(18) Liang, Y.; Gan, S.; Chambers, S. A.; Altman, E. I. Surface Structure of Anatase TiO_2(001): Reconstruction, Atomic Steps, and Domains. *Phys. Rev. B* 2001, *63*, 235402.

(19) Weng, X.; Fisher, P.; Skowronski, M.; Salvador, P. A.; Maksimov, O. Structural Characterization of TiO_2 Films Grown on $LaAlO_3$ and $SrTiO_3$ Substrates using Reactive Molecular Beam Epitaxy. *J. Cryst. Growth* 2008, *310*, 545-550.

(20) Herman, G. S.; Sievers, M. R.; Gao, Y. Structure Determination of the Two-Domain (1x4) Anatase TiO_2(001) Surface. *Phys. Rev. Lett.* 2000, *84*, 3354-3357.

(21) Tanner, R. E.; Sasahara, A.; Liang, Y.; Altman, E. I.; Onishi, H. Formic Acid Adsorption on Anatase TiO_2(001)(1x4) Thin Films Studied by NC-AFM and STM. *J. Phys. Chem. B* 2002, *106*, 8211-8222.

(22) Ohsawa, T.; Lyubinetsky, I.; Du, Y.; Henderson, M. A.; Shutthanandan, V.; Chambers, S. A. Crystallographic Dependence of Visible-Light Photoactivity in Epitaxial $TiO_{2-x}N_x$ Anatase and Rutile. *Phys. Rev. B* 2009, *79*, 085401.

(23) Ohsawa, T.; Lyubinetsky, I.; Henderson, M. A.; Chambers, S. A. Hole-Mediated Photodecomposition of Trimethyl Acetate on a TiO_2(001) Anatase Epitaxial Thin Film Surface. *J. Phys. Chem. C* 2008, *112*, 20050-20056.

(24) Du, Y.; Kim, D. J.; Kaspar, T. C.; Chamberlin, S. E.; Lyubinetsky, I.; Chambers, S. A. In-Situ Imaging of the Nucleation and Growth of Epitaxial Anatase TiO_2(001) Films on $SrTiO_3$(001). *Surf. Sci.* 2012, *606*, 1443-1449.

(25) Tanner, R. E.; Liang, Y.; Altman, E. I. Structure and Chemical Reactivity of Adsorbed Carboxylic Acids on Anatase TiO_2(001). *Surf. Sci.* 2002, *506*, 251-271.

(26) Lazzeri, M.; Selloni, A. Stress-Driven Reconstruction of an Oxide Surface: The Anatase TiO_2(001)(1x4) Surface. *Phys. Rev. Lett.* 2001, *87*, 266105.

(27) Liu, H.; Wang, X.; Pan, C.; Liew, K. M. First-Principles Study of Formaldehyde Adsorption on TiO_2 Rutile (110) and Anatase (001) Surfaces. *J. Phys. Chem. C* 2012, *116*, 8044-8053.

(28) Selcuk, S.; Selloni, A. Surface Structure and Reactivity of Anatase TiO_2 Crystals with Dominant 001 Facets. *J. Phys. Chem. C* 2013, *117*, 6358-6362.

(29) Lee, J. H.; Hevia, D. F.; Selloni, A. Incorporation of Nonmetal Impurities at the Anatase TiO_2(001)-(1x4) Surface. *Phys. Rev. Lett.* 2013, *110*, 016101.

(30) Cheng, H.; Selloni, A. Surface and Subsurface Oxygen Vacancies in Anatase TiO_2 and Differences with Rutile. *Phys. Rev. B* 2009, *79*, 092101.

(31) Lazzeri, M.; Vittadini, A.; Selloni, A. Structure and Energetics of Stoichiometric TiO_2 Anatase Surfaces. *Phys. Rev. B* 2001, *63*, 155409.

(32) Gong, X.; Selloni, A.; Vittadini, A. Density Functional Theory Study of Formic Acid Adsorption on Anatase TiO_2(001): Geometries, Energetics, and Effects of Coverage, Hydration, and Reconstruction. *J. Phys. Chem. B* 2006, *110*, 2804-2811.

(33) Vittadini, A.; Casarin, M.; Selloni, A. Chemistry of and on TiO_2-Anatase Surfaces by DFT Calculations: A Partial Review. *Theor. Chem. Acc.* 2007, *117*, 663-671.

(34) Horcas, I.; Fernandez, R.; Gomez-Rodriguez, J. M.; Colchero, J.; Gomez-Herrero, J.; Baro, A. M. WSXM: A Software for Scanning Probe Microscopy and a Tool for Nanotechnology. *Rev. Sci. Instrum.* 2007, *78*, 013705.

(35) Hengerer, R.; Bolliger, B.; Erbudak, M.; Grätzel, M. Structure and Stability of the Anatase TiO_2(101) and (001) Surfaces. *Surf. Sci.* 2000, *460*, 162-169.

(36) Wang Z.-T.; Deskins N. A.; Henderson M. A.; Lyubinetsky I. Inhibitive Influence of Oxygen Vacancies for Photoactivity on TiO_2(110). *Phys. Rev. Lett.* 2012,*109*, 266103

CHAPTER SIX

Probing Structure of Cross-linked (1 × 2) Rutile TiO_2(110): Adsorption of Trimethyl Acetic Acid[1]

This chapter published as: K. Zhu, Y. Xia, Z. Zhang, K. T. Park Probing Structure of Cross-linked (1 × 2) Rutile TiO_2(110): Adsorption of Trimethyl Acetic Acid. J. Phys. Chem. C, 2016, 120, 15257

Abstract

Cross-linked (1 × 2) rutile TiO_2(110) has been extensively studied, yet the exact atomistic model remains a point of contention. Employing a carboxylic acid as a probing molecule, we studied the structure of cross-linked (1 × 2) TiO_2(110) through the interaction of trimethyl acetic acid (TMAA) with various sites on the surfaces using *in situ* scanning tunneling microscopy (STM). The comparison of the same area before and after various exposures to TMAA reveals three distinctive adsorption sites: in trough between two adjacent strands, on cross-link, and strand. Trough and cross-link are more preferable adsorption sites than strand. Unlike the surface of (1 × 1) TiO_2(110) where TMAA dissociates and de-protonated trimethyl acetate (TMA) is strongly chemisorbed, TMAA diffuses along troughs on (1 × 2) reconstructed TiO_2(110) at low coverages suggesting that TMAA adsorbs molecularly in troughs. At higher coverages, additional TMAA molecules adsorb on strands in both centered and off-centered configurations. We compared three specific atomistic models for (1 × 2) reconstructed TiO_2(110), Ti_2O_3, Ti_2O, and Ti_3O_6. The adsorption of TMAA on strands at room temperature strongly supports the Ti_2O model for cross-linked (1 × 2) reconstructed TiO_2(110).

[1] http://pubs.acs.org/doi/abs/10.1021/acs.jpcc.6b04875

6.1 Introduction

The interaction of organic molecules with TiO_2 is of a broad interest in many technological applications such as degradation of organic pollutants, water purification, water splitting, hydrophilic coatings, and solar cells.[1-5] In these applications, the catalytic processes proceed with surface-mediated redox chemistry.

Faced with structural complexity and heterogeneity in industrial catalysts, surface studies using single-crystal TiO_2 have aimed to provide fundamental insights into catalytic processes in a model system.[6,7] One such example involving the interaction of rutile $TiO_2(110)-(1\times1)$ with a number of carboxylic acids, as surface-anchored carboxylate species play a key role in many catalytic reactions.[8-19] From systematic studies, a general pattern for room-temperature adsorption has emerged, in which the carboxylic acids, from the simplest formic acid to a larger functionalized one such as trimethyl acetic acid (TMAA), decompose into proton and the carboxylate species.[13-17] The acidic proton attaches to basic surface bridging oxygen (O_b) whereas the basic carboxylate species anchors over two acidic 5-fold coordinated titanium (Ti_{5c}) cations in a bi-dentate configuration. At high coverages, carboxylate species form a close-packed overlayer. Moreover, a recent study reported that formic, acetic, and benzoic acids adsorbed on $TiO_2(110)$ via aqueous solutions also show the majority of the carboxylate species in bi-dentate configuration,[20] just as those formed by the vapor deposited acids.

For TiO_2, it is well known that the binary compound is easily reducible as there are numerous stable suboxides, from Magnelli phases to corundum, monoxide, and eventually to metal depending upon the ratio of O to Ti.[21,22] Because these suboxide species possess structures that are markedly different from that of the mother compound, the local charge

distribution and the location of active sites are expected to be unlike those of the mother compound. Hence, the presence of such species in catalysts could significantly influence the adsorption behaviors of organic molecules and consequently the photochemical and catalytic properties of such a partially reduced surface of TiO_2.

For rutile TiO_2(110), such partial reduction is responsible for (1 × 2) reconstructions of the surface. Depending on the level of the partial reduction, rutile TiO_2(110) undergoes a transition from the reduced (1 × 1) phase to the simple (1 × 2) phase and then to the cross-linked (1 × 2) phase. The structure of the reduced (1 × 1) phase is well established. The (1 × 2) reconstructed TiO_2(110) phase has been extensively studied yet remains contentious for the exact atomistic model.[23-37] Among various models, the added Ti_2O_3 row model by Onishi and Iwasawa[27] has long been used to explain the row stoichiometry on both the simple and cross-linked (1 × 2) phases and the linked structures including single-links and cross-links on the cross-linked (1 × 2) phase. According to this model, the repeating unit of the row is considered as 2 Ti and 3 O atoms added on the (1 × 1) TiO_2(110) (Fig. 6.1a). Although the stoichiometry of the added row is like that of the corundum Ti_2O_3, its structure is not related to the corundum as the Ti atom occupies the sites corresponding to the interstitial sites of the rutile lattice.[22] This model is supported by low-energy electron diffraction investigations[32,33] and theory.[34] Later, Park *et al.*[28,29] proposed an alternative model, Ti_2O added row model. In this model, the added Ti atoms are coordinated with surface bridging oxygen atoms to form edge- and face-sharing octahedra chains along [001] direction (Fig. 6.1b). Unlike the Ti_2O_3 model, added Ti atoms are exposed. The structure can be viewed as the edge- and corner-sharing TiO_2 octahedra that are shifted and stacked on the surface as in the reduced TiO_{2-x} bulk phases, for example

at the crystallographic shear planes of the Ti_2O_{2n-1} as well as the corundum Ti_2O_3.[38] This model has been confirmed by a transmission electron microscopy investigation.[30] In contrast to the two models describing (1 × 2) reconstruction as oxygen-deficient sub-stoichiometric structures, Bennett *et al*.[31] proposed a row model made of Ti_3O_6 units for the cross-linked (1 × 2) reconstructed surface (Fig. 6.1c). The separation between two adjacent rows results from a missing row of stoichiometric O-Ti-O units similar to the Ti_3O_5 model proposed earlier by Pang *et al*.[35] However, with the missing bridging oxygen atoms added back onto the Ti_3O_5 row, the Ti_3O_6 row model can be viewed as an essentially bulk-terminated, corrugated surface. Although the stoichiometric nature of the model contradicts the fact that the cross-linked (1 × 2) reconstructed surface requires a higher preparation temperature, the Ti_3O_6 row model was supported by a non-contact atomic force microscopy study.[36] Most recently, various (1 × 2) TiO_2(110) surface structures have been calculated using *ab initio* evolutionary techniques, which allow for both structural and compositional variations.[24] Ti_2O_3 and Ti_2O are found to be the stable and the metastable structures of the (1 × 2) phases, respectively. Simulated STM images of both models can explain the simple (1 × 2) phase and the row structure of the cross-linked (1 × 2) phase.

In this paper, we employ TMAA $(CH_3)_3CCOOH$) to probe the structure of cross-linked (1 × 2) reconstructed rutile TiO_2(110). The adsorption of TMAA on various sites is studied using STM. The comparison of the same area before and after various exposures to TMAA is used to gain insight into the interaction between carboxylic acids and troughs, cross-links, and strands. The three specific atomistic models for the (1 × 2) reconstruction are compared and contrasted to experimentally observed adsorption behaviors of TMAA. The results strongly support the Ti_2O model.

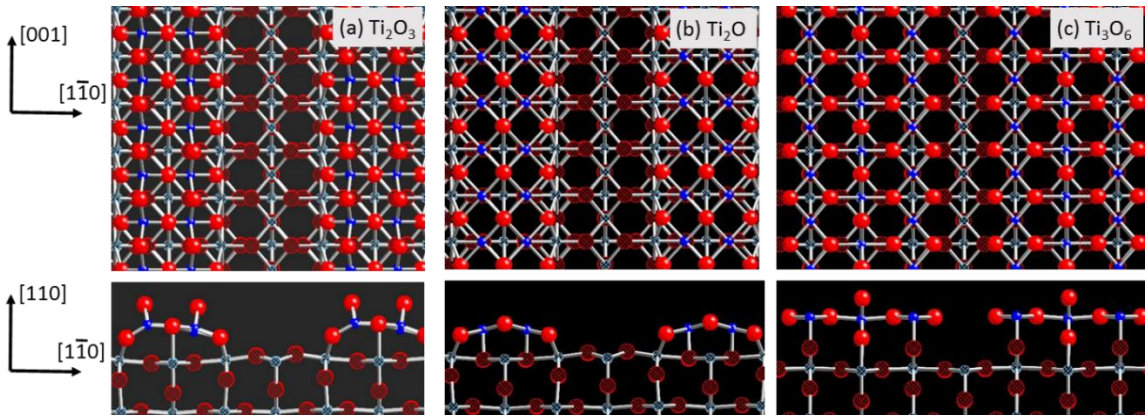

Figure 6.1 Three models for cross-linked (1 × 2) reconstructed TiO_2 (110): (a) Ti_2O_3, (b) Ti_2O, and (c) Ti_3O_6, added-row models in top (top panel) and side (lower panel) views. Small blue spheres are Ti atoms. Large red spheres are O atoms. The atoms below the (1 × 2) added rows are hatched for clarity.

6.2 Experimental Section

Experiments were performed in an ultrahigh vacuum chamber at Baylor University. The UHV system (base pressure < 5×10^{-11} Torr) is equipped with a variable temperature STM (SPECS), quadrupole mass spectrometry (SRS), and an ion gun (SPECS). A rutile TiO_2(110) sample (Princeton Scientific) was initially cleaned by several cycles of Ar-ion sputtering and annealing. A typical Ar-ion sputtering lasted for 15 minutes in the Ar partial pressure of 3 x 10^{-6} Torr. The ion current of about 2 μA was measured at the sample using the accelerating voltage of 1 kV. Following Ar sputtering, the sample was annealed up to 1050 K for 5 minutes. After large terraces of (1x2) reconstruction were observed, the surface was further cleaned only as necessary, by flashing it up to 950K for 5 minutes prior to subsequent experiments. The color of the sample was blue indicating its reduced state.

TMAA was introduced onto the TiO_2(110) surface at the STM stage at room temperature via a retractable tube doser containing a pinhole.[39-41] Freeze-pump-thaw cycles with liquid nitrogen were performed before using TMAA. Prior to dosing TMAA to the surface, the gas-line system and doser assembly were purged with fresh TMAA vapor each

day before preparing the sample. The TMAA exposure is controlled by adjusting the pressure in the gasline and the dosing time. During the exposure, the chamber pressure is below 1×10^{-10} Torr. All STM images (empty states) were collected at room temperature in a constant-current (~0.3 nA) mode at positive sample bias voltages (V_{bias}'s). Images were processed using WSxM software (Nanotech, freeware).[42] The coverage of adsorbed molecules was obtained by a direct count in STM images and expressed in monolayer (ML) units (1 ML corresponds to 5.2×10^{14} cm^{-2} Ti atoms).

6.3 Results and Discussions

Fig. 6.2 shows the images of the same area on (1 × 2) TiO_2(110) before and after several exposures to TMAA molecules. Prior to the adsorption of TMAA, the (1 × 2) reconstructed surface exhibits the characteristic strands running along the [001] direction. The spacing between two adjacent strands is well established as 13 Å.[23] This value, along with the lattice constants from the (1 × 1) surface, is used as a calibration for the STM scanner. The surface also shows cross-links running along the [1-10] direction. Most of the links have the average FWHM of 9 Å, spanning about three lattice constants along the [001] direction, thus they are labeled as cross-links.[31,43,44] Some of the links have an average FWHM of 6 Å and are designated as single-links.

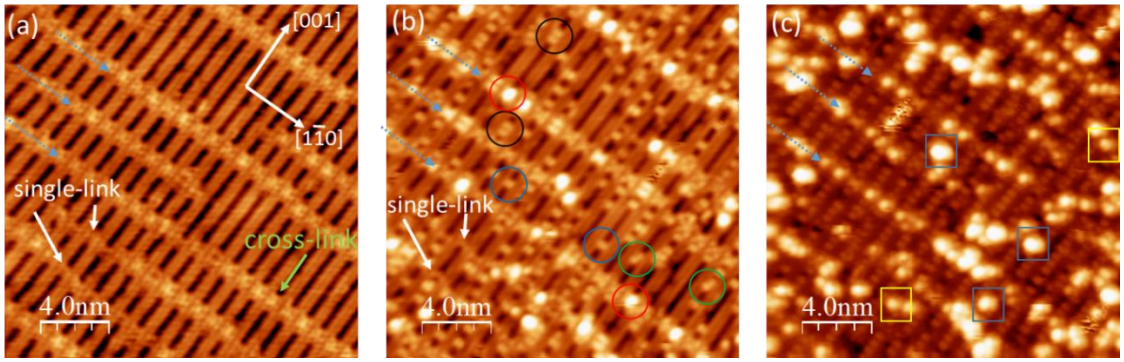

Figure 6.2 Three STM images taken from the same area at room temperature before and after TMAA exposures: (a) clean cross-linked (1 × 2) TiO_2(110), (b) after an exposure to TMAA at 200 mTorr for 10 minutes, and (c) after additional exposure to TMAA at 300 mTorr for 20 minutes on b. The blue and green circles mark the centered and off-centered TMAA in troughs, respectively. The black circles mark the TMAA with neighbors in troughs. The red circles mark the TMAA on cross-links. The squares mark TMAA on strands.

After an exposure of 200 mTorr of TMAA for 10 minutes, the same area reveals bright features adsorbed on various surface sites (Fig. 6.2b). The most TMAA appear as bright spots in troughs (marked by blue circles), and are centered between two adjacent (1 × 2) strands. Under the bias condition used, they are measured 1.0 Å in height and 6 Å in FWHM in the [001] direction. Most of them are isolated. A small number of molecules (< 10%) appear off-centered in the trough (marked by green circles). There are only a few areas, in which the molecules sit next to each other along the trough (marked by black circles). In addition to the troughs, a number of bright adsorbed TMAA species (marked by red circles) appear on the cross links. No TMAA species are observed to adsorb on single-links (marked by white arrows).

An additional exposure of 300 mTorr of TMAA for 20 minutes leads to near saturation of the trough sites (Fig. 6.2c). TMAA molecules are close-packed along troughs. The nearest-neighbor distance between TMAA molecules in troughs is measured to be 6.0 Å on average (see below). Gaps or vacancies are occasionally visible in troughs. The strong preference for TMAA to adsorb to a trough site rather than a (1 × 2) strand site is by now

obvious as the close-packed molecules form quasi-one dimensional chains well separated by (1 × 2) strands. TMAA features that appear on (1 × 2) strands are easily discernable with a bright contrast (marked by squares), consistent with the topographically higher position compared to the trough position. The sizes of the bright TMAA features that appear on strands are different. Some appear to resemble a single molecule in shape and size (yellow squares) whereas others apparently form a cluster of two or more molecules (blue squares). Further discussion is presented below with Fig. 6.5. In addition, the TMAA molecules continue to adsorb on cross-links. As more molecules are found on the cross-links, they form lines (marked by blue dotted arrows) perpendicular to the molecular chains in troughs, providing easy markers for comparing the same area.

The TMAA coverages are calculated by counting the number of sites occupied by the molecules: in troughs between two adjacent strands, on top of the cross-links, and on strands. Each covered area is then subsequently normalized to monolayers (ML), where 1 ML is defined as one molecule per the (1 × 1) unit cell of TiO_2(110) — 3.0 Å × 6.5 Å. For close-packed TMAA molecules in troughs on the (1 × 2) reconstructed surface, the unit cell is 6.0 Å × 13.0 Å corresponding to a 2 × 2 unit cell, thus the saturation coverage is 0.25 ML. The saturation coverage for strands should be the same value of 0.25 ML, since it represents an alternate site in the same 2 × 2 unit cell. Cross-links (double only) are counted as defects on the (1 × 2) surface. Each cross-link occupies an area of a 3 × 2 unit cell. The percentage of (1 × 1) unit cells occupied by cross-links is 24% in Fig. 6.2. Therefore, the saturation coverage of TMAA on cross-links is 0.04 ML with one TMAA molecule per cross-link. For TMAA adsorbed on various sites after each exposure, the calculated ML coverages in Fig. 6.2 are shown in Table 6.1. Also given are the relative

occupancies for a given site; for example, 100% of the trough sites corresponds to the full coverage (0.19 ML = 0.25 ML × 76%) of the available trough sites. The coverage data clearly depicts that the trough is the more favorable adsorption site than the strand for TMAA and the preference for adsorption on the trough and on the cross-link are comparable.

Table 6.1. TMAA coverages on various sites of cross-linked (1 × 2) reconstructed TiO_2 (110) at low total TMAA coverages (< 0.25 ML).

Adsorption sites (site saturation in ML)	After 200 mTorr for 10 min. (percentage to saturation)	After additional 300 mTorr for 20 min. (percentage to saturation)
Trough (0.25 ML)	0.033 ± 0.004 ML (16%)	0.17 ± 0.01 ML (87%)
Strands (0.25 ML)	0.002 ± 0.001 ML (1%)	0.030 ± 0.006 ML (16%)
Crosslink (0.04 ML)	0.007 ± 0.002 ML (18%)	0.022 ± 0.003 ML (55%)

Fig. 6.3a and b are close-up views of closely packed TMAA molecules formed on the (1 × 2) and (1 × 1) surfaces, respectively. The TMAA molecules are lined up in the troughs of the (1 × 2) reconstructed surface with a nearest neighbor distance of 6 Å on average (Fig. 6.3a). The measured value is exactly the same as that measured on (1 × 1) surface along [001] (Fig. 6.3b). The TMAA molecules in adjacent troughs on the (1 × 2) surface do not appear to correlate with one another as some of TMAA positions in adjacent troughs are off by one lattice constant (3 Å) along [001] and some TMAA positions are aligned. This is expected for the negligible interactions between the molecules across the strands since the distance between the troughs is 13 Å. On the (1 × 1) surface, the nearest neighbor distance along [1-10] is 6.5 Å, which is one lattice constant of TiO_2(110) along this direction. Thus the resulting unit cell for the close-packed TMAA overlayer is rectangular (albeit nearly square-like). There are some domain boundaries (black arrows) where two

adjacent rectangular unit cells are shifted with respect to one another by 3 Å along [001] (Fig. 6.3b).

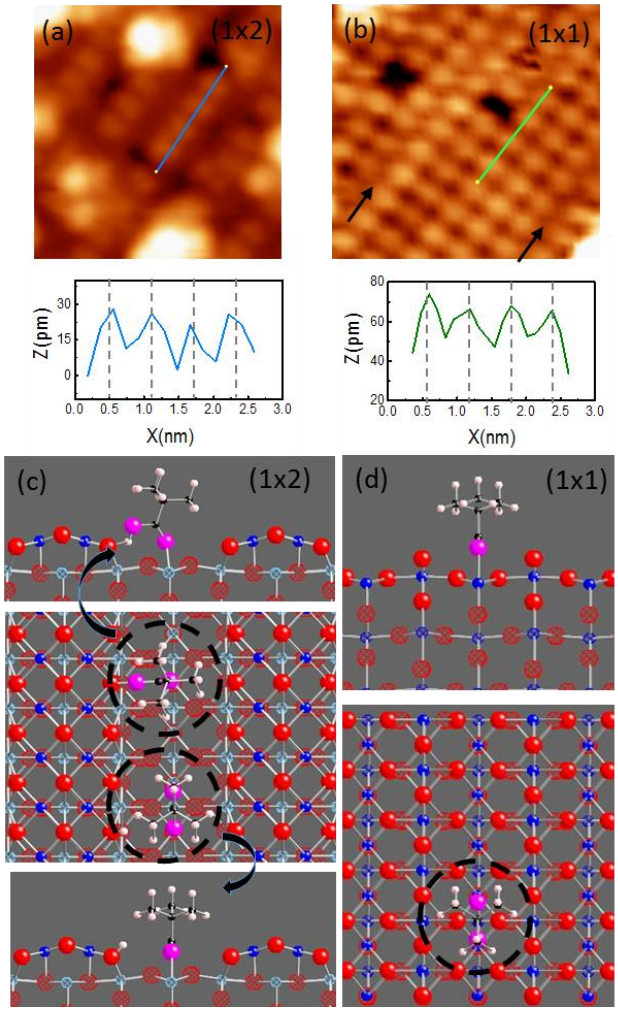

Figure 6.3 STM images with close-up views of close-packed TMAA on (a) (1 × 2) TiO_2(110) and (b) (1 × 1) TiO_2(110). The height profiles along the blue line on (a) and green line on (b) are also shown for comparison. The vertical dashed lines are 6.0 Å apart and show the same nearest-neighbor distances on these two surfaces. (c) Proposed bonding geometry for molecularly adsorbed TMAA in troughs on (1 × 2) TiO_2(110) (top: side view, middle: top view) and for de-protonated TMA in a bi-dentate configuration (bottom: side view, middle: top view), and (d) de-protonated TMA on (1 × 1) TiO_2(110). For TMAA, oxygen, carbon, and hydrogen atoms are shown as pink, black, and white spheres.

The adsorption geometry of TMAA on (1 × 1) TiO_2(110) at 300 K is well established.[9,17,18] TMAA adsorbs with its carboxylic group toward and its tri-methyl groups

away from the surface. The TMAA molecule de-protonates into trimethyl acetate (TMA, $(CH_3)CCOO$), which is bridge-bonded over two adjacent Ti_{5c} sites (Fig. 6.3d). Such bonding geometry has been supported by density functional theory calculations.[18] From the comparison in TMAA positions and nearest neighbor distances along [001] between the (1 × 2) and (1 × 1) surfaces, it is evident that the TMAA molecules in troughs of the (1 × 2) surface can adsorb similarly over two adjacent Ti_{5c} sites in the bi-dentate configuration as on (1 × 1) surface. Of the three (1 × 2) reconstructed models considered, the Ti_3O_6 structural model (Fig. 6.1c) poses a serious conflict with the experimental observation of TMAA adsorbing in troughs because its trough is too narrow (3.8 Å) for TMAA to fit between the two adjacent rows since the diameter of the tert-butyl group is 5.8 Å. In addition, the Ti_3O_6 model has the same Ti_{5c} sites on top of the rows as those in troughs, which are in the same configuration as the Ti_{5c} sites on (1 × 1) TiO_2(110). Those sites should be available and preferable for TMAA adsorption considering the narrow spacing of the trough sites. The STM data clearly show that TMAA preferably adsorbs in troughs, thus the Ti_3O_6 model is not consistent with the observation. On the other hand, both Ti_2O_3 and Ti_2O row models have a trough wide and shallow enough for TMAA to adsorb easily. Fig. 6.3(c) (middle & bottom) shows schematics of the bi-dentate adsorption geometry of de-protonated TMA in the trough between Ti_2O rows, with the carboxylate group bridging two Ti_{5c} sites along [001].

Although de-protonated TMA in the bi-dentate configuration is the most stable geometry on stoichiometric (1 × 1) TiO_2(110), it is not entirely clear that the same is true on (1 × 2) reconstructed TiO_2(110). The surface chemistry of TMAA with a single acid proton and the basic carboxylate involves basic O sites and acidic Ti cation sites. On (1 ×

1) TiO_2(110), the acid proton is bound to two-fold O_b forming bridging hydroxyl (OH_b) species and the basic carboxylate reacts with the acidic Ti_{5c}. Using combined STM and density functional theory (DFT) calculations, Lyubinetsky *et al.*[18] reported that a molecularly-adsorbed TMAA on (1 × 1) TiO_2(110) could serve as a mobile precursor to form the close-packed TMA overlayer. The calculated adsorption energy of the most stable molecularly-adsorbed TMAA via O-Ti_{5c} and H-O_b bonding on (1 × 1) TiO_2(110) is only 0.19 eV higher than that of dissociative bonding. A similar configuration is also plausible for TMAA adsorbed in troughs of both Ti_2O_3 and Ti_2O row models. Fig. 6.3c (top & middle) shows the molecular configuration in troughs of the Ti_2O row model as an example. Given that a redistribution of excess charges is expected not only on the reduced Ti^{3+} sites but also on nearby Ti_{5c} sites,[45] it is plausible that the preference between the dissociated configuration and molecular configuration is different on (1 × 2) reconstructed TiO_2(110).

More tantalizing experimental evidence pointing toward the molecular adsorption of TMAA is the mobility of TMAA. At room temperature, TMAA species are observed diffusing back and forth along troughs at the low coverages (< 0.05 ML) when the TMAA species are isolated. Three snapshots from an STM movie in Fig. 6.4 represent the typical diffusion of TMAA when the same area of a TiO_2(110) surface is imaged for extended periods of time ranging from 30 min to 1 h at 300 K. The TMAA species (marked by a red circle) diffused a distance of one and five lattice spacings in 4.8 min and 14.4 min, respectively. No hydroxyl is observed after the TMAA molecule diffused away, which suggests that the molecule is not dissociated. This is in contrast to the formation of TMA from the dissociation of TMAA on (1 × 1) TiO_2(110).[9,17] Considering the time that is

needed to scan one image (66 s) and using the Arrhenius relation with a typical prefactor (10^{13}), the observation of mobility at room temperature indicates a diffusion barrier smaller than or comparable to 0.8 eV. On the (1×1) rutile TiO_2(110) surface, no substantial TMA mobility at room temperature is observed over several hours. The calculated TMA diffusion barrier is 1.09 eV, which is much higher than that that of the most stable molecular TMAA (0.63 eV).[18] The observed mobility of TMAA species on the (1 × 2) surface is consistent with molecular adsorption. The determination of the detailed configuration of molecular TMAA will need further theoretical calculations.

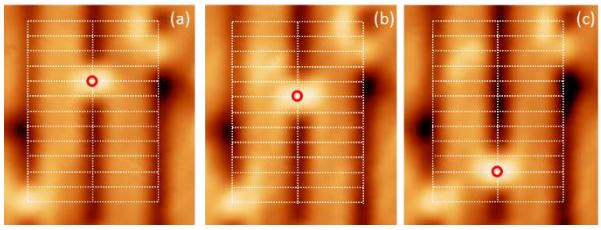

Figure 6.4 Three time-lapse images of TMAA represent the diffusion of TMAA along a trough between two adjacent strands on (1 × 2) TiO_2(110) (20 Å × 45 Å). A white grid is overlaid to show the surface unit cell and lattice spacings. A TMAA species hopped one lattice spacing during the first 4.8 minutes and five spacings between 4.8 and 14.4 minutes along the [001] direction. Circles mark the positions of TMAA.

The adsorption behavior of TMAA at higher coverages is studied with higher exposures. Fig. 6.5 shows the STM images taken from the same area of cross-linked (1 × 2) TiO_2(110) after various amounts of TMAA exposure. After an exposure of 350 mTorr of TMAA for 20 minutes (Fig. 6.5b), TMAA molecules adsorb on all three sites: 0.095 ML in troughs between the 1 × 2 strands, 0.010 ML on top of the 1 × 2 strands, and 0.013 ML on cross-links (Table 6.2). Similar to Fig. 6.2, no TMAA adsorbs on single-links. Additional exposure of 550 mTorr of TMAA for 20 minutes (Fig. 6.5c) leads to the increased coverage of TMAA, 0.058 ML on strands and 0.022 ML on cross-links. As

pointed out in Fig. 6.2, the TMAA species on strands are not uniform in size. We use two molecules per larger species (blue squares) and one molecule per small species to count the coverage. 0.058 ML of TMAA on strands corresponds to the occupation of 27% of the available strand sites. With the higher coverage, the TMAA molecules on strands and cross-links obscure the view of those in troughs and prevent the actual calculation of the coverage. However, glimpses of them in several areas lead to a conclusion that TMAA molecules saturate the troughs.

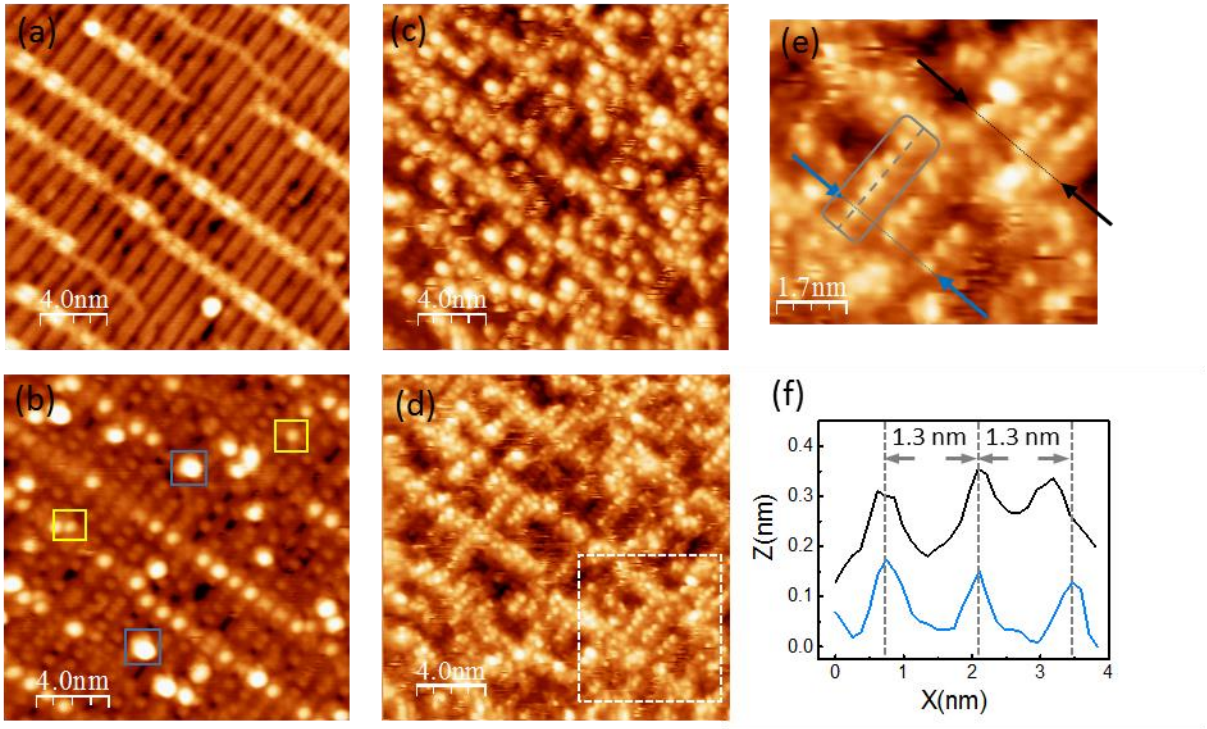

Figure 6.5 Four STM images taken from the same area at room temperature before and after TMAA exposures: (a) clean cross-linked (1 × 2) TiO_2(110), (b) after an exposure to TMAA at 350 mTorr for 20 minutes, (c) after additional exposure to TMAA at 550 mTorr for 20 minutes on b, (d) after additional 20 minute exposure to TMAA at 550 mTorr on c, and (e) close-up view of the square region indicated in d. (f) The height profiles along the black line and the green line one.

After the final exposure of TMAA at 550 mTorr for 20 minutes (Fig. 6.5d), TMAA molecules become uniform in size and shape on 1 × 2 strands. The coverage on strands is

0.089 ML using one TMAA molecule per cluster, corresponding to 42% of the available 1 × 2 strand sites.

Table 6.2. TMAA coverages on various sites of cross-linked (1 × 2) reconstructed TiO_2 (110) at high total TMAA coverages (> 0.25 ML).

Adsorption sites (site saturation in ML)	After 350 mTorr for 20 min. (percentage to saturation)	After additional 550 mTorr for 20 min. (percentage to saturation)	After additional 550 mTorr for 20 min. (percentage to saturation)
Trough (0.25 ML)	0.095 ± 0.006 ML (45%)	_	_
Strands (0.25 ML)	0.010 ± 0.002 ML (5%)	0.058 ± 0.005 ML (27%)	0.089 ± 0.006 ML (42%)
Crosslink (0.025 ML)	0.013 ± 0.002 ML (52%)	0.022 ± 0.003 ML (88%)	0.023 ± 0.003 ML (92%)

Closer-up views of TMAA on strands reveal similar traits of TMAA adsorbed in troughs. TMAA species are generally lined up along the strands (Fig. 6.5d and 6.5e). The measured nearest neighbor distance is ~ 6.0 Å, approximately the same value observed for two adjacent TMAA in troughs as well as on (1 × 1) TiO_2(110). However, there is also considerably more disorder in the adsorption on strands than in troughs. Some TMAA molecules appear right on the center of the strands, e.g. the lower three molecules in the grey box in Fig. 6.5e. Others adsorb off-centered on strands, e.g. the upper two molecules in the grey box. The distances measured between the molecules on the neighboring strands vary (Fig. 6.5f). Some are the same as the distance between the neighboring strands of the (1 × 2) surface (13 Å) as expected, and others are range from 15 Å to 10 Å.

The two added row models, Ti_2O_3 and Ti_2O, offer markedly different surface terminations of the added row. Being terminated with 2-fold-coordinated bridging oxygen atoms, the Ti_2O_3 row structure has no exposed acidic Ti sites that are accessible as reaction

sites for TMAA (Fig. 6.1a). The observation of TMAA species on strands at room temperature indicates that TMAA most likely is chemisorbed on strands. Therefore, the Ti_2O_3 row model poses a serious conflict with the STM observation. On the other hand, the Ti_2O row structure has double rows of Ti cations exposed and running along the [001] direction (Fig. 6.1b). The Ti cations of the double rows are separated by 2.78 Å along [1-10] and 2.96 Å along [001].[28,29]

In summary, an *in situ* room-temperature STM study identifies three adsorption sites: troughs, cross-links, and strands for TMAA molecules on (1 × 2) reconstructed TiO_2(110). At low coverage, the TMAA molecules mostly adsorb in troughs and on cross-links. However, unlike being stationary on (1 × 1) TiO_2(110), TMAA are mobile in troughs suggesting that TMAA adsorbs molecularly in troughs. With increasing coverage, TMAA molecules start forming a close-packed "quasi-1D" chain along [001], separated by (1 × 2) strands. The observed adsorption of TMAA in troughs contradicts the Ti_3O_6 model. At higher coverage, in addition to the adsorption in troughs, TMAA molecules adsorb on strands in both centered and off-centered configurations. The observed adsorption is consistent with the locations of the Ti cations on strands in the Ti_2O model, but not consistent with the Ti_2O_3 model, which has no exposed acidic Ti sites on strands. The adsorption of TMAA strongly supports the Ti_2O model.

References

1. Fujishima, A.; Zhang, X.; Tryk, D. Photocatalysis and Related Surface Phoenomena. *Surf. Sci. Rep*. 2008, *63*, 515–582.

2. Fujishima, A.; Honda, K. Electrochemical photolysis of water at a semiconductor electrode. *Nature* 1972, *238*, 37–38.

3. Mills, A.; Davies, R.H.; Worsley, D. Water-purification by semiconductor photocatalysis. *Chem. Soc. Rev*. 1993, *22*, 417–425.

4. Wang, R.; Hashimoto, K.; Fujishima, A.; Chikuni, M.; Kojima, E.; Kitamura, A.; Shimohigashi, M.; Watanabe, T. *Nature* 1997, *388*, 431.

5. Grätzel, M. Photoelectrochemical Cells. *Nature* 2001, *414*, 338-344.

6. Pang, C. L.; Lindsay, R.; Thornton G. Structure of Clean and Adsorbate-Covered Single-Crystal Rutile TiO_2 Surfaces. *Chem. Rev.* 2013, *113*, 3887-3948.

7. Henderson, M. A.; Lyubinetsky, I. Molecular-level Insights into Photocatalysis from Scanning Probe Microscopy Studies on TiO_2(110). *Chem. Rev.* 2013, *113*, 4428-4455.

8. Sherrill, A. B.; Barteau, M. A. in *Oxide Surfaces*, *The Chemical Physics of Solid Surfaces*, ed. Woodruff, D. P., Elsevier: Amsterdam, 2001, *9*, 409.

9. Henderson, M. A.; White, J. M.; Uetsuka, H.; Onishi, H. Photochemical Charge Transfer and Trapping at the Interface between an Organic Adlayer and an Oxide Semiconductor. *J. Am. Chem. Soc.* 2003, *125*, 14974-14975.

10. White, J. M.; Szanyi, J.; Henderson, M. A. The Photon-Driven Hydrophilicity of Titania: A Model Study Using TiO_2(110) and Adsorbed Trimethyl Acetate. *J. Phys. Chem. B* 2003, *107*, 9029-9033.

11. White, J. M.; Szanyi, J.; Henderson, M. A. Thermal Chemistry of Trimethyl Acetic Acid on TiO_2(110). *J. Phys. Chem. B* 2004, *108*, 3592-3602.

12. Aizawa, M.; Morikawa, Y.; Namai, Y. Morikawa H.; Iwasawa Y. Oxygen Vacancy Promoting Catalytic Dehydration of Formic Acid on TiO_2(110) by in Situ Scanning Tunneling Microscopic Observation. *J. Phys. Chem. B* 2005, *109*, 18831-18838.

13. Onishi, K.; Iwasawa, Y. STM-imaging of formate intermediates adsorbed on TiO_2(110) surface. *Chem. Phys. Lett*. 1994, *226*, 111-114.

14. Bates, S. P.; Kresse, G.; Gillan, M. J. The adsorption and dissociation of ROH molecules on TiO_2(110). *Surf. Sci*. 1998, *409*, 336-349.

15. Hayden, B. E.; King, A.; Newton, M. A. Fourier Transform Reflection-Absorption IR Spectroscopy Study of Formate Adsorption on TiO_2(110). *J. Phys. Chem. B* 1999, *103*, 203-208.

16. Foster, A. S.; Gal, A. Y.; Nieminen, R. M.; Shluger, A. L. Probing Organic Layers on the TiO_2(110) Surface. *J. Phys. Chem. B* 2005, *109*, 4554-4560.

17. Lyubinetsky, I.; Yu, Z. Q.; Henderson, M. A. Direct Observation of Adsorption Evolution and Bonding Configuration of TMMA on TiO_2(110). *J. Phys. Chem. C* 2007, *111*, 4342-4346.

18. Lyubinetsky, I.; Deskins, N. A.; Du, Y.; Vestergaard, E. K.; Kim, D. J.; Dupuis, M. Adsorption states and mobility of trimethylacetic acid molecules on reduced TiO_2(110) surface. *Phys. Chem. Chem. Phys.* 2010, *12*, 5986-5992.

19. Du, Y.; Petrik, N. G.; Deskins, N. A.; Wang, Z.; Henderson, M. A.; Kimmel, G. A.; Lyubinetsky, I. Hydrogen reactivity on highly-hydroxylated TiO_2(110) surfaces prepared *via* carboxylic acid adsorption and photolysis. *Phys. Chem. Chem. Phys.* 2012, *14*, 3066-3074.

20. Grinter, D. C.; Woolcot, T.; Pang, C. L.; Thornton, G. Ordered Carboxylates on TiO_2(110) Formed at Aqueous Interfaces. *J. Phys. Chem. Lett.* 2014, *5*, 4265-4269.

21. Samsonov, G. V. Ed. *The Oxide Handbook*, IFI/Plenum: New York, 1982.

22. Henrich, V. E.; Cox, P. A. *The Surface Science of Metal Oxides*, Cambridge University Press: Cambridge, 1994.

23. Diebold, U. The surface science of titanium dioxide. *Surf. Sci. Rep.* 2003, *48*, 53–229.

24. Wang; Q. Oganov, A. R.; Zhu, Q.; Zhou, X. –F. New Reconstructions of the (110) Surface of Rutile TiO_2 Predicted by an Evolutionary Method. *Phys. Rev. Lett*. 2014, *113*, 266101.

25. Yim, C. M.; Pang, C. L.; Thornton, G. Probing the local electronic structure of the cross-linked (1x2) reconstruction of rutile TiO_2(110). *Surf. Sci.* 2015, 04, 22

26. Sánchez-Sánchez, C.; Martín-Gago, J. A.; López, M. F. Small Pt nanoparticles on the TiO_2(110) – (1 × 2) surface. *Surf. Sci*. 2012, *607*, 159-163.

27. Onishi, H.; Iwasawa, Y. Dynamic visualization of a metal-oxide-surface/gas-phase reaction: Time-resolved observation by scanning tunneling microscopy at 800 K. *Phys. Rev. Lett*. 1996, *76*, 791–794.

28. Park, K.T.; Pan, M.H.; Meunier, V.; Plummer, E.W. Surface reconstructions of TiO_2(110) driven by suboxides. *Phys. Rev. Lett*. 2006, *96*, 226105.

29. Park, K.T.; Pan, M.H.; Meunier, V.; Plummer, E.W. Reoxidation of TiO_2(110) via Ti interstitials and line defects. *Phys. Rev. B* 2007, *75*, 245415.

30. Shibata, N.; Goto, A.; Choi, S.-Y.; Mizoguchi, T.; Findlay, S.D.; Yamamoto, T.; Ikuhara, Y. Direct imaging of reconstructed atoms on TiO_2(110) surfaces. *Science* 2008, *322*, 570–573.

31. Bennett, R.A.; Stone, P.; Price, N.J.; Bowker, M. Two (1 × 2) Reconstructions of TiO_2(110): Surface Rearrangement and Reactivity Studied Using Elevated Temperature Scanning Tunneling Microscopy. *Phys. Rev. Lett*. 1999, *82*, 3831–3834.

32. Blanco-Rey, M.; Abad, J.; Rogero, C.; Mendez, J.; Lopez, M.; Martin-Gago, J.; de Andres, P. Structure of Rutile TiO_2(110)–(1 × 2): Formation of Ti_2O_3 Quasi-1D Metallic Chains. *Phys. Rev. Lett.* 2006, *96*, 055502.

33. Blanco-Rey, M.; Abad, J.; Rogero, C.; Méndez, J.; López, M.; Román, E.; Martín-Gago, J.; de Andrés, P. LEED-IV study of the rutile TiO_2(110)–1 × 2 surface with a Ti-interstitial added-row reconstruction. *Phys. Rev. B* 2007, *75*, 081402.

34. Elliott, S. D.; Bates, S. P. Assignment of the (1 × 2) surface of rutile TiO_2(110) from first principles. *Phys. Rev. B* 2003, *67*, 035421.

35. Pang, C. L.; Haycock, S. A.; Raza, H.; Murray, P. W.; Thornton G.; Gülseren, O.; James, R.; Bullett, D. W. Added row model of TiO_2(110)1 × 2. *Phys. Rev. B* 1998, *58*, 1586.

36. Pieper, H. H.; Venkataramani, K.; Torbrügge, S; Bahr, S.; Lauritsen, J. V.; Besenbacher, F.; Kühnle, A.; Reichling, M. Unravelling the atomic structure of cross-linked (1 × 2) TiO_2(110). *Phys. Chem. Chem. Phys.* 2010, *12*, 12436-12441.

37. Zhang, W.; Liu, L.; Wan, L.; Liu, L.; Cao, L.; Xu, F.; Zhao, J.; Wu, Z. Electronic structures of bare and terephthalic acid adsorbed TiO_2(110) - (1×2) reconstructed surfaces: origin and reactivity of band gap states. *Phys. Chem. Chem. Phys.* 2015, *17*, 20144-20153.

38. Bursill, L.A.; Hyde, B.G. Crystallographic shear in the higher titanium oxides: Structure, texture, mechanisms and thermodynamics. *Prog. Solid State Chem*. 1972, *7*, 177–253.

39. Zhu, K.; Xia, Y.; Tang, M.; Wang, Z. –T.; Lyubinetsky, I.; Ge, Q.; Dohnalek, Z.; Park, K. T.; Zhang, Z. Low-Temperature Reductive Coupling of Formaldehyde on Rutile TiO_2(110). *J. Phys. Chem. C* 2015, *119*, 18452-18457.

40. Zhu, K.; Xia, Y.; Tang, M.; Wang, Z.; Jan, B.; Lyubinetsky, I.; Dohnálek, Z.; Ge, Q.; Park, K. T.; Zhang, Z. Tracking Site-Specific C-C Coupling of Formaldehyde Molecules on Rutile TiO_2(110). *J. Phys. Chem. C* 2015, *119*, 14267– 14272.

41. Zhang, Z.; Tang, M.; Wang, Z.; Ke, Z.; Xia, Y.; Park, K.; Lyubinetsky, I.; Dohnalek, Z.; Ge, Q. Imaging of Formaldehyde Adsorption and Diffusion on TiO_2(110). *Top. Catal*. 2015, *58*, 103– 113.

42. Horcas, I.; Fernandez, R.; Gomez-Rodriguez, J. M.; Colchero, J.; Gomez-Herrero, J.; Baro, A. M. WSXM: A Software for Scanning Probe Microscopy and a Tool for Nanotechnology. *Rev. Sci. Instrum*. 2007, *78*, 013705.

43. Takakusagi, S.; Fukui, K. –I.; Nariyuki, F.; Iwasawa, Y. STM study on structures of two kinds of wide strands formed on TiO_2(110). *Surf. Sci*. 2003, *523*, L41-46.

44. Maksymovych, P.; Mezhenny, S.; Yates, J. T. STM study of water adsorption on the TiO_2(110)-(1 × 2) surface. *Chem. Phys. Lett*. 2003, *382*, 270-276.

45. Kowalski, P. M.; Camellone, M. F.; Nair, N. N.; Meyer, B.; Marx, D. Charge Localization Dynamics Induced by Oxygen Vacancies on the TiO_2(110) Surface. *Phys. Rev. Lett.* 2010, *105*, 146405.

CHAPTER SEVEN

Conclusion and Future Work

In this dissertation, the surface structure and properties of TiO_2 surfaces were studied by UHV VT-STM.

On reduced TiO_2(110) (1×1) surface, the diffusion of V_O mediated by the combination of two acetone diffusion channels was presented. The STM images show that at 300 K acetone prefers to adsorb on V_O sites. The sequential isothermal STM images directly show V_O-bounded acetone can diffuse both along the Ti row and along the O_b row. On O_b row, acetone heals the oxygen vacancy by losing its oxygen and diffuses as an alkyl group. Subsequently, the alkyl group can combine with an O_b atom and diffuse to and then along Ti^{4+} row as an acetone which creates a new oxygen vacancy. The acetone diffusion barriers calculated using DFT agree with experimental results.

On partially oxidized TiO_2(110) (1×1) surfaces, the consecutive reaction steps of acetone with O_a and V_O are studied using STM at 300 K and two types of acetone-O_a species were revealed. One species was formed by a V_O-bound acetone combining with a nearby O_a which appears as a bright V_O-bound acetone-O_a complex. Once formed, the V_O-bound acetone-O_a complex becomes stationary. The other species was formed by a Ti_{5c}-bound acetone reacting with an O_a as a Ti_{5c}-bound diolate which assists the diffusion of the surface O_a. The diolate can be observed both on a single O_a and on an O_a pair. The lifetimes of the Ti_{5c}-bound acetone-O_a diolate, the V_O-bound acetone and the Ti_{5c}-bound acetone indicate that their adsorption energies follow $E_{ads}^{\text{Ti-bound acetone}} > E_{ads}^{\text{diolate}} > E_{ads}^{\text{Vo-bound acetone}}$.

The structure of (1×4) anatase TiO_2(001) epitaxial thin films was studied. High bias STM images show three types of features on the bright rows of the (1×4) reconstruction. The high-resolution images taken from the same area at different bias voltages show that the three types of features are made of two common types of atomic building blocks. We propose a modified added molecule model. In this model, the twofold oxygen at the center of the added TiO_3 row is removed non-uniformly and replaced with surface bridging oxygen atoms of the (1×1) surface. The observed STM image can be qualitatively explained by the combination of reported "theoretical STM images" for the AMR model and ADM model.

On cross-linked (1×2) rutile TiO_2(110), TMAA molecules were found to be adsorbed on three sites: troughs, cross-links and strands from an in situ room-temperature STM study. At low coverage, the TMAA molecules mostly adsorb in troughs and on cross-links. In troughs, TMAA are mobile suggesting that TMAA adsorbs molecularly. With increasing coverage, TMAA molecules start forming a close-packed "quasi-1D" chain along [001], separated by (1 × 2) strands. At higher coverage, in addition to the adsorption in troughs, TMAA molecules adsorb on strands in both centered and off-centered configurations. The adsorption of TMAA in troughs and on strands strongly supports the Ti_2O model.

For further research, there are several directions. As observed, two types of acetone-O_a species were formed on partially oxidized TiO_2(110) surface. Further study of photo-catalytic reactions of these two species would be interesting and important to understand the photo-oxidation of ketones on metal oxide surfaces. On anatase TiO_2(001) surfaces, the chemical reactions and photo-catalytic reactions of organic molecules at defect sites can

provide new evidence to support the theoretic model and also contribute to a better understanding of heterogeneous catalytic reactions on anatase TiO_2. Although the photoreaction of TMAA on cross-linked (1×2) rutile TiO_2(110) was studied without reasonable results, it is still a good direction to explore. Since some changes were observed after UV light exposure, O_2 exposure is a possible method to enhance the photoreaction.

REFERENCES

(1) Henrich, V. E. and Cox, P. A., The Surface Science of Metal Oxides. (Cambridge, New York, 1994), pp. 2, 421.

(2) Diebold, U. The Surface Science of Titanium Dioxide. *Surf. Sci. Rep.* 2003, *48*, 53.

(3) Henderson, M. A., A Surface Science Perspective on Photo-catalysis. Surf. Sci. Rep. 2011, 66, 185.

(4) Schmidt, C. M.; Buchbinder, A. M.; Weitz, E.; Geiger, F. M., Photochemistry of the Indoor Air Pollutant Acetone on Degussa P25 TiO_2 Studied by Chemical Ionization Mass Spectrometry. *J. Phys. Chem. A*, 2007, 111, 13023.

(5) Carter, E.; Carley, A. F., Murphy, D. M., Free-Radical Pathways in the Decomposition of Ketones over Polycrystalline TiO_2: The Role of Organoperoxy Radicals. *ChemPhysChem,* 2007, 8, 113.

(6) Senanayake, S. D.; Gordon, W. O.; Overbury, S. H., Mullins, D. R., Adsorption and Reaction of Acetone over CeOx(111) Thin Films. *J. Phys. Chem. C,* 2009, 113, 6208.

(7) Mattsson, A., Osterlund, L., Adsorption and Photoinduced Decomposition of Acetone and Acetic Acid on Anatase, Brookite, and Rutile TiO_2 Nanoparticles. *J. Phys. Chem. C*, 2010, 114, 14121.

(8) El-Maazawi, M.; Finken, A. N.; Nair, A. B., Grassian, V. H., Adsorption and Photocatalytic Oxidation of Acetone on TiO_2: An in Situ Transmission FT-IR Study. *J. Catal.*, 2000, 191, 138.

(9) Hernandez-Alonso, M. D.; Tejedor-Tejedor, I.; Coronado, J. M.; Anderson, M. A., Soria, J., Operando FTIR Study of the Photocatalytic Oxidation of Acetone in Air over TiO_2-ZrO_2 Thin Films. *Catal. Today*, 2009, 143, 364.

(10) Henderson, M. A., Photooxidation of Acetone on TiO_2(110): Conversion to Acetate via Methyl Radical Ejection. *J. Phys. Chem. B*, 2005, 109, 12062.

(11) Grant, F.A., Properties of Rutile (Titanium Dioxide). Rev. Mod. Phys. 1959, 31, 646-674

(12) Brinkley, D.; Engel, T. Evidence for Structure Sensitivity in the Thermally Activated and Photocatalytic Dehydrogenation of 2-Propanol on TiO_2. *J. Phys. Chem. B* 2000, *104*, 9836-9841.

(13) Farfan-Arribas, E.; Madix, R. Different Binding Sites for Methanol Dehydrogenation and Deoxygenation on Stoichiometric and Defective TiO_2(110)Surfaces. *Surf. Sci.* 2003, *544*, 241-260.

(14) Zhang, Z.; Bondarchuk, O.; White, J. M.; Kay, B. D.; Dohnalek, Z. Imaging Adsorbate O-H Bond Cleavage: Methanol on TiO_2(110). *J. Am. Chem. Soc.* 2006, *128*, 4198-4199.

(15) Gamble, L.; Jung, L.; Campbell, C. Decomposition and Protonation of Surface Ethoxys on TiO_2(110). *Surf. Sci.* 1996, *348*, 1-16.

(16) Wendt, S.; Schaub, R.; Matthiesen, J.; Vestergaard, E. K.; Wahlstrom, E.; Rasmussen, M. D.; Thostrup, P.; Molina, L. M.; Laegsgaard, E.; Stensgaard, I. et al. Oxygen Vacancies on TiO_2(1 1 0) and their Interaction with H_2O and O_2: A Combined High-Resolution STM and DFT Study. *Surf. Sci.* 2005, *598*, 226-245.

(17) Hugenschmidt, M. B.; Gamble, L.; Campbell, C. T. The Interaction of H_2O with a TiO_2(110) Surface. *Surf. Sci.* 1994, *302*, 329-340.

(18) Henderson, M. A. Structural Sensitivity in the Dissociation of Water on TiO_2 Single-Crystal Surfaces. *Langmuir* 1996, *12*, 5093-5098.

(19) Bikondoa, O.; Pang, C. L.; Ithnin, R.; Muryn, C. A.; Onishi, H.; Thornton, G. Direct Visualization of Defect-Mediated Dissociation of Water on TiO_2(110). *Nat. Mater.* 2006, *5*, 189-192.

(20) Wendt, S.; Sprunger, P. T.; Lira, E.; Madsen, G. K. H.; Li, Z.; Hansen, J. O.; Matthiesen, J.; Blekinge-Rasmussen, A.; Laegsgaard, E.; Hammer, B. et al. The Role of Interstitial Sites in the Ti3d Defect State in the Band Gap of Titania. *Science* 2008, *320*, 1755-1759.

(21) Haubrich, J.; Kaxiras, E.; Friend, C. M. The Role of Surface and Subsurface Point Defects for Chemical Model Studies on TiO_2: A First-Principles Theoretical Study of Formaldehyde Bonding on Rutile TiO_2(110). *Chem. Eur. J.* 2011, *17*, 4496-4506.

(22) Bowker, M.; Bennett, R. A. The Role of Ti_{3+} Interstitials in TiO_2(110) Reduction and Oxidation. *J. Phys. Condens. Matter.* 2009, *21*, 474224.

(23) Mattsson, A.; Osterlund, L. Adsorption and Photoinduced Decomposition of Acetone and Acetic Acid on Anatase, Brookite, and Rutile TiO_2 Nanoparticles. *J. Phys. Chem. C* 2010, *114*, 14121-14132.

(24) Kim, J.; Kay, B. D.; Dohnalek, Z. Formaldehyde Polymerization on $(WO_3)_3/TiO_2$(110) Model Catalyst. *J. Phys. Chem. C* 2010, *114*, 17017-17022.

(25) Henderson, M. A. Photooxidation of Acetone on TiO_2(110): Conversion to Acetate Via Methyl Radical Ejection. *J. Phys. Chem. B* 2005, *109*, 12062-12070.

(26) El-Maazawi, M.; Finken, A.; Nair, A.; Grassian, V. Adsorption and Photocatalytic Oxidation of Acetone on TiO_2: An in Situ Transmission FT-IR Study. *J. Cata.* 2000, *191*, 138-146.

(27) Hernandez-Alonso, M. D.; Tejedor-Tejedor, I.; Coronado, J. M.; Anderson, M. A.; Soria, J. Operando FTIR Study of the Photocatalytic Oxidation of Acetone in Air Over TiO_2-ZrO_2 Thin Films. *Catal. Today* 2009, *143*, 364-373.

(28) Henderson, M. A. Acetone Chemistry on Oxidized and Reduced TiO_2(110). *J. Phys. Chem. B* 2004, *108*, 18932-18941.

(29) Yasuo, M.; Sasahara, A.; Onishi, H. Acetone Adsorption on Oxidized and Reduced TiO_2(110): A Scanning Tunneling Microscope Study. *J. Phys. Chem. C* 2010, *114*, 14579-14582.

(30) Henderson, M. A. Effect of Coadsorbed Water on the Photodecomposition of Acetone on TiO_2(110). *J. Cata.* 2008, *256*, 287-292.

(31) Qiu, H.; Idriss, H.; Wang, Y.; Woell, C. Carbon-Carbon Bond Formation on Model Titanium Oxide Surfaces: Identification of Surface Reaction Intermediates by High-Resolution Electron Energy Loss Spectroscopy. *J. Phys. Chem. C* 2008, *112*, 9828-9834.

(32) Marquez, A. M.; Plata, J. J.; Fdez Sanz, J. Role of Coverage and Surface Oxidation Degree in the Adsorption of Acetone on TiO_2(110). A Density Functional Study. *J. Phys. Chem. C* 2009, *113*, 19973-19980.

(33) Benz, L.; Haubrich, J.; Jensen, S. C.; Friend, C. M. Molecular Imaging of Reductive Coupling Reactions: Interstitial-Mediated Coupling of Benzaldehyde on Reduced TiO_2(110). *ACS Nano* 2011, *5*, 834-843.

(34) Almeida, A. R.; Moulijn, J. A.; Mul, G. Photocatalytic Oxidation of Cyclohexane Over TiO_2: Evidence for a Mars-Van Krevelen Mechanism. *J. Phys. Chem. C* 2011, *115*, 1330-1338.

(35) Trovarelli, A. In *Catalysis by Ceria and Related Materials;* Catalytic science series; Imperial College Press: London, 2002; Vol. 2, pp 508.

(36) Masel, R. I. In *Chemical Kinetics and Catalysis;* Wiley-Interscience: New York, 2001; pp 952.

(37) Zehr, R. T.; Henderson, M. A. Acetaldehyde Photochemistry on TiO_2(110). *Surf. Sci.* 2008, *602*, 2238-2249.

(38) Pierce, K. G.; Barteau, M. A. Ketone Coupling on Reduced TiO_2 (001) Surfaces: Evidence of Pinacol Formation. *J. Org. Chem.* 1995, *60*, 2405-2410.

(39) Cheng, H.; Selloni, A. Energetics and Diffusion of Intrinsic Surface and Subsurface Defects on Anatase TiO_2(101). *J. Chem. Phys.* 2009, *131*, 054703.

(40) Zhang, Z.; Rousseau, R.; Gong, J.; Li, S. C.; Kay, B. D.; Ge, Q.; Dohnalek, Z. Vacancy-Assisted Diffusion of Alkoxy Species on Rutile TiO_2(110). *Phys. Rev. Lett.* 2008, *101*, 156103.

(41) Li, S. C.; Chu, L. N.; Gong, X. Q.; Diebold, U. Hydrogen Bonding Controls the Dynamics of Catechol Adsorbed on a TiO_2(110) Surface. *Science* 2010, *328*, 882-884.

(42) Tatsuma, T.; Tachibana, S., Fujishima, A., Remote Oxidation of Organic Compounds by UV-Irradiated TiO_2 via the Gas Phase. *J. Phys. Chem. B,* 2001, 105, 6987.

(43) Nakamura, R., Sato, S., Oxygen Species Active for Photooxidation of *n*-Decane over TiO_2 Surfaces. *J. Phys. Chem. B,* 2002, 106, 5893.

(44) Szczepankiewicz, S. H.; Colussi, A. J., Hoffmann, M. R., Infrared Spectra of Photoinduced Species on Hydroxylated Titania Surfaces. *J. Phys. Chem. B,* 2000, 104, 9842.

(45) Yates, J. T., Photochemistry on TiO_2: Mechanisms behind the surface chemistry. *Surf. Sci.*, 2009, 603, 1605.

(46) Wendt, S.; Sprunger, P. T.; Lira, E.; Madsen, G. K. H.; Li, Z.; Hansen, J. O.; Matthiesen, J.; Blekinge-Rasmussen, A.; Laegsgaard, E.; Hammer, B., Besenbacher, F., The Role of Interstitial Sites in the Ti*3d* Defect State in the Band Gap of Titania. *Science*, 2008, 320, 1755.

(47) Pang, C. L.; Bikondoa, O.; Humphrey, D. S.; Papageorgiou, A. C.; Cabailh, G.; Ithnin, R.; Chen, Q.; Muryn, C. A.; Onishi, H., Thornton, G., Tailored TiO_2(110) Surfaces and Their Reactivity. *Nanotechnology*, 2006, 17, 5397.

(48) Du, Y.; Deskins, N. A.; Zhang, Z.; Dohnalek, Z.; Dupuis, M., Lyubinetsky, I., Imaging Consecutive Steps of O_2 Reaction with Hydroxylated TiO_2(110): Identification of HO_2 and Terminal OH Intermediates. *J. Phys. Chem. C,* 2009, 113, 666.

(49) Petrik, N. G., Kimmel, G. A., Electron- and Hole-Mediated Reactions in UV-Irradiated O_2 Adsorbed on Reduced Rutile TiO_2(110). *J.Phys.Chem.C,* 2011, 115, 152.

(50) Henderson, M. A.; Epling, W. S.; Perkins, C. L.; Peden, C. H. F., Diebold, U., Interaction of Molecular Oxygen with the Vacuum-Annealed TiO_2(110) Surface: Molecular and Dissociative Channels. *J. Phys. Chem. B,* 1999, 103, 5328.

(51) Scheiber, P.; Riss, A.; Schmid, M.; Varga, P., Diebold, U., Observation and Destruction of An Elusive Adsorbate with STM: O_2/TiO_2(110). *Phys.Rev.Lett.,* 2010, 105, 216101.

(52) Lira, E.; Hansen, J. Ø.; Huo, P.; Bechstein, R.; Galliker, P.; Lægsgaard, E.; Hammer, B.; Wendt, S., Besenbacher, F., Dissociative and Molecular Oxygen Chemisorption Channels on Reduced Rutile TiO_2(110): An STM and TPD Study. *Surf.Sci.,* 2010, 604, 1945.

(53) Du, Y.; Deskins, N. A.; Zhang, Z.; Dohnalek, Z.; Dupuis, M., Lyubinetsky, I., Formation of O Adatom Pairs and Charge Transfer upon O(2) Dissociation on Reduced TiO_2(110). *Phys. Chem. Chem. Phys.,* 2010, 12, 6337.

(54) Tan, S.; Ji, Y.; Zhao, Y.; Zhao, A.; Wang, B.; Yang, J., Hou, J. G., Molecular Oxygen Adsorption Behaviors on the Rutile TiO_2(110)-1x1 Surface: An in Situ Study with Low-Temperature Scanning Tunneling Microscopy. *J.Am.Chem.Soc.,* 2011, 133, 2002.

(55) Jayaweera, P. M.; Quah, E. L., Idriss, H., Photoreaction of Ethanol on TiO_2(110) Single-Crystal Surface. *J.Phys.Chem.C,* 2007, 111, 1764.

(56) Yasuo, M.; Sasahara, A., Onishi, H., Acetone Adsorption on Oxidized and Reduced TiO_2(110): A Scanning Tunneling Microscope Study. *J. Phys. Chem. C,* 2010, 114, 14579.

(57) Brinkley, D., Engel, T., Evidence for Structure Sensitivity in the Thermally Activated and Photocatalytic Dehydrogenation of 2-Propanol on TiO_2. *J. Phys. Chem. B,* 2000, 104, 9836.

(58) Idriss, H.; Légare, P., Maire, G., Dark and Photoreactions of Acetates on TiO_2(110) Single Crystal Surface. *Surf.Sci.,* 2002, 515, 413.

(59) Shen, M.; Henderson, M. A., Identification of the Active Species in Photochemical Hole Scavenging Reactions of Methanol on TiO_2. *J. Phys. Chem. Lett.,* 2011, 2, 2707.

(60) Phillips, K. P.; Jensen, S. C.; Baron, M.; Li, S. C.; Friend, C. M., Sequential Photo-oxidation of Methanol to Methyl Formate on TiO_2(110). *J. Am. Chem. Soc.,* 2013, 135, 574.

(61) Henderson, M. A., Acetone Chemistry on Oxidized and Reduced TiO_2(110). *J. Phys. Chem. B,* 2004, 108, 18932.

(62) Henderson, M. A., Effect of Coadsorbed Water on the Photodecomposition of Acetone on TiO_2(110). *J. Catal.*, 2008, 256, 287.

(63) Henderson, M. A., Relationship of O_2 Photodesorption in Photooxidation of Acetone on TiO_2. *J. Phys. Chem. C*, 2008, 112, 11433.

(64) Henderson, M. A., Ethyl Radical Ejection during Photodecomposition of Butanone on TiO_2(110). *Surf.Sci.*, 2008, 602, 3188.

(65) Zehr, R. T., Henderson, M. A., Acetaldehyde Photochemistry on TiO_2(110). *Surf.Sci.*, 2008, 602, 2238.

(66) Zehr, R. T.; Deskins, N. A.; Henderson, M. A., Photochemistry of 1,1,1-Trifluoroacetone on Rutile TiO_2(110). *J. Phys. Chem. C*, 2010, 114, 16900.

(67) Zehr, R. T.; Henderson, M. A., Thermal Chemistry and Photochemistry of Hexafluoroacetone on Rutile TiO_2(110). *Phys. Chem. Chem. Phys.*, 2010, 12, 8085.

(68) Wang, T.; Dixon, D. A., Henderson, M. A., C-C and C-Heteroatom Bond Dissociation Energies in $CH_3R\dot{C}(OH)_2$: Energetics for Photocatalytic Processes of Organic Diolates on TiO_2 Surfaces. *J. Phys. Chem. B*, 2010, 114, 14083.

(69) Henderson, M. A.; Deskins, N. A.; Zehr, R. T., Dupuis, M., Generation of Organic Radicals during Photocatalytic Reactions on TiO_2. *J. Catal.*, 2011, 279, 205.

(70) Jensen, S. C.; Shank, A.; Madix, R. J., Friend, C. M., Butyrophenone on O-TiO_2(110): One-Dimensional Motion in a Weakly Confined Potential Well. *ACS Nano*, 2012, 6, 2925.

(71) Zhang, D.; Li, G.; Yang, X.; Yu, J. C. A Micrometer-size TiO_2 Single-crystal Photocatalyst with Remarkable 80% Level of Reactive Facets. *Chem. Commun.* 2009, *45*, 4381-4383.

(72) Liu, S.; Yu, J.; Jaroniec, M. Tunable Photocatalytic Selectivity of Hollow TiO_2 Microspheres Composed of Anatase Polyhedra with Exposed {001} Facets. *J. Am. Chem. Soc.* 2010, *132*, 11914-11916.

(73) Han, X.; Kuang, Q.; Jin, M.; Xie, Z.; Zheng, L. Synthesis of Titania Nanosheets with a High Percentage of Exposed (001) Facets and Related Photocatalytic Properties. *J. Am. Chem. Soc.* 2009, *131*, 3152-3153.

(74) Yang, H. G.; Sun, C. H.; Qiao, S. Z.; Zou, J.; Liu, G.; Smith, S. C.; Cheng, H. M.; Lu, G. Q. Anatase TiO_2 Single Crystals with a Large Percentage of Reactive Facets. *Nature* 2008, *453*, 638-641.

(75) Wen, C. Z.; Zhou, J. Z.; Jiang, H. B.; Hu, Q. H.; Qiao, S. Z.; Yang, H. G. Synthesis of Micro-sized Titanium Dioxide Nanosheets Wholly Exposed with High-Energy {001} and {100} Facets. *Chem. Commun.* 2011, *47*, 4400-4402.

(76) Gong, X. Q.; Selloni, A. Reactivity of Anatase TiO_2 Nanoparticles: the Role of the Minority (001) Surface. *J. Phys. Chem. B* 2005, *109*, 19560-19562.

(77) Pan, J.; Liu, G.; Lu, G. Q.; Cheng, H. On the True Photoreactivity Order of {001}, {010}, and {101} Facets of Anatase TiO_2 Crystals. *Angew. Chem. Int. Ed.* 2011, *50*, 2133-2137.

(78) Zheng, Z.; Huang, B.; Lu, J.; Qin, X.; Zhang, X.; Dai, Y. Hierarchical TiO_2 Microspheres: Synergetic Effect of {001} and {101} Facets for Enhanced Photocatalytic Activity. *Chem. Eur. J.* 2011, *17*, 15032-15038.

(79) Scheiber, P.; Fidler, M.; Dulub, O.; Schmid, M.; Diebold, U.; Hou, W.; Aschauer, U.; Selloni, A. (Sub)Surface Mobility of Oxygen Vacancies at the TiO_2 Anatase (101) Surface. *Phys. Rev. Lett.* 2012, *109*, 136103.

(80) He, Y.; Dulub, O.; Cheng, H.; Selloni, A.; Diebold, U. Evidence for the Predominance of Subsurface Defects on Reduced Anatase TiO_2(101). *Phys. Rev. Lett.* 2009, *102*, 106105.

(81) Thomas, A. G.; Flavell, W. R.; Kumarasinghe, A. R.; Mallick, A. K.; Tsoutsou, D.; Smith, G. C.; Stockbauer, R.; Patel, S.; Gratzel, M. Resonant Photoemission of Anatase TiO_2 (101) and (001) Single Crystals. *Phys. Rev. B* 2003, *67*, 035110.

(82) Sandell, A.; Sanyal, B.; Walle, L. E.; Richter, J. H.; Plogmaker, S.; Karlsson, P. G.; Borg, A.; Uvdal, P. Probing and Modifying the Empty-State Threshold of Anatase TiO_2: Experiments and *Ab Initio* Theory. *Phys. Rev. B* 2008, *78*, 075113.

(83) Liang, Y.; Gan, S.; Chambers, S. A.; Altman, E. I. Surface Structure of Anatase TiO_2(001): Reconstruction, Atomic Steps, and Domains. *Phys. Rev. B* 2001, *63*, 235402.

(84) Weng, X.; Fisher, P.; Skowronski, M.; Salvador, P. A.; Maksimov, O. Structural Characterization of TiO_2 Films Grown on $LaAlO_3$ and $SrTiO_3$ Substrates using Reactive Molecular Beam Epitaxy. *J. Cryst. Growth* 2008, *310*, 545-550.

(85) Herman, G. S.; Sievers, M. R.; Gao, Y. Structure Determination of the Two-Domain (1x4) Anatase TiO_2(001) Surface. *Phys. Rev. Lett.* 2000, *84*, 3354-3357.

(86) Tanner, R. E.; Sasahara, A.; Liang, Y.; Altman, E. I.; Onishi, H. Formic Acid Adsorption on Anatase TiO_2(001)(1x4) Thin Films Studied by NC-AFM and STM. *J. Phys. Chem. B* 2002, *106*, 8211-8222.

(87) Ohsawa, T.; Lyubinetsky, I.; Du, Y.; Henderson, M. A.; Shutthanandan, V.; Chambers, S. A. Crystallographic Dependence of Visible-Light Photoactivity in Epitaxial $TiO_{2-x}N_x$ Anatase and Rutile. *Phys. Rev. B* 2009, *79*, 085401.

(88) Ohsawa, T.; Lyubinetsky, I.; Henderson, M. A.; Chambers, S. A. Hole-Mediated Photodecomposition of Trimethyl Acetate on a TiO_2(001) Anatase Epitaxial Thin Film Surface. *J. Phys. Chem. C* 2008, *112*, 20050-20056.

(89) Ramamoorthy, M.; Vanderbilt, D.; Kingsmith. R.M. First-principles calculations of the energetics of stoichiometric TiO2 surfaces. Phys. Rev. 1994, B 49, 16721-16727

(90) Kauzmann, W. Kinetic Theory of Gases. W.A.Benjamin, New York, 1966, 232

(91) Oura, K.; Lifshits, V.G.; Saranin, A. A.; Zotov, A. V.; Katayama, M. Surface Science: An introduction. Springer, 2003, 19

(92) Binnig, G.; Rohrer, H. Scanning tunneling microscopy. IBM Journal of Research and Development, 1986, 30, 355

(93) Bai, C. Scanning Tunneling Microscopy and Its Applications. Springer-Verlag Berlin Heidelberg New York, 2000, 3

(94) Chen, C. J. Introduction to Scanning Tunneling Microscopy. Oxford Science Publications, 2007, 3